SANDIA REPORT
SAND2014-5038
Unlimited Release
Printed July 2014

Electromagnetic Field Limits Set By The V-Curve

Larry K. Warne, Roy E. Jorgenson, and H. Gerald Hudson

Prepared by
Sandia National Laboratories
Albuquerque, New Mexico 87185 and Livermore, California 94550

Sandia National Laboratories is a multi-program laboratory managed and operated by Sandia Corporation, a wholly owned subsidiary of Lockheed Martin Corporation, for the U.S. Department of Energy's National Nuclear Security Administration under contract DE-AC04-94AL85000.

Issued by Sandia National Laboratories, operated for the United States Department of Energy by Sandia Corporation.

Available to DOE and DOE contractors from
U.S. Department of Energy
Office of Scientific and Technical Information
P.O. Box 62
Oak Ridge, TN 37831

Telephone:	(865) 576-8401
Facsimile:	(865) 576-5728
E-Mail:	reports@adonis.osti.gov
Online ordering:	http://www.osti.gov/bridge

Available to the public from
U.S. Department of Commerce
National Technical Information Service
5285 Port Royal Rd.
Springfield, VA 22161

Telephone:	(800) 553-6847
Facsimile:	(703) 605-6900
E-Mail:	orders@ntis.fedworld.gov
Online order:	http://www.ntis.gov/help/ordermethods.asp?loc=7-4-0#online

SAND2014-5038
Unlimited Release
Printed July 2014

Electromagnetic Field Limits Set by the V-Curve

Larry K. Warne and Roy E. Jorgenson,
Electromagnetic Theory Dept. 1352,

and H. Gerald Hudson, Retired

Sandia National Laboratories
P. O. Box 5800
Albuquerque, NM 87185-1152

Abstract

When emitters of electromagnetic energy are operated in the vicinity of sensitive components, the electric field at the component location must be kept below a certain level in order to prevent the component from being damaged, or in the case of electro-explosive devices, initiating. The V-Curve is a convenient way to set the electric field limit because it requires minimal information about the problem configuration. In this report we will discuss the basis for the V-Curve. We also consider deviations from the original V-Curve resulting from inductive versus capacitive antennas, increases in directivity gain for long antennas, decreases in input impedance when operating in a bounded region, and mismatches dictated by transmission line losses. In addition, we consider mitigating effects resulting from limited antenna sizes.

Acknowledgments

The authors would like to thank Kenneth C. Chen of Sandia National Laboratories for many helpful discussions on the V-Curve. We would also like to thank Kelvin S. H. Lee for helpful discussions regarding modal series represenations.

Contents

Figures

Intentionally Left Blank

Electromagnetic Field Limits Set by the V-Curve

Larry K. Warne and Roy E. Jorgenson,
Electromagnetic Theory Dept. 1352,

and H. Gerald Hudson, Retired

Sandia National Laboratories
P. O. Box 5800
Albuquerque, NM 87185-1152

1 SUMMARY

This summary discusses the basis for the V-Curve to set limits on field levels and briefly touches on issues relating to its use.

1.1 The V-Curve

The V-Curve is intended to serve as a bounding susceptibility curve for sensitive components, such as electro-explosive devices, for which a power threshold can be set. The basic idea of the model is that part of the attached wiring acts as an antenna, receiving power from a surrounding field, and part of the wiring acts as a transmission line between the device load and the antenna. The right arm of the V-Curve assumes the transmission line acts a transformer matching the antenna to the load, and the response is dictated by the wavelength (or frequency) as well as the directivity gain of the antenna. The left arm of the V-Curve assumes the transmission line is too short to effect matching (which typically occurs when the length of the transmission line is shorter than a quarter wavelength). Figure 1 shows a summary of the V-Curve model. To be conservative, the actual low frequency asymptote for capacitive antennas, depicted by the dotted curve labeled as C_{dip} in Figure 2, is usually replaced by the solid curve that intersects the right arm at the minimum matching frequency. Each of these two arms then set out an allowed electric field level as a function of frequency. The corresponding two straight curves (on a log-log electric field versus frequency plot) extrapolate to an intersection, at the minimum matching frequency of the V as depicted by the solid curve in Figure 2. Inductive loop antennas are also considered and demonstrated to lead to the same general characteristics for the allowed magnetic field (taken to be implied by the standard V-Curve requirement). Loops can be more efficient receivers at low frequencies, as depicted by the widely spaced dots labeled by L_{oop} in Figure 2 for very large loops, however reasonable antenna size constraints lead to the standard V-Curve (and implied magnetic field) still being applicable.

1.2 Directivity Of Antennas

The directivity gain of the antenna is usually set to that of a resonant dipole. Short dipoles exhibit nearly the same gain level. Up on the right side of the V-Curve (high frequencies) reasonable sized antennas can exhibit directivity gains exceeding the simple dipole when the wave impinges near grazing. These enhancements cause the actual susceptibility to fall below the right arm of the V-Curve, but occur in a region where the allowed field levels are quite high, as depicted by the long dashed curve labeled by G in Figure 2. In addition, dielectric (and other) losses in the matching transmission line may begin to play a mitigating role in this frequency region. Another issue is the enhancement of gain caused by bringing a neighboring conducting plane (ground plane) into the configuration. This ground plane causes a doubling of the antenna gain, which could be incorporated into the basic V-Curve.

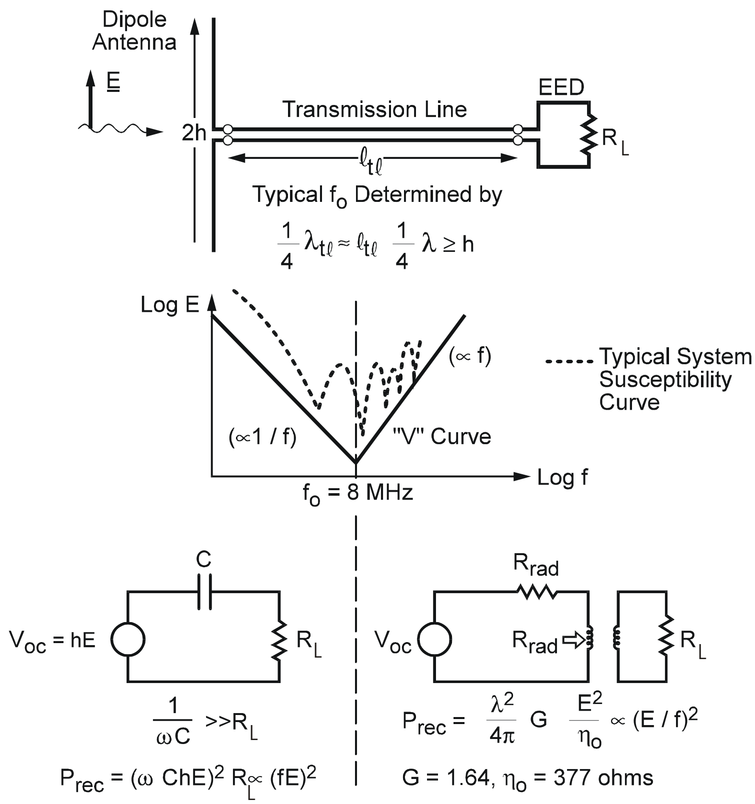

Figure 1. Summary of the V-Curve model.

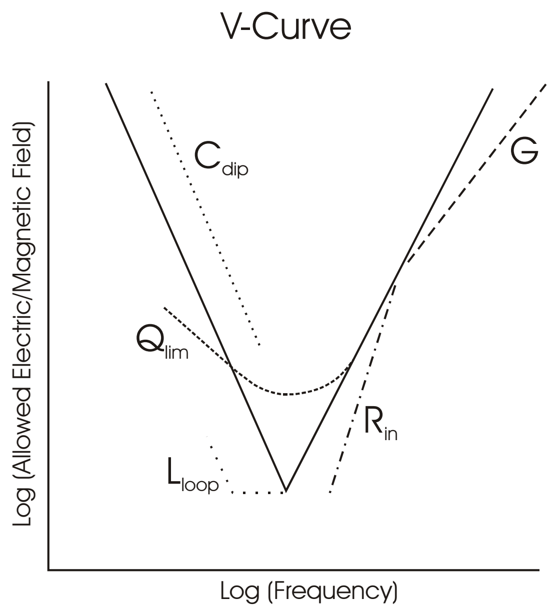

Figure 2. Generic V-Curve and various issues discussed in this report.

1.3 Loss Limits On Matching

The typical V-Curve requirement assumes a lossless transmission line. However for realistic metallic losses, we can place a bound on the quality factor of the matching network. For reasonable antenna size limits these losses place an addition limit on the lowest frequency where conjugate matching is possible. The resulting curve modifications, which tend to raise the bottom of the V, are depicted as the dashed curve modification with label Q_{lim} in Figure 2. This additional limit is useful not only to exhibit some of the conservatism in the original V-Curve, but also to help mitigate effects which reduce the antenna input impedance (such as operation in conducting enclosures).

1.4 Enclosures

The antenna circuit model used in the V-Curve calculation for received power involves the inverse of the radiation resistance. This quantity results from the long range radiation field of the antenna. When the antenna is operated in a bounded region or cavity (room or enclosure), this radiation resistance is modified to reflect the losses in the walls of the room; in some situations the value can be reduced, dropping the allowed level, as depicted by the bounding curve with label R_{in} in Figure 2. In this report we examine two canonical cavities and this effect down near the bottom of the V (below the lowest resonant cavity mode), as well as at high frequencies. At sufficiently high frequencies this effect is reduced due to overlap of the resonant modes. Near the bottom of the V, this effect can be mitigated by the loss limits on matching discussed above (which are made more difficult by the room). Nevertheless, there is a region between these two limits where the room will likely cause a reduction in the input resistance of the antenna. Measurements of the loss properties of typical rooms (quality factor of the resonances) are proposed so that this can be more quantitatively assessed. In high quality factor cases another mitigating factor is that the transmitter field is likely suppressed at the same frequencies as the receiver impedance. Taking this into account requires the transmitter to be part of the problem (a two-port description rather then the single-port receiver centric V-Curve), which is out of scope of the present report.

2 INTRODUCTION

The V-Curve model places limits on field levels in the vicinity of susceptible devices that are attached to cabling. The cabling couples the power due to the surrounding field into the susceptible device, which acts as a load. Part of the cabling is assumed to act as a section of transmission line and part is assumed to act as an antenna. Note that we are using the term "cabling" in a very general sense. The cabling could consist of random conductors such as containers, wire and so forth that are accidently touching each other and the susceptible devices, and could include metal holding fixtures in combination with test leads. The topology of the entire system is shown in Figure 3.

The crucial feature of this three-part structure (antenna, transmission line and load) is that the transmission line at a discrete set of frequencies can, in principle, match the antenna impedance at one end to the load impedance at the opposite end. The V-Curve model provides a practical worst case by assuming that the impedance matching occurs at every frequency above a "minimum" frequency (ω_0) – the frequency where the allowed field is the smallest. Above the minimum frequency the allowed field level rises because the receiving cross section decreases with wavelength; below the "minimum" the field level rises because of the antenna and load impedance mismatch. The allowed electric field levels calculated by this model appear as a "V" shape on a log-log electric field versus frequency plot, which is the source of the model's name. Figure 4 shows a sketch of a V-Curve in relation to a typical susceptibility curve obtained by taking more detailed information into account.

One of the model's requirements is that the susceptible device must be characterized by a known, allowed received power level P_L. If the calculated power delivered to the load is less than P_L we assume the susceptible device will not be damaged (or will not initiate – a "no-fire" level); above P_L it may be damaged (or may initiate). We use a power threshold here in preference to a current threshold because variations in impedance (from say the skin effect) may make the current a less reliable threshold in some cases. The ability by an antenna to absorb power from an incident field is characterized by the antenna's gain parameter (G) so the gain of the portion of cabling acting as the antenna is another quantity required by the V-Curve model. Fortunately, G does not vary widely for quite large variations of antenna geometry over the range of frequencies where the V-Curve predicts the lowest field levels. This allows us to choose a reasonable value for G even though the geometry is uncertain. The value of ω_0 is set by the length of cabling that functions as a transmission line (ℓ). This quantity can be set conservatively by using the longest length of cabling that could conceivably be available in the scenario. If the V-Curve is being applied inside an enclosed space, the reflections from the walls of the room can also play a role; the room quality factor (Q) and volume (V) can be used to assess the importance of this effect. All of the parameters that go into the model will be be discussed in more detail in the remainder of the report. The ability of the V-Curve model to give a reasonable bound for the field level without requiring detailed knowledge of what could be a highly-variable geometry is its great strength.

The scientific justification and assumptions for the V-Curve used by Sandia were first documented in an undated note written by R. L. Parker [1], although aspects of such bounding models have been discussed previously [2]. It is included in this report for historical purposes in Appendix A. Appendix B [3] compares the electric field bound calculated by the V-Curve to the bound calculated by other models. It is included because the bound given by the V-Curve is not strictly a worst case bound. At high frequencies, say larger than 1 GHz, there are situations where the receiving antenna could be many wavelengths long giving it a somewhat higher gain and resulting in a lower allowed electric field than that predicted by the V-Curve using a constant half-wavelength dipole gain. This typically does not result in a significant problem using the V-Curve, however because, at high frequencies the level of field allowed by the V-Curve is large. This situation is shown in Figures B-13 and B-14. The advantage of the V-Curve in terms of requiring minimal information outweigh its inability to capture the strict bound at high frequencies. Nevertheless, it is prudent to use caution if a proposed field level gets close to the V-Curve limit at frequencies greater than 1

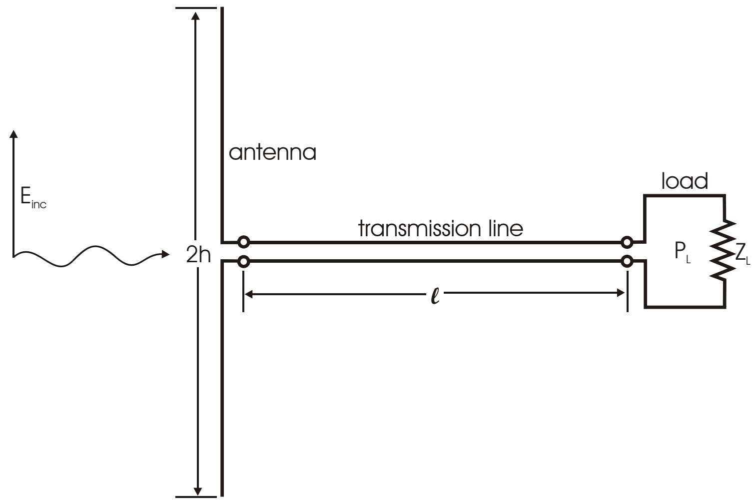

Figure 3. Sensitive load attached to cables that act like an antenna and transmission line.

GHz. Another issue is the possible variation of the power level P_L with frequency, since this threshold is frequently experimentally verified in ordnance at low frequencies.

Near the bottom of the V-Curve, for antennas of limited size, losses in the transmission lines responsible for the matching place limits on how low the frequency can be before matching becomes impossible. This is discussed and is a useful addition to the line length criterion in constraining the lowest matching frequency, particularly in situations where the antenna input impedance is suppressed.

In the past V-Curves were developed for unbounded environments like what would be encountered out-doors. Section 3 in this report discusses the V-Curve for an unbounded environment. The V-Curve model for unbounded environments has been widely used to establish electromagnetic field specifications in explosive handling areas. Often these areas consist of rooms with concrete walls containing reinforcing bar which are electrically tied together to form a type of conducting boundary. When the area is enclosed by conducting boundaries as shown in Figure 5 it is natural to ask about the effect of the bounded region on the underlying theory of the V-Curve. This was first considered at Sandia in some internal reports [4], [5] that are included as Appendices C and D. This report will attempt to estimate the effect of the bounded region on the electromagnetic field specification in Section 6.

3 THE V-CURVE

This section reviews the standard V-Curve in an unbounded region [1], [3]. We assume in this section that a receiving antenna is immersed in a plane field (generated a large distance away). Interactions with a closely spaced transmitter, or other objects in the vicinity of the receiver (including boundaries of the region), are not considered. The receiving circuit includes a section of transmission line between the antenna and the load which facilitates matching if it is sufficiently long. We examine the resulting circuit and what restrictions it places on the field surrounding the receiver. Note that the spirit of the V-Curve is to place limits on the field surrounding the receiver, for an allowed received power to the load, with minimal information on the details of the receiving setup.

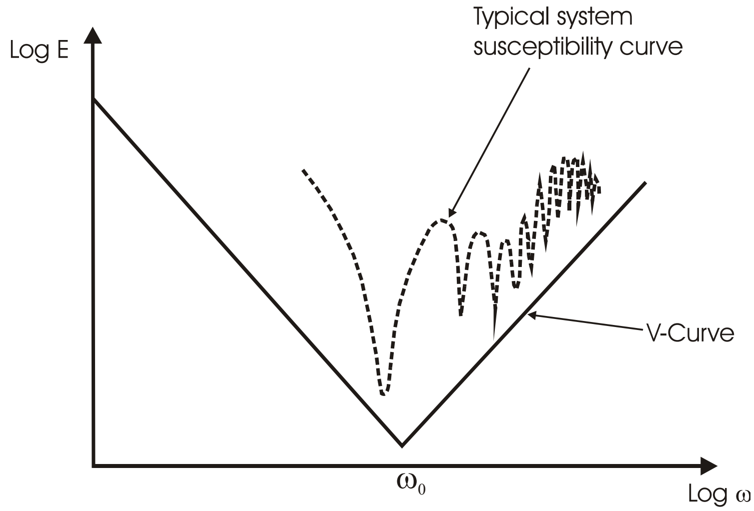

Figure 4. Form of a typical V-Curve (solid line) along with a susceptibility curve of a typical system calculated with more detailed information (dashed curve). The V-Curve typically gives a lower bound to the curves calculated with more detailed information.

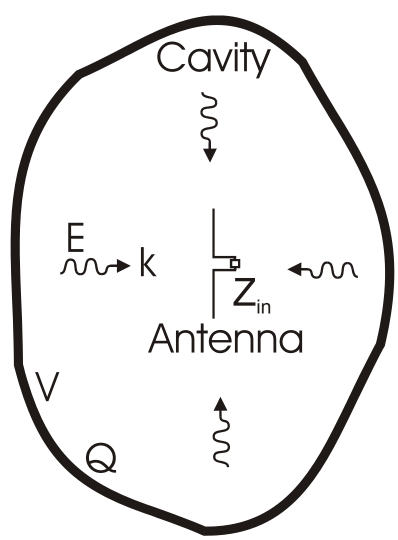

Figure 5. Typical geometry of receiving linear antenna in a cavity.

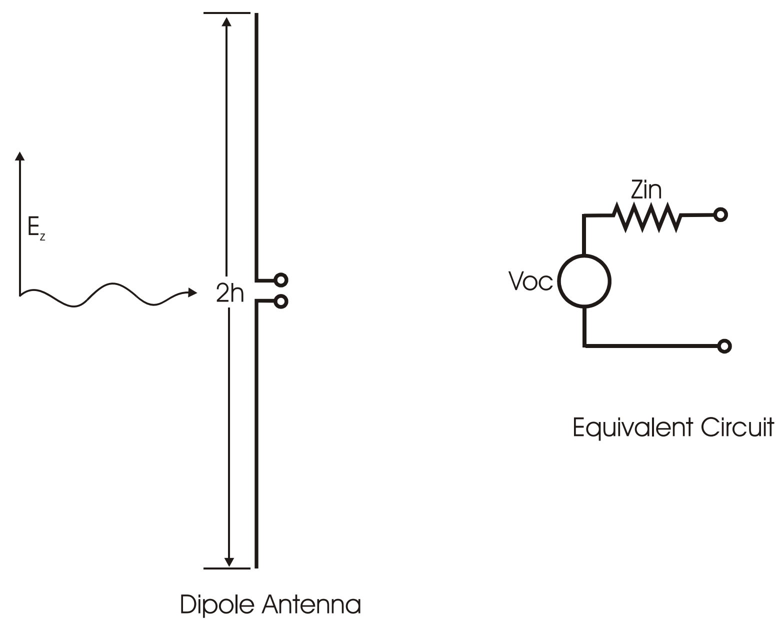

Figure 6. Dipole dimensions and equivalent circuit.

3.1 Antenna and Transmission Line Circuit Representation

We begin by considering an electric dipole or capacitive antenna, but also briefly summarize the inductive or loop antenna.

3.1.1 Capacitive Antenna

The receiving dipole antenna with length $2h$ can be described by an equivalent circuit model as shown in Figure 6 [6], [7]. The open circuit voltage in the circuit is

$$V_{oc} = -h_e E_z \tag{1}$$

where the effective height is h_e and the electric field (in the z direction) along the antenna, without the antenna present, is E_z. The effective height for an electrically short dipole is the half length

$$h_e \sim h \tag{2}$$

The effective height of a resonant half-wave dipole is

$$h_e \approx 1.28h \tag{3}$$

The impedance of the antenna has both a resistive and a reactive part (with harmonic time dependence $e^{-i\omega t}$ suppressed)

$$Z_{in} = R_{in} - iX_{in} \tag{4}$$

If the resistance of the conducting materials that make up the antenna is ignored then the resistive part is the radiation resistance of the antenna

$$R_{in} = R_{rad} \tag{5}$$

The electrically short dipole antenna has radiation resistance

$$R_{rad} \sim \eta_0 \frac{(kh)^2}{6\pi} = O\left(\omega^2\right) \tag{6}$$

where $\eta_0 = \sqrt{\mu_0/\varepsilon_0} \approx 120\pi$ ohms is the intrinsic impedance of free space, $\mu_0 = 4\pi \times 10^{-7}$ H/m is the magnetic permeability of free space, $\varepsilon_0 \approx 8.854 \times 10^{-12}$ F/m is the electric permittivity of free space, and the wavenumber is

$$k = \omega/c \tag{7}$$

where ω is the temporal frequency and $c = 1/\sqrt{\mu_0\varepsilon_0} \approx 3 \times 10^8$ m/s is the vacuum velocity of light. The value of the radiation resistance for a resonant half-wave dipole is

$$R_{rad} \approx 73 \text{ ohms} \tag{8}$$

The reactance of the antenna is dependent on the antenna cross section and other geometrical features in practical situations. The electrically short antenna has capacitive reactance

$$X_{in} \sim -1/\left(\omega C_{dip}\right) = O\left(\omega^{-1}\right) \tag{9}$$

whose capacitance is given by

$$C_{dip} \sim \frac{2\pi\varepsilon_0 h}{\Omega_e} \tag{10}$$

where

$$\Omega_e = \Omega - 2\left(1 + \ln 2\right) \tag{11}$$

and the fatness parameter of the dipole of radius a is

$$\Omega = 2\ln\left(2h/a\right) \tag{12}$$

The resonant antenna has vanishing reactance

$$X_{in} = 0 \tag{13}$$

3.1.2 Inductive Antenna

In the case of an electrically small inductive loop antenna the open circuit voltage is

$$V_{oc} = A_r\mu_0\left(-i\omega\right)H_n \tag{14}$$

where H_n is the component of magnetic field through the loop and the radiation resistance is

$$R_{rad} \sim \frac{1}{6\pi}\eta_0\left(k^2 A_r\right)^2 = O\left(\omega^4\right) \tag{15}$$

where the loop area is A_r

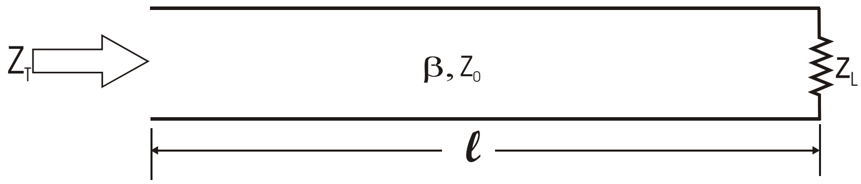

Figure 7. Transmission line characteristics with attached load.

$$A_r = \pi b^2 \text{ (circular loop of radius } b\text{)}$$

$$= s^2 \text{ (square loop of side length } s\text{)} \tag{16}$$

The input reactance is inductive

$$X_{in} \sim \omega L_{loop} = O(\omega) \tag{17}$$

where the inductance is [8], [9]

$$L_{loop} \sim \mu_0 b \left[\ln(8b/a) - 2\right] \text{ (circular loop)}$$

$$\sim \frac{\mu_0}{\pi} 2s \left[\ln(s/a) - 0.77401284\right] \text{ (square loop)} \tag{18}$$

3.1.3 Transmission Line And Load

The transmission line and load are shown in Figure 7. The susceptible device is usually taken to be a resistive load $Z_L = R_L$ with a relatively low value (1 ohm is typical). The connecting transmission line section of length ℓ, characteristic impedance Z_0, and transmission line wave number β, transforms the load impedance Z_L to the impedance looking into the transmission line [8]

$$Z_T = R_T - iX_T = Z_0 \left[\frac{Z_L \cos(\beta\ell) - iZ_0 \sin(\beta\ell)}{Z_0 \cos(\beta\ell) - iZ_L \sin(\beta\ell)}\right] \tag{19}$$

Because the transmission line characteristic impedance (100 ohms is typical) is generally much larger than the load impedance, this section of transmission line becomes an effective transformer (capable of transforming the load to much larger impedances) when the transmission line electrical length approaches a quarter wave

$$\beta\ell \approx \pi/2 \tag{20}$$

yielding the large value

$$Z_T \approx Z_0^2/Z_L \tag{21}$$

Detuning off this particular frequency will introduce reactive elements useful for matching and will eventually drop this value. Thus, this quarter wave criterion of the transmission line length can be taken to conservatively set the minimum matching frequency as low as possible

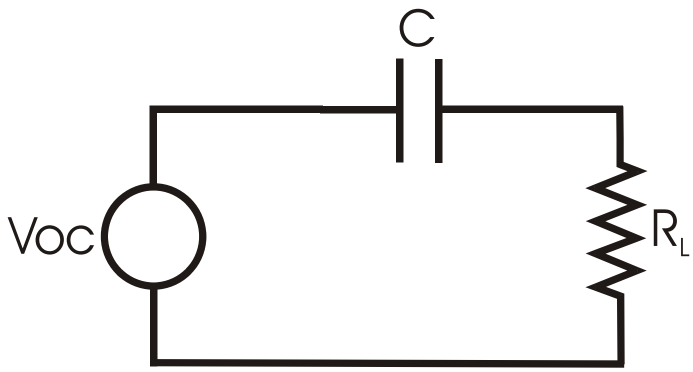

Figure 8. Equivalent circuit for the left-hand side of the V-Curve.

$$\omega = \omega_0 \tag{22}$$

for a given length of transmission line with known transmission line wavenumber; in other words it sets the frequency of the minimum field level of the V-Curve joining the left and right arms of the "V". The minimum matching frequency is related to β in Equation 20 by

$$\beta = \omega_0 \sqrt{\mu_r \varepsilon_r}/c \tag{23}$$

where μ_r and ε_r are the relative permeability and permittivity of insulation that forms the transmission line section of the cabling (these may be effective quantities if this region is inhomogeneous).

Note that for shorter antennas (below resonant) the real part of the antenna impedance (the radiation resistance) will already be smaller and could conceivably be of the same order as Z_L (or smaller than the load as in the inductive antenna below).

Conservation of power for a lossless transmission line means that the power delivered to the load is the same as that delivered to the input terminals of the transmission line section

$$P_L = P_T = \mathrm{Re}\left(Z_T\right)\left|\frac{V_{oc}}{Z_{in}+Z_T}\right|^2 = \frac{R_T\left|V_{oc}\right|^2}{\left(R_{in}+R_T\right)^2+\left(X_{in}+X_T\right)^2} \tag{24}$$

where V_{oc} is an RMS quantity.

3.2 Left Arm Of V-Curve

The left arm of the V-Curve assumes the transmission line is too short to accomplish matching.

3.2.1 Capacitive Antenna

The equivalent circuit in this case for the capacitive antenna is shown in Figure 8. Thus we have

$$P_L \sim R_L \left|h_e E_z/X_{in}\right|^2 \sim R_L \left|hE_z\right|^2 \omega^2 C_{dip}^2 \tag{25}$$

where we have assumed that the reactance of the antenna is much larger than R_L. We are neglecting the transmission line inductive reactance in series with the load in this circuit because of the low frequencies and high level of capacitive reactance of the antenna (the transmission line is responsible for matching to the right arm of the V-Curve, as discussed next). Note that we also define E_z in terms of its RMS value rather than its peak value. For a fixed value of P_L (typically 1 W) we see that the allowed electric field level (E_z) is inversely proportional to the frequency. Thus for simplicity as well as to insure continuity with the right arm of the curve (and because the reactive elements of the system are not precisely known) this is typically written in terms of the V-Curve minimum frequency as

$$P_L \sim (\omega/\omega_0)^2 A_0 |E_z|^2 / \eta_0 \tag{26}$$

where A_0 is effective area at the V-Curve minimum from the right arm description below.

3.2.2 Inductive Antenna

In the inductive antenna the capacitor of Figure 8 is replaced by an inductance $L_{loop} + L_{TL}$ (the transmission line also has a capacitive reactance across the load that we are ignoring)

$$X_T \sim \omega L_T \sim \omega L_{TL} \tag{27}$$

and in the lossless transmission line the line inductance is the inductance per unit length L times the length

$$L_{TL} = \ell L = \beta \ell Z_0 / \omega$$

and the power at the load is again that fed into the line

$$P_L = R_T \left| \frac{A_r \mu_0 (-i\omega) H_n}{Z_T + Z_{in}} \right|^2 \sim \frac{R_L}{R_L^2 + \omega^2 (L_{loop} + L_{TL})^2} |A_r \mu_0 \omega H_n|^2 \tag{28}$$

In the unmatched case if $\omega (L_{loop} + L_{TL}) >> R_L$, this power is initially constant in frequency, however as one moves to lower frequencies, we eventually have $\omega (L_{loop} + L_{TL}) << R_L$ and

$$P_L \sim \omega^2 A_r^2 |\mu_0 H_n|^2 / R_L = k^2 A_r^2 |\eta_0 H_n|^2 / R_L \tag{29}$$

We thus see again that the allowed field (in this case the magnetic field) is allowed to rise inversely with frequency to maintain the same limit on received power. At low frequencies the electric and magnetic fields are not necessarily connected by the free space impedance η_0. Nevertheless, to get a feel for how this inductive case compares with the capacitive case we associate $\eta_0 H_n$ with the V-Curve requirement on E_z and see that the power in the inductive case dominates the capacitive case as $(|\eta_0 H_n| A_r \eta_0 / R_L)^2 >> (|E_z| h C_{ant}/\varepsilon_0)^2 \sim \left(|E_z| 2\pi h^2/\Omega_e\right)^2$, since we expect that $\eta_0/R_L >> 1/\Omega_e$; the loop is thus more efficient at low frequencies.

We will compare in the next section how these low frequency results compare to the standard left arm of the V-Curve when they are extrapolated upward to the V-Curve minimum.

3.3 Right Arm of V-Curve

On the right arm of the V-Curve it is assumed that the transformer action of the connecting transmission line section matches the load to the antenna, where the real parts are as shown in Figure 9. Thus the transformed load is

$$Z_T = Z_{in}^* = R_{rad} + iX_{in} \tag{30}$$

3.3.1 Capacitive Antenna

This produces received power

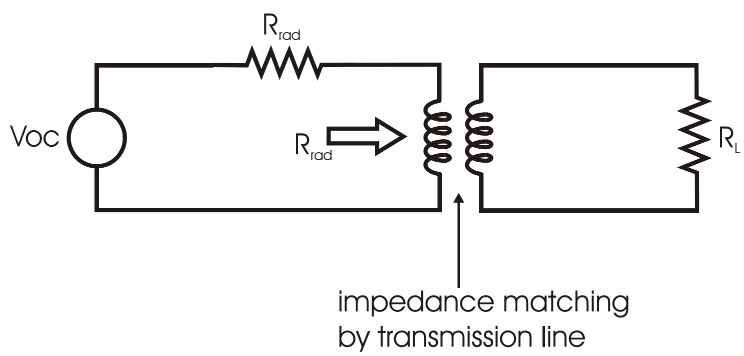

Figure 9. Equivalent circuit for the right-hand side of the V-Curve.

$$P_L = \frac{|V_{oc}|^2}{4R_{rad}} = \frac{|h_e E_z|^2}{4R_{rad}} \tag{31}$$

Noting that $R_{rad} = O\left(\omega^2\right)$ with $h_e \sim h$ for the short antenna, and that $h_e = O\left(\lambda/2\right) = O\left(1/\omega\right)$ with $R_{rad} \approx 73$ ohms for a resonant antenna, we see that for a fixed power level the allowed electric field is proportional to frequency. This can be rewritten in terms of the effective area A_e of the antenna as

$$P_L = A_e \left|E_z\right|^2 / \eta_0 \tag{32}$$

where (here we are assuming that the electric field polarization is aligned for maximal coupling)

$$A_e = \frac{|h_e|^2}{4R_{rad}} \eta_0 = \frac{\lambda^2}{4\pi} G \tag{33}$$

where G is the directivity gain of the antenna. Note that the right hand side of (33) is derived in [10] for an infinite space surrounding the antenna by a reciprocity argument. The value at the minimum $k_0 = 2\pi/\lambda_0 = \omega_0/c = 2\pi f_0/c$ is

$$A_0 = \pi G / k_0^2 \tag{34}$$

which is the quantity used in equation (26). The directivity gain G is 1.64 for a resonant antenna and is 1.5 for a short antenna.

It is instructive to ask, if we make the extrapolated low frequency result agree with the matched case at the V-Curve minimum ω_0

$$\frac{3}{2} \frac{\lambda_0^2}{4\pi} \left|E_z\right|^2 / \eta_0 = P_L \sim R_L \left|h E_z\right|^2 \omega_0^2 C_{dip}^2 \tag{35}$$

what is the required antenna dimension h^2

$$h^2 \left(\frac{2\pi}{\Omega_e}\right) \sim \sqrt{\frac{3\eta_0}{2\pi R_L}} \left(\frac{\lambda_0^2}{4\pi}\right) \tag{36}$$

As we see in the example to follow, the frequency at the minimum is low enough that this is a very large dipole antenna (for the larger load value $R_L = 4.5$ ohm and $f_0 = 8$ MHz it is $h^2 \left(2\pi/\Omega_e\right) \sim 708$ m^2), and hence the normal V-Curve definition will constitute an upper bound for typical capacitive antenna dimensions.

3.3.2 Inductive Antenna

For the small inductive antenna we obtain the same result (with $G = 1.5$ and $\eta_0 \left|H_n\right|^2$ the counterpart of $\left|E_z\right|^2 / \eta_0$)

$$P_L = \frac{|V_{oc}|^2}{4R_{rad}} = \frac{|A_r \mu_0 \omega H_n|^2}{4R_{rad}} = \frac{3}{2} \frac{\lambda^2}{4\pi} \eta_0 \left|H_n\right|^2 \tag{37}$$

Because the loop pickup at low frequencies is larger than the dipole pickup, it is important to compare the resulting levels with the extrapolation of this low frequency result toward the V-Curve minimum at ω_0

$$\frac{3}{2}\frac{\lambda_0^2}{4\pi}\eta_0\left|H_n\right|^2 = P_L \sim k_0^2 A_r^2 \left|\eta_0 H_n\right|^2 / R_L \tag{38}$$

which means that the loop area for these to match is

$$A_r \sim \sqrt{\frac{3R_L}{2\pi\eta_0}\frac{\lambda_0^2}{4\pi}} \tag{39}$$

As we see in the example to follow, the frequency at the minimum is low enough that this is a fairly large area loop (for the smaller load value $R_L = 1$ ohm and $f_0 = 8$ MHz it is $A_r \approx 4$ m^2), and hence the normal V-Curve definition (and implied magnetic field requirement) will constitute a bound able to accommodate inductive loops up to this size.

3.4 An Example V-Curve And Choice Of Minimum

So to summarize the V-Curve we first substitute and re-arrange equation (32) to obtain for the right hand side of the V-Curve

$$|E_z| = \sqrt{\frac{4\pi\eta_0}{c^2}}\sqrt{\frac{P_L}{G}}f \tag{40}$$

Re-arranging equation (26) we obtain for the left hand side of the V-Curve

$$|E_z| = \sqrt{\frac{4\pi\eta_0}{c^2}}\sqrt{\frac{P_L}{G}}\frac{f_0^2}{f} \tag{41}$$

Note from the definition of power used in this report that E_z is RMS field and not the peak field. At $f = f_0$, both sides of the V-Curve meet at the value

$$|E_z| = \sqrt{\frac{4\pi\eta_0}{c^2}}\sqrt{\frac{P_L}{G}}f_0 \tag{42}$$

where f_0 is given by the equation

$$f_0 \approx \frac{c}{4\ell\sqrt{\mu_r\varepsilon_r}} \tag{43}$$

In calculating the V-Curve in an unbounded environment we only need to know three quantities: the maximum power that is guaranteed not to damage or initiate the susceptible device (P_L), the directive gain of the attached conductors that could function as the antenna (G), the maximum electrical length of the attached conductors that could function as the matching transmission line (ℓ), which leads to the establishment of the V-Curve minimum frequency (ω_0). We then must keep the fields due to electromagnetic emitters below this limit set by the V-Curve.

Let us assume that the no-fire level of the susceptible device is $P_L = 45$ mW and that the antenna gain is that of a resonant half-wave dipole $(G = 1.64)$. We could then examine the electrical length of the longest cables attached to this device and also determine if they have the potential for being even longer due to touching other conductors in the operational area to set the minimum matching frequency f_0 (the bottom of the V). Because this frequency has traditionally been taken as ($f_0 = 8$ MHz), we instead work backward to examine the implied cable length. For an air line ($\mu_r = \varepsilon_r = 1$) equation (43) implies the longest attached cable is near 9.37 m in length. For a cable having insulation with ($\mu_r = 1, \varepsilon_r = 4$) the longest attached cable is half this length. Most cable insulation fall in this range of effective permittivities. For $f_0 = 8$ MHz the resulting V-Curve is shown in Figure 10.

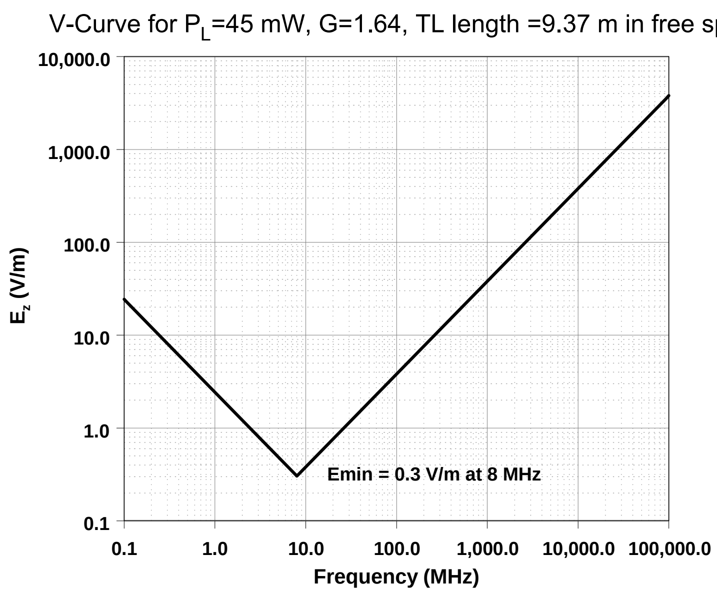

Figure 10. V-Curve associated with a 45 mW device assuming a half-wave dipole as a receiving antenna and $f_0 = 8$ MHz.

4 DIRECTIVITY OF ANTENNAS

This section considers practical antenna directivities exceeding the usual dipole level, arising from either ground planes in proximity to the receiver or receiving antennas in the form of long wire dipoles. These enhancements in antenna directivity gain, if included, would tend to reduce the allowed field levels associated with the standard V-Curve.

4.1 Ground Plane Directivity Enhancement

Taking into account the fact that the sensitive device and cabling may be in the presence of a conducting half-space such as a floor or ground if outside, this situation could be bounded by assuming that the antenna gain is that of a quarter-wave monopole ($G \rightarrow 2G = 3.28$) which would shift the field of the previous V-Curve down by a factor of $\sqrt{2}$, i.e. $E_{\min} = 0.212$ V/m at 8 MHz.

4.2 Long Wire Antennas At Grazing Incidence

The directivity gain G of long wire antennas is maximized for fields impinging near grazing incidence angles as demonstrated in Appendix B [3]. This reduces the allowed levels of field up on the right hand section of the V-Curve if such lengths are present. An expression for the directivity of a dipole antenna of length $2h$ that is simpler than that given by the Wiener-Hopf method in Appendix B is [11]

$$G = \frac{2F(\theta)\,|_{\max}}{D} \tag{44}$$

The denominator of the directivity expression is given by

$$\begin{aligned} D \quad = \quad & \gamma + \ln(2kh) + \mathrm{Ci}(2kh) + \frac{1}{2}\sin(2kh)\left[\mathrm{Si}(4kh) - 2\,\mathrm{Si}(2kh)\right] \\ & + \frac{1}{2}\cos(2kh)\left[\gamma + \ln(kh) + \mathrm{Ci}(4kh) - 2\,\mathrm{Ci}(2kh)\right] \end{aligned} \tag{45}$$

$\mathrm{Ci}(x)$ and $\mathrm{Si}(x)$ are the cosine and sine integrals given by

$$\mathrm{Ci}(x) = \int_{\infty}^{x} \frac{\cos(y)}{y}\,dy \tag{46}$$

and

$$\mathrm{Si}(x) = \int_{0}^{x} \frac{\sin(y)}{y}\,dy \tag{47}$$

and $\gamma = 0.5772$ is Euler's constant. The numerator of the directivity expression is given by

$$F(\theta) = \left[\frac{\cos(kh\cos\theta) - \cos(kh)}{\sin\theta}\right]^2 \tag{48}$$

where θ is the angle with respect to the antenna axis and $F(\theta)\,|_{\max}$ means we find the maximum value of this function. A first guess at the maximum of $F(\theta)$ for the standing wave antenna being considered here can be taken as

$$\theta_{\max} = \arccos\left(1 - \frac{\lambda}{4h}\right) \tag{49}$$

which is the angle of the major lobe for a traveling wave antenna. Note that dielectric (and other) losses in the connecting transmission line may become a mitigating factor in this high frequency region.

5 LOSS LIMITS ON MATCHING

The maximum transmission line length played a role above in setting the minimum frequency for which matching of the load was possible. However, the antenna dimensions were only used to discuss the low frequency behavior of the power and how this compared to the standard V-Curve. Nonetheless, the antenna dimensions do play a role in the issue of matching near the bottom of the V-Curve once inevitable losses are brought into the picture. This limitation to matching is an issue worth exploring since it is made even more difficult by cavity loading effects discussed later in this report (and hence it can help to mitigate effects resulting from the boundary, near the bottom of the V-Curve, when the antenna dimensions are limited).

5.1 Antenna Quality Factor

In a previous report [12], and later in an external publication [13], a limit on the quality factor of the matching network to the antenna was introduced. The idea was that as the frequency is reduced, the radiation resistance of the antenna rapidly decreases and hence the apparent antenna quality factor (input reactance over input resistance) rapidly increases, requiring the matching network to exhibit a very high quality factor (noting that for a conjugate match $X_T = -X_{in}$ and $R_T = R_{in} = R_{rad}$)

$$Q_{ant} = |X_{in}| / R_{rad} = Q_T \tag{50}$$

Then if we force a limit on the load quality factor

$$Q_T \leq Q_{\text{lim}} \tag{51}$$

a conjugate match is no longer possible below a frequency $\omega_m = 2\pi f_m$.

5.1.1 Capacitive Antenna

The required quality factor for matching here is

$$Q_{dip} = |X_{in}| / R_{rad} \sim \frac{1}{\omega C R_{rad}} \sim \frac{3\Omega_e}{k^3 h^3} = \frac{6\left[\ln\left(2h/a\right) - 1 - \ln 2\right]}{k^3 h^3} = O\left(\omega^{-3}\right) \tag{52}$$

5.1.2 Inductive Antenna

For the small inductive antenna or a loop

$$Q_{loop} = |X_{in}| / R_{rad} \sim \frac{\omega L_{loop}}{R_{rad}} \sim \frac{6\left[\ln\left(8b/a\right) - 2\right]}{\pi k^3 b^3} = O\left(\omega^{-3}\right) \text{ (circular loop)}$$

$$\sim \frac{12\left[\ln\left(s/a\right) - 0.77401284\right]}{k^3 s^3} = O\left(\omega^{-3}\right) \text{ (square loop)} \tag{53}$$

Both of these are similar to the capacitive antenna (the half length h is approximately replaced by $\pi^{1/3} b$ or by $s/2^{1/3}$).

5.2 Limiting Quality Factor Example

To choose the limiting quality factor we first imagine a transmission line having a large wire diameter $2a_{TL} = 5$ mm and a conductivity of copper $\sigma = 5.8 \times 10^7$ S/m, some height over a ground plane, with characteristic impedance $Z_0 \approx 100$ ohms, and propagation constant $\beta \approx 2k$ (index of refraction equal to two). The quality factor of a resonance (here we take the frequency to be $O\left(10 \text{ MHz}\right)$ since we are interested in frequencies near the bottom of the V-Curve)

$$Q_{TL} = \omega L/R \approx O\left(1000\right) \tag{54}$$

where for a low impedance load the line reactance per unit length is

$$\omega L = \beta Z_0 \tag{55}$$

$R_s = \sqrt{\omega\mu_0/\left(2\sigma\right)}$ is the surface resistance (here we assume the material is nonmagnetic) and we took the skin depth $\delta = \sqrt{2/\left(\omega\mu_0\sigma\right)}$ much smaller than the wire radius so that the resistance per unit length is

$$R \sim \frac{R_s}{2\pi a_{TL}} \tag{56}$$

From this example we take a limiting value on the transformed load quality factor typical of transmission line systems

$$Q_T \leq Q_{\lim} = 1000 \tag{57}$$

Suppose now we take the antenna dimensions to be of limited extent and inquire about the minimum possible matching frequency. For example, if the dipole antenna has length $2h \leq 1$ m we find (we will take $2a = 5$ mm and $\Omega_e \approx 8.6$)

$$Q_{dip} \sim \frac{3\Omega_e}{k^3 h^3} \leq Q_{\lim} \tag{58}$$

implies that $f \geq f_m = 28$ MHz.

For the magnetic antenna we take $2s \leq 1.25$ m (we again take $2a = 5$ mm)

$$Q_{loop} \sim \frac{12\left[\ln\left(s/a\right) - 0.77401284\right]}{k^3 s^3} \leq Q_{\lim} \tag{59}$$

and find that $f \geq f_m = 29$ MHz.

We see from these results that loss puts restrictions on the lowest frequency for a conjugate match when the antenna component of the receiving system has limited spatial extent. This can be helpful in raising the bottom of the V-Curve. We next examine what the loaded transmission line implies about Q_T.

5.2.1 Transmission Line Loss Example

Suppose we consider the limits on the value of

$$Q_T = \left|\text{Im}\left(Z_T\right)\right| / \text{Re}\left(Z_T\right) \tag{60}$$

The contributions to the real part come from both the transmission line losses as well as the load. Let us examine how large this quality factor can become and how it relates to these losses. Let us take the transmission line to be characterized by the usual parameters per unit length $Z = R - i\omega L, Y = G - i\omega C$ and write

$$\beta = \sqrt{-ZY} = \beta' + i\beta'' \approx \omega\sqrt{LC}\left(1 + iR/\left(2\omega L\right) + iG/\left(2\omega C\right)\right) \tag{61}$$

We presume that $\beta'' << \beta'$, and in addition that $\beta''\ell << 1$, so that

$$\cos\left(\beta\ell\right) \approx \cos\left(\beta'\ell\right) - i\beta''\ell\sin\left(\beta'\ell\right) \tag{62}$$

$$\sin\left(\beta\ell\right) \approx \sin\left(\beta'\ell\right) + i\beta''\ell\cos\left(\beta'\ell\right) \tag{63}$$

and that

$$Z_0 = \sqrt{Z/Y} = Z_0' + iZ_0'' \approx \sqrt{L/C}\left(1 + iR/\left(2\omega L\right) - iG/\left(2\omega C\right)\right) \tag{64}$$

Then we can write

$$Z_T = \left(Z_0' + iZ_0''\right)$$

$$\left[\frac{Z_L\left\{\cos\left(\beta'\ell\right) - i\beta''\ell\sin\left(\beta'\ell\right)\right\} - i\left(Z_0' + iZ_0''\right)\left\{\sin\left(\beta'\ell\right) + i\beta''\ell\cos\left(\beta'\ell\right)\right\}}{\left(Z_0' + iZ_0''\right)\left\{\cos\left(\beta'\ell\right) - i\beta''\ell\sin\left(\beta'\ell\right)\right\} - iZ_L\left\{\sin\left(\beta'\ell\right) + i\beta''\ell\cos\left(\beta'\ell\right)\right\}}\right] \tag{65}$$

Let us simplify the problem by ignoring dielectric losses $G = 0$. Then

$$\beta\ell \approx \omega\sqrt{LC}\ell\left(1 + iR/\left(2\omega L\right)\right) \approx \omega\sqrt{LC}\ell + iR\ell/\left(2\sqrt{L/C}\right) \approx \omega\sqrt{LC}\ell\left(1 + \frac{i}{2Q_{TL}}\right)$$

$$\approx \beta'\ell\left(1 + \frac{i}{2Q_{TL}}\right) \tag{66}$$

$$Z_0 \approx \sqrt{L/C}\left\{1 + iR/\left(2\omega L\right)\right\} \approx \sqrt{L/C}\left(1 + \frac{i}{2Q_{TL}}\right) \approx Z_0'\left(1 + \frac{i}{2Q_{TL}}\right) \tag{67}$$

and

$$Z_T = Z_0'\left(1 + \frac{i}{2Q_{TL}}\right)$$

$$\left[\frac{Z_L\left\{\cos\left(\beta'\ell\right) - i\frac{\beta'\ell}{2Q_{TL}}\sin\left(\beta'\ell\right)\right\} - iZ_0'\left(1 + \frac{i}{2Q_{TL}}\right)\left\{\sin\left(\beta'\ell\right) + i\frac{\beta'\ell}{2Q_{TL}}\cos\left(\beta'\ell\right)\right\}}{Z_0'\left(1 + \frac{i}{2Q_{TL}}\right)\left\{\cos\left(\beta'\ell\right) - i\frac{\beta'\ell}{2Q_{TL}}\sin\left(\beta'\ell\right)\right\} - iZ_L\left\{\sin\left(\beta'\ell\right) + i\frac{\beta'\ell}{2Q_{TL}}\cos\left(\beta'\ell\right)\right\}}\right] \tag{68}$$

In the case where we have a short circuit end condition $Z_L = 0$

$$Z_T = -iZ_0'\left(1+\frac{i}{2Q_{TL}}\right)\left[\frac{\sin\left(\beta'\ell\right)+i\frac{\beta'\ell}{2Q_{TL}}\cos\left(\beta'\ell\right)}{\cos\left(\beta'\ell\right)-i\frac{\beta'\ell}{2Q_{TL}}\sin\left(\beta'\ell\right)}\right]$$

$$= \frac{-iZ_0'}{\cos^2\left(\beta'\ell\right)+\left(\frac{\beta'\ell}{2Q_{TL}}\right)^2\sin^2\left(\beta'\ell\right)}\left(1+\frac{i}{2Q_{TL}}\right)\left[\sin\left(\beta'\ell\right)\cos\left(\beta'\ell\right)+i\frac{\beta'\ell}{2Q_{TL}}\right]$$

$$= \frac{Z_0'}{\cos^2\left(\beta'\ell\right)+\left(\frac{\beta'\ell}{2Q_{TL}}\right)^2\sin^2\left(\beta'\ell\right)}\left[-i\sin\left(\beta'\ell\right)\cos\left(\beta'\ell\right)+\frac{\beta'\ell+\sin\left(\beta'\ell\right)\cos\left(\beta'\ell\right)}{2Q_{TL}}+i\frac{\beta'\ell}{\left(2Q_{TL}\right)^2}\right] \tag{69}$$

We see in this case that the quality factor of Z_T is

$$Q_T = 2Q_{TL}\frac{\left|\sin\left(\beta'\ell\right)\cos\left(\beta'\ell\right)-\frac{\beta'\ell}{\left(2Q_{TL}\right)^2}\right|}{\beta'\ell+\sin\left(\beta'\ell\right)\cos\left(\beta'\ell\right)} \sim 2Q_{TL}\frac{\left|\sin\left(2\beta'\ell\right)\right|}{2\beta'\ell+\sin\left(2\beta'\ell\right)} \tag{70}$$

Finding the maximum of the function

$$\frac{d}{dx}\left(\frac{\sin x}{x+\sin x}\right) = \frac{x\cos x-\sin x}{\left(x+\sin x\right)^2} = 0 \tag{71}$$

gives

$$x = 0, 4.4935, ... \tag{72}$$

For $x \to 0$

$$\frac{\sin x}{x+\sin x} \to 1/2 \tag{73}$$

Thus the maxima are

$$Q_T \leq Q_{TL}, 0.555Q_{TL}, ... \tag{74}$$

In the case where we have an open circuit end condition $Z_L = \infty$

$$Z_T = iZ_0'\left(1+\frac{i}{2Q_{TL}}\right)\left[\frac{\cos\left(\beta'\ell\right)-i\frac{\beta'\ell}{2Q_{TL}}\sin\left(\beta'\ell\right)}{\sin\left(\beta'\ell\right)+i\frac{\beta'\ell}{2Q_{TL}}\cos\left(\beta'\ell\right)}\right]$$

$$= \frac{iZ_0'}{\sin^2\left(\beta'\ell\right)+\left(\frac{\beta'\ell}{2Q_{TL}}\right)^2\cos^2\left(\beta'\ell\right)}\left(1+\frac{i}{2Q_{TL}}\right)\left[\sin\left(\beta'\ell\right)\cos\left(\beta'\ell\right)-i\frac{\beta'\ell}{2Q_{TL}}\right]$$

$$= \frac{Z_0'}{\sin^2\left(\beta'\ell\right)+\left(\frac{\beta'\ell}{2Q_{TL}}\right)^2\cos^2\left(\beta'\ell\right)}\left[i\sin\left(\beta'\ell\right)\cos\left(\beta'\ell\right)+\frac{\beta'\ell-\sin\left(\beta'\ell\right)\cos\left(\beta'\ell\right)}{2Q_{TL}}+i\frac{\beta'\ell}{\left(2Q_{TL}\right)^2}\right] \tag{75}$$

We see in this case that the quality factor of Z_T is

$$Q_T = 2Q_{TL}\frac{\left|\sin\left(\beta'\ell\right)\cos\left(\beta'\ell\right)+\frac{\beta'\ell}{(2Q_{TL})^2}\right|}{\beta'\ell-\sin\left(\beta'\ell\right)\cos\left(\beta'\ell\right)} \sim 2Q_{TL}\frac{\left|\sin\left(2\beta'\ell\right)\right|}{2\beta'\ell-\sin\left(2\beta'\ell\right)} \tag{76}$$

Finding the maximum

$$\frac{d}{dx}\left(\frac{\sin x}{x-\sin x}\right) = \frac{x\cos x-\sin x}{\left(x-\sin x\right)^2} = 0 \tag{77}$$

gives the same second value of $x = 4.4935$, yielding $Q_T = 0.36Q_{TL}$. However, we see in this open circuited case that for $x \to 0$, $\sin x/\left(x-\sin x\right) \to 6/x^2$ and thus we obtain the expected result from the capacitance per unit length C of the open circuited transmission line

$$Q_T \to \frac{3}{\left(\beta'\ell\right)^2}Q_{TL} = \frac{1}{\omega C\ell R\ell/3} \to \infty \tag{78}$$

But in this limit we have an electrically short section of line and the actual load resistance cannot be ignored. The actual quality factor would become

$$Q_T \sim \omega L\ell/R_L \tag{79}$$

It seems reasonable therefore that a limit on the load quality factor can be set from losses and is close to what was taken in the preceding section.

5.2.2 Antenna Loss

The antenna also has associated metal losses. The input resistance will have the additive term

$$R_{dip} = \frac{2}{3}\frac{R_s}{2\pi a}h \tag{80}$$

$$R_{loop} = P\frac{R_s}{2\pi a} \tag{81}$$

where $P = 2\pi b$ or $4s$ is the loop perimeter. If the radiation resistance is suppressed, as discussed in the next section, these contributions may become important.

5.3 Continuation For Lower Frequencies

If only the reactive elements are taken to be matched at lower frequencies

$$X_T = -X_{in} \tag{82}$$

than this conjugate match limit ω_m, then the received power is

$$P_L = \frac{\left|V_{oc}\right|^2 R_T}{\left(R_T+R_{in}\right)^2} \tag{83}$$

Taking the input resistance to the antenna to be progressing toward small values at low frequencies, we replace the input resistance to the transmission line with the smallest value possible (this lower limit for the capacitive antenna leads to load powers that are decreasing for lower frequencies, but not for the inductive antenna, as discussed below)

$$R_T \geq |X_T| / Q_{\lim} = |X_{in}| / Q_{\lim} \tag{84}$$

Then

$$P_L = \frac{|V_{oc}|^2 |X_{in}| / Q_{\lim}}{\left(|X_{in}| / Q_{\lim} + R_{in}\right)^2} = \frac{4 |X_{in}| / Q_{\lim}}{\left(|X_{in}| / Q_{\lim} + R_{in}\right)^2} \left[R_{in}(\omega_m) P_L(\omega_m)\right] \tag{85}$$

where the load power at the minimum matching frequency is

$$P_L(\omega_m) = \frac{|V_{oc}|^2}{4 R_{in}(\omega_m)} \tag{86}$$

5.3.1 Capacitive

Now for the capacitive antenna in free space the minimum matching frequency is (where $R_{in} = R_{rad} = O\left(\omega^2\right)$)

$$\omega_m^3 = 1 / \left(Q_{\lim} C_{dip} R_{rad} / \omega^2\right) \tag{87}$$

and we can write the power

$$P_L / P_L(\omega_m) = \frac{4 / \left(\omega C_{dip} Q_{\lim}\right)}{\left[1 / \left(\omega C_{dip} Q_{\lim}\right) + R_{rad}\right]^2} \left[(\omega_m / \omega)^2 R_{rad}\right] = \frac{4 (\omega_m / \omega)^5}{\left[(\omega_m / \omega)^3 + 1\right]^2} \tag{88}$$

or

$$P_L / P_L(\omega_m) = f(\omega / \omega_m) \ , \ \omega < \omega_m \tag{89}$$

$$f(x) = \frac{4x}{\left(1 + x^2\right)^3} \tag{90}$$

which has a peak at $x_p = 5^{-1/3} \approx 0.585$ and peak value $f_p = 5^{5/3}/9 \approx 1.6$. Thus the allowed field is $3/5^{5/6} \approx 0.785$ of the point where matching is no longer possible. Note that this is shrinking only as $O(\omega)$ below the match point versus the usual $O\left(\omega^2\right)$ for the reactive mismatch of the left arm of the V-Curve. This behavior is illustrated qualitatively as the dashed curve labeled as $Q_{\lim}$ in Figure 2. Eventually for shorter line lengths we would find $R_T \geq R_L$, and the $O\left(\omega^2\right)$ behavior discussed previously. Nevertheless, it exhibits limits set by losses with respect to the matching criterion, near the bottom of the V-Curve. If the $R_{rad} \to R_{in}$ is made smaller, as in the case of a cavity, then this has an even greater effect.

5.3.2 Inductive

In the case of an inductive antenna (where $R_{in} = R_{rad} = O\left(\omega^4\right)$) the minimum matching frequency is

$$\omega_m^3 = L_{loop} / \left(Q_{\lim} R_{rad} / \omega^4\right) \tag{91}$$

and we find

$$P_L/P_L(\omega_m) = \frac{4\omega L_{loop}/Q_{\lim}}{\left[\omega L_{loop}/Q_{\lim} + R_{rad}\right]^2}\left[(\omega_m/\omega)^4 R_{rad}\right] = \frac{4(\omega_m/\omega)^7}{\left[(\omega_m/\omega)^3 + 1\right]^2} \tag{92}$$

or

$$P_L/P_L(\omega_m) = (\omega_m/\omega)^2 f(\omega/\omega_m)\ ,\ \omega < \omega_m \tag{93}$$

The power received continues to grow as $O(1/\omega)$ for frequencies below the match point ω_m, but at a rate that is reduced versus the typical growth on the right arm of the V-Curve $O\left(1/\omega^2\right)$. Furthermore, unlike the growing capacitive antenna reactance, the loop reactance diminishes as frequency is reduced and the expression (84) rapidly fails, so that we reach the limit

$$R_T = O(R_L) \tag{94}$$

sooner, below which we find the previous behavior (29).

The loss limits still reduce the coupled power near the bottom of the V-Curve, but not as dramatically as in the capacitive antenna. The change in characteristics between the two antennas is thus similar to the change associated with the standard V-Curve.

6 EFFECTS OF REGION BOUNDARY

Because the V-Curve is often applied to operations in rooms or enclosures, it is prudent to ask what effect this has on the prior unbounded model; the directivity gain enhancement associated with a ground plane in proximity, discussed in the preceding section, is an analogous boundary effect. The region boundaries mean that the receiver input impedance can be affected by reflections from the walls of the region; although the effective height of the antenna h_e can be modified as well by the cavity boundary, we will focus on a very short dipole receiver where we can neglect this effect. The antenna directivity gain is connected to these circuit quantities (33) and is thus being modified by the boundaries.

In addition, the field from the transmitter, whether outside or inside the bounded region will be modified relative to the unbounded case (the presence of a transmitter can also affect the room quality factor). In the spirit of the original V-Curve our focus will be on the receiver properties, and how they are affected by the boundary reflections. Hence we are continuing to place limits on the allowed field at the receiver. We will briefly consider the transmitter at the end of this section since the resonant effects can to some extent mitigate the changes in the receiver properties, but this is not the main focus.

The bounded region will be taken to have a quality factor (Q) and volume (V). We are examining the extension of the preceding model as the quality factor rises from small values to see when modifications must be included in the receiver model. The short dipole receiver behavior will be assessed by examining how the input impedance is affected by the cavity. For the matched case we write the received power from the circuit model as

$$P_L = \frac{|V_{oc}|^2}{4R_{in}} \sim \frac{|hE_z|^2}{4R_{in}} = \frac{|hE_z|^2}{4R_{rad}}\frac{1}{r_{in}}\ \text{, short dipole} \tag{95}$$

We begin by a general discussion of the cavity behavior. Next we examine two canonical geometries, spherical and rectangular cavities, where we focus on the fundamental cavity modes occurring down near the minimum of the V-Curve [5], but also touch on high frequency limits of the sphere. We then discuss these effects in more general cavities at higher frequencies.

6.1 Description of Frequency Regions

The cavity field can be thought of as having three frequency regions. The lowest modes constitute the fundamental mode region where the field is a standing wave that could, in principle, be accurately modeled if the geometry of the cavity boundary and contents are known and taken into account. The square of the field fluctuates in an ordered manner about a mean value with maxima, in three dimensions, reaching perhaps eight times the mean. As we proceed to higher-order modes, the complexity of practical cavities renders the field difficult to predict in a deterministic way (small perturbations change the field distribution and the mode is made up of many plane waves or rays). This region has been denoted as the undermoded region because it is still possible for the modes to be separate and discrete in frequency. Finally for very high frequencies the cavity becomes highly overmoded with many overlapping modes. Figures 11 and 12 illustrate the spectra in the undermoded and overmoded regions respectively. Statistical treatments of the field have been introduced at high frequencies. The parameter that describes the transition between under and over moding is [14]

$$\alpha_n = \frac{\pi}{2} \frac{\omega_n / Q_n}{\langle \Delta\omega_n \rangle} \sim \frac{k_n^3 V}{2\pi Q_n} \tag{96}$$

where ω_n is the radian frequency of a particular mode number n, $k_n = \omega_n / c$, the quality factor of the mode is Q_n (may depend somewhat on n), the 3 dB width of a mode is ω_n / Q, the cavity volume is V, and the mean modal spacing for high frequencies is [15]

$$\langle \Delta\omega_n \rangle = \omega_{n+1} - \omega_n \sim \pi^2 c^3 / \left(V \omega_n^2 \right) \ , \ \omega_n \to \infty \tag{97}$$

We define

$$\alpha = \frac{\pi}{2} \frac{\omega / Q}{\langle \Delta\omega \rangle} = \frac{k^3 V}{2\pi Q} \tag{98}$$

where for large n, the quality factor is assumed to be the mean value Q

$$Q \sim \frac{3k\eta_0 V}{4R_s S} \sim \frac{3}{2} \frac{V}{\delta S} \text{ (for nonmagnetic materials)} \tag{99}$$

where $\delta = \sqrt{2/(\omega\mu\sigma)}$ is the skin depth in the wall, σ is the wall conductivity, and the wall resistance per square is $R_s = 1/(\sigma\delta)$. Thus for $\alpha << 1$, the cavity is undermoded with separate and discrete spectra. Alternatively for $\alpha >> 1$, the cavity is overmoded with overlapping spectra. The transition where the modes begin to overlap is $\alpha = O(1)$. The input impedance of an antenna tends toward the fixed values of the unbounded region as $\alpha \to \infty$, whereas it fluctuates with position and frequency for $\alpha \to 0$.

As an example, for a cavity volume $V = 500$ m^3 and assumed quality factor $Q = 100$, we find $\alpha = 7.3$ at 100 MHz.

6.2 Sphere Cavity

The canonical problem of a short dipole at the center of a spherical cavity of radius b with wall impedance $Z_s = R_s (1 - i)$ can be easily solved [16], [4]. The result for the normalized input impedance is

$$r_{in} = \left(R_{in} - R_{dip} \right) / R_{rad} = \left(R_s / \eta_0 \right) / \left| D_{sp} \right|^2 \tag{100}$$

and

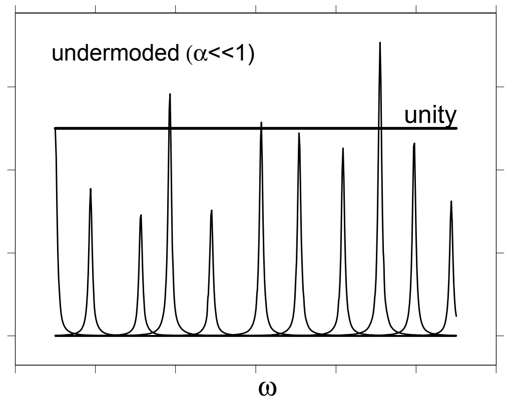

Figure 11. Illustration of separate discrete spectra in the undermoded limit.

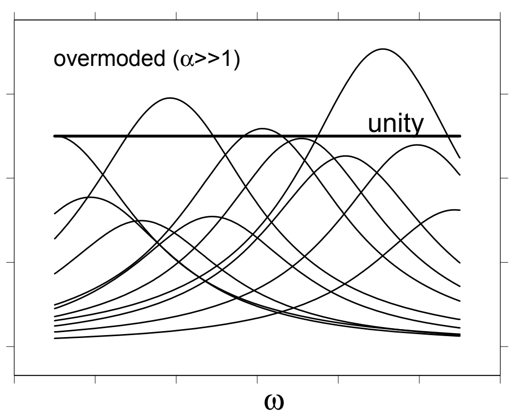

Figure 12. Illustration of overlapping spectra in the overmoded limit.

$$x_{in} = (X_{in} - X)/R_{rad} = \left[-\frac{1}{2}\left(1 - \frac{3}{k^2b^2} + \frac{1}{k^4b^4}\right)\sin(2kb) - \frac{1}{kb}\left(1 - \frac{1}{k^2b^2}\right)\cos(2kb) \right.$$

$$- (R_s/\eta_0)\left\{\left(1 - \frac{2}{k^2b^2}\right)\cos(2kb) - \frac{1}{kb}\left(2 - \frac{1}{k^2b^2}\right)\sin(2kb)\right\}$$

$$\left. + (R_s/\eta_0)^2\left\{\left(1 - \frac{1}{k^2b^2}\right)\sin(2kb) + \frac{2}{kb}\cos(2kb)\right\}\right] / |D_{sp}|^2 \quad (101)$$

where

$$D_{sp} = \left(1 - \frac{1}{k^2b^2}\right)\sin(kb) + \frac{1}{kb}\cos(kb) + i(Z_s/\eta_0)\left\{\cos(kb) - \frac{1}{kb}\sin(kb)\right\} \quad (102)$$

where R_{dip} is the ohmic loss of the antenna, $X \sim 1/(\omega C_{dip})$ is the local capacitive reactance of a short antenna given above, and R_{rad} is the radiation resistance of the short antenna.

6.2.1 High Frequency Region

Simplifying for $kb >> 1$ and taking the limiting cases we find [4]

$$r_{in} \sim R_s/\eta_0\,,\; kb \sim (n - 1/2)\pi \quad (103)$$

$$x_{in} \sim (-1)^{n-1}/(kb)\,,\; kb \sim (n - 1/2)\pi$$

$$r_{in} \sim \eta_0/R_s\,,\; kb \sim n\pi \quad (104)$$

$$x_{in} \sim \pm\eta_0/(2R_s)\,,\; kb \sim n\pi \quad (105)$$

the second set of two results being near resonance and the first two being between resonances, giving the overall range

$$R_s/\eta_0 < r_{in} < \eta_0/R_s \quad (106)$$

Note that the quality factor of the TM_{n01} mode is [8]

$$Q_n = \eta_0/(2R_s)\left[kb/\sin^2(kb) - 1/(kb) - kb\right]/(kb)^2 = [kb - 2/(kb)]\,\eta_0/(2R_s) \quad (107)$$

where the modes $k = k_n$ are the roots of

$$\left(1 - \frac{1}{k^2b^2}\right)\sin(kb) + \frac{1}{kb}\cos(kb) = 0 \quad (108)$$

or

$$\tan(kb) = kb/\left[1 - (kb)^2\right] \quad (109)$$

For large kb this becomes

$$Q_n \sim kb\eta_0/(2R_s) = (\mu_0/\mu)\,b/\delta = 3(\mu_0/\mu)\frac{V}{\delta S} \quad (110)$$

and thus the preceding result can be written for higher frequencies as

$$\frac{kb}{2Q_n} < r_{in} < \frac{2Q_n}{kb} \tag{111}$$

$$|x_{in}| < \frac{Q_n}{kb} \tag{112}$$

Unlike the general three-dimensional case introduced in the preceding section, the modal spacing in this one-dimensional resonant case is fixed in frequency $\Delta k = \Delta\omega/c \sim \pi/b$, and the parameter α in this case becomes

$$\alpha^{(1D)} = \frac{\pi}{2}\frac{\omega/Q}{\langle\Delta\omega\rangle} \sim \frac{kb}{2Q_n} \tag{113}$$

The power balance extremes, discussed in the high frequency section below, reproduce the results (111) if we take $M_0 = 1$ (and $\alpha^{(1D)} << 1$) giving $\alpha^{(1D)} < r_{in} < 1/\alpha^{(1D)}$. The reflected field in this case has near unit amplitude (this results in a two-to-one maximum to mean ratio of the standing wave field).

6.2.2 Fundamental Mode Region

It is important to examine the region near the first resonances of the cavity. The first resonance is at $(kb)_1 \approx 2.74370727$ and the denominator near resonance is minimized for small surface impedance

$$D_{sp} \sim i\left(R_s/\eta_0\right)\left\{\cos\left(kb\right) - \frac{1}{kb}\sin\left(kb\right)\right\} \approx -i1.0631\left(R_s/\eta_0\right)\ ,\ R_s/\eta_0 \to 0 \tag{114}$$

The input resistance then becomes

$$r_{in} = \left(R_s/\eta_0\right)/\left|D_{sp}\right|^2 \approx 0.8848\left(\eta_0/R_s\right) \tag{115}$$

which is only slightly less than the high frequency result (106). Noting that the quality factor is

$$Q_1 \approx 1.00738\left(\eta_0/R_s\right) \tag{116}$$

we can write this as

$$r_{in} < \frac{2.41Q_1}{(kb)_1} \tag{117}$$

which is slightly greater than the high frequency result in terms of the quality factor (111). The second resonance is near $(kb)_2 \approx 6.116764$ with quality factor $Q_2 \approx 2.8949\left(\eta_0/R_s\right)$, and the third is near $(kb)_3 \approx 9.316616$ with quality factor $Q_3 \approx 4.551\left(\eta_0/R_s\right)$.

For low frequencies $kb << 1$

$$D_{sp} \sim \frac{2}{3}kb - i\left(Z_s/\eta_0\right)\frac{1}{3}k^2b^2 \to \frac{2}{3}kb\ ,\ kb << 1, Z_s/\eta_0 << 1 \tag{118}$$

and

$$r_{in} \sim \left(R_s/\eta_0\right)/\left(\frac{2}{3}kb\right)^2 \approx \left[Q_1\left(\frac{2}{3}kb\right)^2\right]^{-1} > 2/Q_1\ ,\ kb << 1, Z_s/\eta_0 << 1 \tag{119}$$

$$x_{in} \sim \frac{1}{3}\left[\frac{2}{kb}+(R_s/\eta_0)-2kb\,(R_s/\eta_0)^2\right]/\left|D_{sp}\right|^2 \to \frac{1}{(kb)^2} > 1\ ,\ kb << 1, Z_s/\eta_0 << 1 \tag{120}$$

Locating the maxima of the first term of D_{sp} for $R_s/\eta_0 \to 0$ gives

$$\frac{\partial}{\partial x}\left[\left(1-\frac{1}{x^2}\right)\sin x+\frac{1}{x}\cos x\right]=\left(1-\frac{2}{x^2}\right)\left(\cos x-\frac{1}{x}\sin x\right)=0 \tag{121}$$

or

$$x=(kb)_{0n}=0,\sqrt{2},4.493409,7.725252,... \tag{122}$$

The minimum point (maximum of the denominator in r_{in}) is $(kb)_{01} \approx \sqrt{2}$, for which the denominator becomes

$$D_{sp} \approx \left[1-1/(kb)^2\right]\sin kb+\frac{\cos kb}{kb}$$

$$\approx \left[\sin\left(\sqrt{2}\right)+\sqrt{2}\cos\left(\sqrt{2}\right)\right]/2 \approx 0.60415\,,\ R_s/\eta_0 \to 0 \tag{123}$$

and

$$r_{in} \approx 2.73973\,(R_s/\eta_0) \tag{124}$$

The preceding high frequency limits still bracket the values at the first resonance although the minimum value (124) is more than two times larger than the high frequency range (106). The peak of the first terms of D_{sp} for $(kb)_{02} = 4.493409$ has the value -0.97612

$$r_{in} \approx 1.04953\,(R_s/\eta_0) \tag{125}$$

The peak of the first terms of D_{sp} for $(kb)_{03} = 7.725252$ has the value 0.991726

$$r_{in} \approx 1.001676\,(R_s/\eta_0) \tag{126}$$

We see from these that we are approaching the lower high frequency limit. Unlike full three-dimensional resonances this one-dimensional resonance has constant modal spacing and thus a fixed minimum r_{in} (for fixed R_s).

If we were to choose the sphere radius to have a volume of 500 m^3 we would arrive at $b \approx 4.9237$ m. This gives a first resonance near $f_1 = 26.6$ MHz, a minimum value at $f_{01} = 13.7$ MHz with value $r_{in} = 2.74\,(R_s/\eta_0)$, a second resonance at $f_2 = 59.3$ MHz, and a second minimum at $f_{02} = 43.6$ MHz with value $r_{in} = 1.05\,(R_s/\eta_0)$, a third resonance at $f_3 = 90.0$ MHz, and a third minimum at $f_{03} = 74.9$ MHz with value $r_{in} = R_s/\eta_0)$. We will compare these values with calculations for the rectangular cavity given in the next section. The main points of this section are that the reduction in the real part of the input resistance r_{in} of the dipole is bounded at the low frequencies and that for the one-dimensional resonances being examined this reduction in value persists to high frequencies.

6.3 Rectangular Cavity

The rectangular cavity conforms more to actual rooms encountered. The modes in a rectangular cavity with perfectly conducting walls are simple sinusoids. However, when lossy walls are introduced a perturbation approach is used to represent the vector potential as [17], [18], [19] (here we are approximately ignoring the modes which are TE with respect to the dipole direction even though the surface impedance of the walls will generate these)

$$\underline{A}(\underline{r}) = -\frac{1}{\varepsilon_0 V}\sum_n \frac{\underline{A}_n(\underline{r})\int_V \underline{A}_n(\underline{r}')\cdot\underline{J}(\underline{r}')\,dV'}{\omega^2\{1+(1+i)/Q_n\}-\omega_n^2} \tag{127}$$

$$\left(\nabla^2 + k_n^2\right)\underline{A}_n = 0\ ,\ \nabla\cdot\underline{A}_n = 0 \tag{128}$$

$$\frac{1}{V}\int_V \underline{A}_n\cdot\underline{A}_{n'}dV = \delta_{nn'} \tag{129}$$

and the quality factor is

$$Q_n = \frac{\omega\mu_0\int_V \underline{H}_n\cdot\underline{H}_n dV}{R_s\oint_S \underline{H}_n\cdot\underline{H}_n dS} \approx Q \tag{130}$$

$$\mu_0\underline{H}_n = \nabla\times\underline{A}_n \tag{131}$$

where $\delta_{nn'}$ is the Kronecker delta. Evaluation of this for a very short electric dipole with current distribution

$$\underline{J}(\underline{r}) = I_1(0)\left(1-|z-z_1|/h_1\right)\delta(x-x_1)\,\delta(y-y_1)\,\underline{e}_z \tag{132}$$

gives

$$\underline{A}(\underline{r}) \sim -\frac{I_1(0)\,h_1}{\varepsilon_0 V}\sum_n \frac{\underline{A}_n(\underline{r})\,A_{nz}(\underline{r}_1)}{\omega^2\{1+(1+i)/Q_n\}-\omega_n^2} \tag{133}$$

The open circuit voltage on a second antenna is [6]

$$V_{oc} = -\frac{1}{I_2(0)}\int_V \underline{E}_1\cdot\underline{J}_2 dV \tag{134}$$

where the subscript 1 indicates the field due to the first antenna and the subscript 2 indicates the transmitter current due to the second antenna. The electric field in general is

$$\underline{E} = -\nabla\phi + i\omega\underline{A} \tag{135}$$

where the scalar potential in the Coulomb gauge satisfies Poisson's equation in the cavity and

$$\underline{n}\times\underline{E} = 0 \text{ on the walls} \tag{136}$$

Thus taking the second antenna to also be z directed

$$V_{oc} \sim \frac{I_1(0)}{-i\omega C_{12}} + \frac{i\omega I_1(0)\,h_1 h_2}{\varepsilon_0 V}\sum_n \frac{A_{nz}(\underline{r}_2)\,A_{nz}(\underline{r}_1)}{\omega^2\{1+(1+i)/Q_n\}-\omega_n^2} \tag{137}$$

where C_{12} is the mutual capacitance between the antennas arising from the scalar potential term. For simplicity we take the scalar potential to be the same as the value without the cavity (assuming the cavity walls are not near the antennas).

Now if we take the antennas to be identical $h_1 \to h_2 = h$, divide by $I_1(0) = I(0)$, and take the real part, while evaluating for $\underline{r}_2 \to \underline{r}_1 = \underline{r}_0$, we obtain the real part of the input impedance (the imaginary part will lead to divergence for an infinitesimal dipole source)

$$r_{in} = R_{in}/R_{rad} \sim \frac{2\pi}{k^3 V} \sum_n \frac{\left(\omega^4/Q_n\right) 3A_{nz}^2\left(\underline{r}_0\right)}{\left|\omega^2\left\{1 + (1+i)/Q_n\right\} - \omega_n^2\right|^2} \tag{138}$$

For the rectangular cavity with dimensions a_0, b_0, c_0 the eigenfunctions are simple sines and cosines, and we write the normalization condition in the indices n, j, m as

$$\int_V \underline{A}_{njm}(x,y,z) \cdot \underline{A}_{n'j'm'}(x,y,z)\, dxdydz = a_0 b_0 c_0 \delta_{nn'} \delta_{jj'} \delta_{mm'} \tag{139}$$

Thus we have the z component

$$A_{njmz} = \sqrt{8/(1+\delta_{m0})} \sqrt{1 - \left(m\pi/\left(c_0 k_{njm}\right)\right)^2} \sin(n\pi x/a_0) \sin(j\pi y/b_0) \cos(m\pi z/c_0) \tag{140}$$

and magnetic field

$$\mu_0 \underline{H}_{njm} \approx \frac{\sqrt{8/(1+\delta_{m0})}}{\sqrt{1 - \left(m\pi/\left(c_0 k_{njm}\right)\right)^2}}$$

$$\left\{\underline{e}_x (j\pi/b_0) \sin(n\pi x/a_0) \cos(j\pi y/b_0) - \underline{e}_y (n\pi/a_0) \cos(n\pi x/a_0) \sin(j\pi y/b_0)\right\}$$

$$\sin(n\pi x_0/a_0) \sin(j\pi y_0/b_0) \cos(m\pi z/c_0) \cos(m\pi z_0/c_0) \tag{141}$$

with eigenfrequencies

$$k_{njm}^2 = \omega_{njm}^2/c^2 = (n\pi/a_0)^2 + (j\pi/b_0)^2 + (m\pi/c_0)^2 \tag{142}$$

and quality factors

$$Q_{njm} = \frac{1}{4}\left(\frac{\eta_0}{R_s}\right) k \left[\frac{(j/b_0)^2 + (n/a_0)^2}{(j/b_0)^2 \left(1/b_0 + 1/\left((1+\delta_{m0}) c_0\right)\right) + (n/a_0)^2 \left(1/a_0 + 1/\left((1+\delta_{m0}) c_0\right)\right)}\right] \tag{143}$$

The normalized input resistance is

$$r_{in} \sim \frac{6\pi}{k^3 V} \sum_{n=1}^{\infty} \sum_{j=1}^{\infty} \sum_{m=0}^{\infty} \frac{\left(\omega^4/Q_{njm}\right)\left[1 - \left(m\pi/\left(c_0 k_{njm}\right)\right)^2\right]}{\left|\omega^2\left\{1 + (1+i)/Q_{njm}\right\} - \omega_{njm}^2\right|^2}$$

$$\frac{8}{1+\delta_{m0}} \sin^2(n\pi x_0/a_0) \sin^2(j\pi y_0/b_0) \cos^2(m\pi z_0/c_0) \tag{144}$$

We see that this rectangular result has the same form as that given previously in the general case (138). However, because the antenna only excites TM modes with respect to the z direction, and the TE modes are missing from the problem (in the exact solution they are generated by the small wall impedance and could be significant near the resonances of these modes), the modal spacing is twice the average value given previously for the general cavity. Let us define

$$\alpha^{(TM)} = \frac{\pi}{2}\frac{\omega/Q}{\langle\Delta\omega\rangle} \sim \frac{k^3 V}{4\pi Q_{njm}} \tag{145}$$

If the observation position is taken to be a position of symmetry in this rectangular cavity (such as the cavity center) then many additional modes are eliminated in the expansion, and the effective value of $\alpha^{(TM)}$ is decreased further, suppressing the values of r_{in}.

A representative set of dimensions giving $V = 500\ \mathrm{m}^3$ is $a_0 = 8.5$ m, $b_0 = 6$ m, and $c_0 = 9.8$ m ($S = 386.2\ \mathrm{m}^2$). Note that

$$Q_{110} = \left(\frac{3k\eta_0 V}{4R_s S}\right)\frac{2}{3}\left[\frac{(a_0 b_0 + a_0 c_0 + b_0 c_0)\left(b_0^2 + a_0^2\right)}{a_0^3\,(c_0 + b_0/2) + b_0^3\,(c_0 + a_0/2)}\right] \approx 1.279Q \tag{146}$$

where Q is the simple formula above (99). Suppose we consider an observation frequency $f = 10$ MHz, which is below the first resonance $f_{110} = 30.6$ MHz. Keeping only the first mode at the cavity center gives

$$r_{in} \approx \frac{24\pi/Q_{110}}{k^3 V}\frac{\omega^4}{\left(\omega^2 - \omega_{110}^2\right)^2} \approx \frac{2c^4 S\,(R_s/\eta_0)}{1.279\pi^3 V^2\left(f^2 - f_{110}^2\right)^2} \approx 0.9\,(R_s/\eta_0) \tag{147}$$

This form is similar to the sphere result (124).

The quality factor in the preceding expansion was determined using a single cavity mode. Because the modes are not, in general, orthogonal on the surface of the cavity [17], it is more accurate (particularly observing between modes at low frequencies) to find the input resistance by integration of the square of the magnetic field over the surface (between modes we can simplify the expression by dropping the quality factor terms)

$$P_{in} = R_{in}\,|I(0)|^2 = r_{in} R_{rad}\,|I(0)|^2 = R_s \oint_S |\underline{H}|^2\,dS$$

$$\approx \frac{24\pi}{k^4 V}\,(R_s/\eta_0)\,R_{rad}\,|I(0)|^2 \sum_{n=1}^{\infty}\sum_{j=1}^{\infty}\sum_{m=0}^{\infty} \frac{\omega^2 2/(1+\delta_{m0})}{\omega^2\left\{1 + (1+i)/Q_{njm}\right\} - \omega_{njm}^2} S_{njm} \tag{148}$$

where

$$S_{njm} = \sum_{m'=0}^{\infty} \frac{2}{c_0\,(1+\delta_{m'0})} \frac{\left\{\left(\frac{j\pi}{b_0}\right)^2 + \left(\frac{n\pi}{a_0}\right)^2\right\}\left\{1 + (-1)^{m+m'}\right\}}{k^2\left\{1 + (1-i)/Q_{njm'}\right\} - k_{njm'}^2}$$

$$\sin^2(n\pi x_0/a_0)\sin^2(j\pi y_0/b_0)\cos(m\pi z_0/c_0)\cos(m'\pi z_0/c_0)$$

$$+\sum_{j'=1}^{\infty} \frac{2}{b_0} \frac{\left(\frac{j\pi}{b_0}\right)\left(\frac{j'\pi}{b_0}\right)\left\{1 + (-1)^{j+j'}\right\}}{k^2\left\{1 + (1-i)/Q_{nj'm}\right\} - k_{nj'm}^2}$$

$$\sin^2(n\pi x_0/a_0)\sin(j\pi y_0/b_0)\sin(j'\pi y_0/b_0)\cos^2(m\pi z_0/c_0)$$

$$+\sum_{n'=1}^{\infty}\frac{2}{a_0}\frac{\left(\frac{n\pi}{a_0}\right)\left(\frac{n'\pi}{a_0}\right)\left\{1+(-1)^{n+n'}\right\}}{k^2\{1+(1-i)/Q_{n'jm}\}-k_{n'jm}^2}$$

$$\sin(n\pi x_0/a_0)\sin(n'\pi x_0/a_0)\sin^2(j\pi y_0/b_0)\cos^2(m\pi z_0/c_0) \tag{149}$$

This is the quantity reported in the table below (the previous results are reported in parentheses).

6.4 Numerical Simulation Of Rectangular Cavity

Numerical simulations were also performed on the rectangular cavity. In this subsection we will compare the value of r_{in} obtained analytically using equation (148) (and (144)) to that obtained numerically using the boundary element code EIGER for an example rectangular cavity filled with free-space and again dimensioned $a_0 = 8.5$ m by $b_0 = 6.0$ m by $c_0 = 9.8$ m. We will examine r_{in} at 10 MHz, a frequency that is below the lowest fundamental mode of this cavity and near the minimum frequency of the V-Curve. The lowest fundamental modes of a PEC cavity with these dimensions occur at 23.34 MHz (TE_{101}), 23.29 MHz (TE_{011}), and 30.58 MHz (TM_{110}) where we are designating modes that are transverse electric (TE) or transverse magnetic (TM) to the $\hat{z}$ direction. The dominant modes that are excited by the dipole are TM_{dip}, where the subscript is the direction of the dipole, which will be oriented either in $\hat{y}$ (b_0) or $\hat{z}$ (c_0) directions. In the simulation we calculate r_{in} for a PEC dipole antenna dimensioned $h = 0.1$ m and $a = 1$ mm and positioned at the center of the cavity with the two orientations. For convenience we have taken $\sigma = 1$ S/m (the results scale as $Q, 1/r_{in} \propto \sqrt{\sigma}$ for higher conductivities). We grid the walls of the cavity with square elements 50 cm on a side (~ 20 unknowns/wavelength at 30 MHz) and the dipole with two linear elements. The unknowns on the elements are linear, edge-based functions. The results are summarized in the table below. The last column gives r_{in} for a spherically shaped cavity (124), where the frequency is taken at the first sphere minimum 13.7 MHz.

The analytic rectangular and numerical results are similar to each other, errors may be due to some of the approximations mentioned previously. Since the $\hat{z}$ oriented antenna does not itself generate the TE to $\hat{z}$ modes, we expect r_{in} for this orientation to be smaller than for the $\hat{y}$ orientation and we see from the table that this is indeed the case. Numerical results indicate that r_{in} is smallest in the center of the cavity and increases as the antenna moves closer to the walls. This seems reasonable both because loss of the cavity should increase as the current flowing on the wall being approached becomes larger to fulfill the wall's boundary condition, and the fact that moving off the center symmetry location brings more modes into play. The fact that the analytical approach and numerical approach are similar in the center of the cavity where the conditions are worst-case give us some confidence in the results.

Next we examine r_{in} between resonances. A $\hat{z}$ directed dipole in the center of the rectangular cavity will excite the TM_{110} at 30.58 MHz and TM_{112} at 43.25 MHz (the TM_{111} mode at 34.20 MHz is not excited because E_z has odd symmetry about the cavity center). For the $\hat{y}$ directed, centered dipole the TE_{101} mode at 23.34 MHz and the TE_{103} mode at 49.16 MHz are excited. We will take 37 MHz as the approximate midpoint between the TM_{110} and TM_{112} resonances and between the TE_{101} and TE_{103} resonances. The results are shown in the following table (the sphere results were evaluated at the second minimum 43.6 MHz). Unlike the previous table, in this case the $\hat{y}$ directed dipole has a smaller value of r_{in} than the $\hat{z}$ directed dipole. This is because the modes excited by the $\hat{y}$ dipole are further away in frequency from the chosen center point of 37 MHz than the modes excited by the $\hat{z}$ dipole.

Next we examine r_{in} between the next higher-order resonances. For a $\hat{y}$ directed, centered dipole, the

TE_{103} mode at 49.16 MHz and the TE_{121} mode at 55.15 MHz are excited. We will take 52.1 MHz as the approximate midpoint between the two resonances for this polarization. A $\widehat{z}$ directed dipole in the center of the rectangular cavity will excite the TM_{112} at 43.25 MHz and the TM_{310} at 58.51 MHz. We chose the frequency 50.9 MHz as the midpoint between these two resonances. The results are shown in the following table (the sphere results are at the third minimum 74.9 MHz).

Frequency (MHz)	Orientation	Q	Analytic r_{in}	Numerical r_{in}	Spherical r_{in}
10	$\widehat{y}$	12	0.17 (0.064)	0.15	0.053
10	$\widehat{z}$	12	0.089 (0.028)	0.062	0.053
37	$\widehat{y}$	23	0.065 (0.076)	0.061	0.037
37	$\widehat{z}$	23	0.27 (0.24)	0.27	0.037
52.1	$\widehat{y}$	28	0.75 (0.77)	0.74	0.046
50.9	$\widehat{z}$	28	0.11 (0.13)	0.10	0.046

Summarizing the preceding table: we see at 10 MHz that a factor of $r_{in} = 0.06$ reduction in input resistance is possible for $Q \approx 12$ (the results scale as $Q, 1/r_{in} \propto \sqrt{\sigma}$ for higher conductivities); at 37 MHz we observe a $r_{in} = 0.06$ reduction in input resistance possible for $Q \approx 23$ ($\alpha \approx 1.61$); and at 51 MHz a reduction in input resistance $r_{in} = 0.1$ for $Q \approx 28$ ($\alpha \approx 3.46$).

6.4.1 Alternative Form Of Modal Expansion

An alternative form for the modal expansion

$$\underline{A}(\underline{r}) = -\frac{1}{\varepsilon_0 V} \sum_n \frac{\underline{A}_n(\underline{r}) \int_V \underline{A}_n(\underline{r}') \cdot \underline{J}(\underline{r}')\, dV'}{\omega^2 + \omega\omega_n (1+i)/Q_n - \omega_n^2} \tag{150}$$

with the quality factor at the n^{th} mode defined by

$$Q_n = \frac{\omega_n \mu_0 \int_V \underline{H}_n \cdot \underline{H}_n dV}{R_{sn} \oint_S \underline{H}_n \cdot \underline{H}_n dS} \tag{151}$$

where the surface impedance is now calculated at the modal resonant frequency

$$R_{sn} = \sqrt{\omega_n \mu_0 / (2\sigma)} \tag{152}$$

is sometimes used. Because of the cancellation of ω_n in the denominator (150) and in the new definition of Q_n (151), the net effect is the replacement of R_s, evaluated at the operating frequency ω, in the formula for Q_n (130) and (143) by $R_{sn} = \sqrt{\omega_n \mu_0 / (2\sigma)}$, evaluated at the resonant frequency ω_n. The received voltage and input resistance are then

$$V_{oc} \sim \frac{I_1(0)}{-i\omega C_{12}} + \frac{i\omega I_1(0) h_1 h_2}{\varepsilon_0 V} \sum_n \frac{A_{nz}(\underline{r}_2) A_{nz}(\underline{r}_1)}{\omega^2 + \omega\omega_n (1+i)/Q_n - \omega_n^2}$$

$$r_{in} = R_{in}/R_{rad} \sim \frac{2\pi}{k^3 V} \sum_n \frac{(\omega^3 \omega_n / Q_n)\, 3A_{nz}^2(\underline{r}_0)}{|\omega^2 + \omega\omega_n (1+i)/Q_n - \omega_n^2|^2}$$

The results in this case for the rectangular cavity with $R_{snjm} = \sqrt{\omega_{njm} \mu_0 / (2\sigma)}$, can then be written as

$$r_{in} \sim \frac{6\pi}{k^3 V} \sum_{n=1}^{\infty} \sum_{j=1}^{\infty} \sum_{m=0}^{\infty} \frac{\left(\omega^3 \omega_{njm}/Q_{njm}\right)\left[1-\left(m\pi/\left(c_0 k_{njm}\right)\right)^2\right]}{\left|\omega^2+\omega\omega_{njm}\left(1+i\right)/Q_{njm}-\omega_{njm}^2\right|^2}$$

$$\frac{8}{1+\delta_{m0}} \sin^2\left(n\pi x_0/a_0\right)\sin^2\left(j\pi y_0/b_0\right)\cos^2\left(m\pi z_0/c_0\right) \tag{153}$$

with modal quality factors

$$Q_{njm} = \frac{1}{4}\left(\frac{\eta_0}{R_{snjm}}\right) k_{njm} \left[\frac{\left(j/b_0\right)^2+\left(n/a_0\right)^2}{\left(j/b_0\right)^2\left(1/b_0+1/\left(\left(1+\delta_{m0}\right)c_0\right)\right)+\left(n/a_0\right)^2\left(1/a_0+1/\left(\left(1+\delta_{m0}\right)c_0\right)\right)}\right] \tag{154}$$

If this approach is adopted then the values in parenthesis of the table are changed to (0.13), (0.076), (0.10), (0.27), (0.81), and (0.15); the first two 10 MHz results are thus significantly improved versus the values from the original form of the modal expansion (although there is some corresponding degradation in accuracy for higher frequencies). For nondispersive wall surface impedances (R_s not dependent on frequency), either of the two preceding forms of the modal expansion gives the same result. The preceding exact solution of the spherical cavity can be used to develop insight as to the best form of the modal expansion to use for dispersive wall surface impedances; however, even though the resulting residues forming the modal expansion would lead to an evaluation of the surface impedance at the resonant frequencies R_{sn} rather than R_s, there are additional contributions from branch cut integrals arising form the dispersive wall impedance.

6.5 High Frequency Cavities

At high frequencies the antenna input impedance takes on a stochastic character dependent on frequency, location, shape and properties of the cavity [14], [20].

6.5.1 Modal Statistics In High Q Cavity

The cavity eigenvalues (resonant frequencies) ω_n have spacings that can be described by a slowly varying mean $\langle\Delta\omega_n\rangle$ given previously times a random variable s_n

$$\Delta\omega_n = \omega_{n+1} - \omega_n = \langle\Delta\omega_n\rangle s_n \tag{155}$$

The probability density function for the normalized spacing s_n is Poisson (exponential) when the cavity geometry is simple (for example, separable cases where eigenvalue degeneracy occurs frequently) [21], [22]

$$f_{s_n}^P\left(s_n\right) = e^{-s_n}\,,\ 0 < s_n < \infty \tag{156}$$

and is Rayleigh (Wigner) when the cavity is complex [21], [22]

$$f_{s_n}^W\left(s_n\right) = \frac{\pi}{2} s_n e^{-s_n^2\pi/4}\,,\ 0 < s_n < \infty \tag{157}$$

Complex geometry is typical of electromagnetic compatibility applications and thus the Rayleigh spacing is more frequently encountered.

The cavity eigenfunctions are taken to be made up of a random collection of plane waves and modeled by (all three components have similar statistics) a normal density [23], [21]

$$\zeta = \sqrt{3} A_{nz} \tag{158}$$

$$f_\zeta(\zeta) = \frac{1}{\sqrt{2\pi}} e^{-\zeta^2/2} \tag{159}$$

which follows the chosen normalization [23]

$$3 \int_{-\infty}^{\infty} A_{nz}^2 f_{A_{nz}}(A_{nz})\, dA_{nz} = \int_{-\infty}^{\infty} \zeta^2 f_\zeta(\zeta)\, d\zeta = 1 \tag{160}$$

The normalization is assumed to be the same throughout the cavity (homogeneity). Cavities can exhibit deviations from this simple density (the modal spacings can also deviate) due to periodic ray trajectories [21], [24], [25], [26], as well as proximity to the source (of course in low quality factor situations we would also expect field inhomogeneity).

The correlation function for the modal components is different from that for scalar modes [21] and is given by [27], [28]

$$\rho_z^n(\underline{r}_1, \underline{r}_2) = \frac{\langle A_{nz}(\underline{r}_1) A_{nz}(\underline{r}_2) \rangle}{\sqrt{\langle A_{nz}^2(\underline{r}_1) \rangle \langle A_{nz}^2(\underline{r}_2) \rangle}} \sim \frac{3}{2} \left(1 + \frac{1}{k_n^2} \frac{\partial^2}{\partial z_1^2} \right) \frac{\sin[k_n |\underline{r}_1 - \underline{r}_2|]}{k_n |\underline{r}_1 - \underline{r}_2|} \tag{161}$$

where the asymptotic symbol indicates the high-order modes.

Monte Carlo simulations can be used to determine properties of the input impedance [14], [20].

6.5.2 Power Balance Fit

To get a handle on the variability of the real part of the input impedance at high frequencies we make use of a simple power balance approach coupled with a statistical fit for the underlying reflected field from the wall. Defining the normalized impedance as [14]

$$z_{in} = (Z_{in} - X - R_{dip}) / R_{rad} = r_{in} - i x_{in} \tag{162}$$

These normalized quantities obey the equations

$$\tau = -\frac{\mathrm{Re}\left(E_z^{ref}\right)}{\sqrt{\left\langle |E_z|^2 \right\rangle_V}} = (r_{in} - 1) / \sqrt{r_{in}/\alpha} \tag{163}$$

$$\zeta = \frac{\mathrm{Im}\left(E_z^{ref}\right)}{\sqrt{\left\langle |E_z|^2 \right\rangle_V}} = x_{in} / \sqrt{r_{in}/\alpha} \tag{164}$$

where E_z^{ref} is the field at the antenna that has been reflected by the cavity boundary and

$$\left\langle |E_z|^2 \right\rangle_V = (1/V) \int_V |E_z|^2\, dV \tag{165}$$

is the volumetric mean of the square of the field. These two quantities, τ and ζ, represent the normalized reflected field from the boundary and are random variables at high frequencies. The exact probability density functions are very complicated, but a simple fit is given by by the simple Gaussian density [29]

$$f(\zeta) = \frac{1}{\sqrt{2\pi\sigma_r^2}} e^{-\zeta^2/\left(2\sigma_r^2\right)}, \; -\infty < \zeta < \infty \tag{166}$$

and the asymmetrical Gaussian density

$$f(\tau) = \frac{1}{\sqrt{2\pi\sigma_r^2}} \left[1 - \frac{\tau}{\sqrt{\tau^2 + 4\alpha}}\right] e^{-\tau^2/\left(2\sigma_r^2\right)}, \; -\infty < \tau < \infty \tag{167}$$

which accounts for the fact that when the cavity is highly undermoded $\alpha << 1$ the normalized reflected field only has a positive real part near the modal peaks with resulting probability $O(\alpha)$; it also accounts for the highly overmoded limit $\alpha >> 1$ where the modes are overlapping and thus the density function becomes a symmetrical Gaussian. Substitution of the relation between τ and r_{in} gives a density function for r_{in}. To obtain values for x_{in} we can invert the quadratic equation to obtain

$$r_{in} = \left(\sqrt{\tau^2 + 4\alpha} + \tau\right)^2 / (4\alpha) \tag{168}$$

and

$$x_{in} = \zeta \frac{1}{2\alpha} \left(\sqrt{\tau^2 + 4\alpha} + \tau\right) \tag{169}$$

The density for the normalized real input impedance is then

$$f(r_{in}) = \frac{1}{r_{in}\sqrt{2\pi r_{in}\sigma_r^2/\alpha}} e^{-\alpha(r_{in}-1)^2/\left(2\sigma_r^2 r_{in}\right)} \tag{170}$$

In the overmoded limit $\alpha \to \infty$ both distributions become Gaussian

$$f(r_{in}) \sim \frac{1}{\sqrt{2\pi/\alpha}} e^{-\alpha(r_{in}-1)^2/2} \tag{171}$$

$$f(x_{in}) \sim \frac{1}{\sqrt{2\pi/\alpha}} e^{-\alpha x_{in}^2/2} \tag{172}$$

The approximate fit given in [29]

$$\sigma_r^2 = \arctan\left(1/\sqrt{4\alpha}\right) + 1/\left(1 + 1/\sqrt{4\alpha}\right) \tag{173}$$

can be used for the variance. More exact results for this quantity can be found in [20].

6.5.3 Extreme Values

The impedance variations in the cavity can be bounded in a practical sense by taking extreme values for the normalized reflected field statistics [14]. It is somewhat standard practice to take the three standard deviation point of a Gaussian density

$$|\zeta|, |\tau| < M_0 = 3\sigma_r \tag{174}$$

Taking

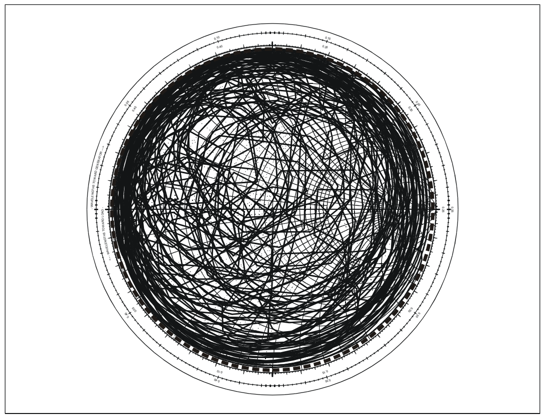

Figure 13. Fifty ohm Smith chart ($e^{j\omega t}$ is suppressed in experiments) for 32.9 cm (2.591 mm diameter) monopole antenna in the wall of the mode stirred chamber. There are 4800 equally spaced frequency points over a 10 MHz span centered at 220 MHz. This is the undermoded $\alpha \approx 0.0609$ region of the chamber. The "bounding" dashed curve is from the power balance formulas.

$$-\frac{E_z^{ref}}{\sqrt{\left\langle \left|E_z\right|^2 \right\rangle_V}} = \left(z_{in} - 1\right) / \sqrt{r_{in}/\alpha} < M_0 e^{i\varphi} \tag{175}$$

generates the bounding (dashed curves) circles shown on the impedance Smith charts in Figures 13,14, and 15 (in these figures $M_0 = 3$ was used). The experiments were carried out in the mode stirred chamber cavity, which is a large rectangular room with a volume of $V \approx 313$ m^3, with a stationary (for these experiments) mode stirrer. These experiments are one-port experiments where the scattering parameter (reflection coefficient) S_{11} is measured and related to the antenna input impedance by means of the formula

$$S_{11} = \frac{Z_{in} - Z_0}{Z_{in} + Z_0} \tag{176}$$

where $Z_0 = 50$ ohms. The quality factor of this room $O\left(10^5\right)$ is thought to be considerably higher than typical rooms where the V-Curve is used. Nevertheless it constitutes a useful test of models. The monopoles used for the impedance experiments had near resonant lengths for each of the frequency ranges used. The extreme values produced by this level of reflected field are

$$1 + \frac{1}{2\alpha}M_0^2 - \sqrt{\left(1 + \frac{1}{2\alpha}M_0^2\right)^2 - 1} < r_{in} < 1 + \frac{1}{2\alpha}M_0^2 + \sqrt{\left(1 + \frac{1}{2\alpha}M_0^2\right)^2 - 1} \tag{177}$$

$$\left|x_{in}\right| < \sqrt{\left(1 + \frac{1}{2\alpha}M_0^2\right)^2 - 1} \tag{178}$$

The undermoded limit $\alpha << 1$ gives $1/\left(2 + M_0^2/\alpha\right) < r_{in} < \left(2 + M_0^2/\alpha\right)$ and $2\left|x_{in}\right| < 2 + M_0^2/\alpha$, which is a large variation from the free space value $r_{in} \to 1$ and $x_{in} \to 0$. The overmoded limit $\alpha >> 1$ gives $(1 - M_0/\sqrt{\alpha}) < r_{in} < (1 + M_0/\sqrt{\alpha})$ and $\left|x_{in}\right| < M_0/\sqrt{\alpha}$. Thus if measurements of the cavity quality factor place the cavity in the overmoded limit with $\alpha >> 1$ we may be able to show that the variation about the mean

$$r_{in} = 1 \pm M_0/\sqrt{\alpha} \tag{179}$$

is acceptably small to justify the use of the free space impedance.

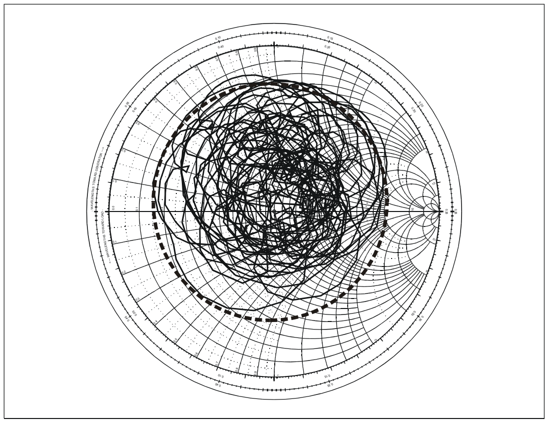

Figure 14. Fifty ohm Smith chart ($e^{j\omega t}$ is suppressed in experiments) for 7.544 cm (2.591 mm diameter) monopole antenna in the wall of the mode stirred chamber. There are 801 equally spaced frequency points over a 1 MHz span centered at 920 MHz. This is the transition $\alpha \approx 2.16$ region of the chamber. The "bounding" dashed curve is from the power balance formulas.

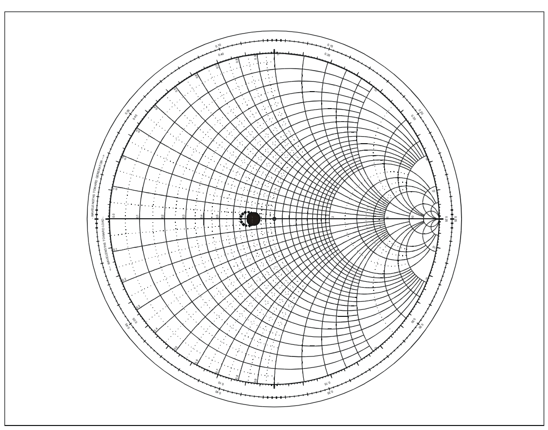

Figure 15. Fifty ohm Smith chart ($e^{j\omega t}$ is suppressed in experiments) for 4.325 mm (1.51 mm diameter) monopole antenna in the wall of the mode stirred chamber. There are 801 equally spaced frequency points over a 10 MHz span centered at 15 GHz. This is the overmoded $\alpha \approx 1200$ region of the chamber. The "bounding" dashed curve is from the power balance formulas.

The following table illustrates the lower extreme value (177) for $V = 500$ m^3 and the frequencies examined above for the rectangular cavity, along with 100 MHz, with an effective wall conductivity $\sigma = 1$ S/m. The first entries do not agree as might be expected since this frequency is below the fundamental resonance of the cavity (denoted by parentheses on these entries). The results at 37 MHz and 51 MHz are not too far off from the preceding rectangular cavity values. Perhaps the preceding rectangular cavity values achieved these low numbers due to the fact that we chose the symmetry point for evaluation, where the impedance reached a minimum, or because of the regularity of the spectrum versus what would be expected with a cluttered cavity (in addition to the predominance of only the TM_{dip} modes for the perfect rectangular room). The small reduction at 100 MHz indicates that the modes are overlapping to a relatively high degree.

f (MHz)	Q	α	r_{in}
10	12	(0.061)	(0.0047)
37	23	1.6	0.12
51	28	3.5	0.22
100	39	18.7	0.50

The numbers in this table can be scaled for other wall conductivities and corresponding room quality factors. We do not know the quality factors of typical rooms, but suspect they may be fairly low due to lossy wall materials. Measurement of these resonant quality factors would be helpful in pinning down the issue. It may also be possible to examine the fluctuations of the input impedance of an antenna in these rooms to get a feel for the issue. Material properties of the walls would also be useful.

6.6 Matching In Cavity

The low values of r_{in} near the V-Curve bottom could be cause for some concern with respect to the original unbounded V-Curve. However, for limited size antennas, and limited quality factors of the matching network, the result (58) will be modified to

$$Q_{dip} \sim \frac{3\Omega_e}{k^3 h^3 r_{in}} \leq Q_{\lim} = 1000 \tag{180}$$

and thus pushes the minimum matching frequency upward. For the preceding example, with a dipole antenna having length $2h \leq 1$ m (we will take $2a = 5$ mm and $\Omega_e \approx 8.6$) and from the preceding table setting $r_{in} = 0.2$, we find a minimum matching frequency of approximately $f_m \approx 50$ MHz. The allowed electric field level would thus be reduced by a factor of two ($\sqrt{0.2}$) (lowering the matched curve) at $f_m \approx 50$ MHz, but certainly constituting less of an effect than otherwise might be anticipated without limits imposed by the matching transmission line losses. Again, realistic estimates for the cavity effect based on loss measurements are needed to make more definitive statements.

6.7 Transmitter Field In Enclosure

The V-Curve criterion, which sets a limit on the allowed field at the receiver, has focused our attention on issues with the receiver, and in this section on the cavity effects associated with the input impedance. However, there is a mitigating factor to these reductions in real input impedance associated with the field of the source or transmitter. In situations where the quality factor of the room is significant, it was shown that the minimum input impedance occurred between modes (or below the first mode). The second term of the open circuit voltage (137), due to the cavity, will also tend to be suppressed in amplitude at precisely these frequencies, leading to reductions in the field at the receiver (the absorption by the transmitter also affects the input impedance of the receiver). To deal more quantitatively with this effect we would need to bring the transmitter into the problem as illustrated in Figure 16 (making the problem a two-port instead

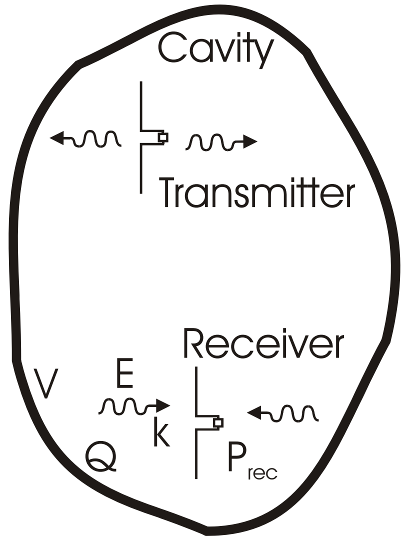

Figure 16. Typical geometry of transmitting and receiving linear antennas in a cavity.

of single port problem [30], [31]). This is probably a reasonable extension of the overall bounding approach, but because the present report is limited to the receiver V-Curve criterion, it is out of scope.

7 CONCLUSIONS

The V-Curve criterion has been summarized for an antenna (modeling exposed cabling attached to a susceptible load) immersed in an incident field in an unbounded region in Section 3. The right arm (where the antenna is assumed to be matched to the load) and the left arm (where the antenna is mismatched) are both included. We discuss both electric dipole and magnetic loop antennas in this context. Although loops can be more efficient at low frequencies, and are sensitive to the surrounding magnetic field, if reasonable antenna size constraints are applied, the allowed magnetic field still falls above that implied by the standard V-Curve when the free space impedance is used to connect the level of the electric field with the magnetic field (the two fields may not actually be so connected at low frequencies, but we take the requirement to imply a magnetic field limit also).

Higher antenna directivity gains, for example, as occur with a ground plane present, imply reduced field levels versus the standard V-Curve, which are briefly discussed in Section 4. On the right arm of the V-Curve at high frequencies, the directivity gain of a long wire antenna near grazing incidence can exceed that of a resonant dipole and thus cause a lack of conservatism in the levels allowed by the standard V-Curve. This usually occurs in the GHz region where the allowed field levels are quite high. In addition, transmission line dielectric (or other) losses may play a role in mitigating this long wire effect.

To quantify additional conservatism in this model we consider losses of the wiring making up the matching transmission line section in the V-Curve model in Section 5. It turns out that the required quality factor for matching becomes very high if size constraints are placed on the antenna dimensions. The effect of this is that conjugate impedance matches (as assumed on the right arm of the V-Curve) near the bottom of the V-Curve become impossible. Hence the standard V-Curve near the bottom of the V is overly conservative if antenna size is limited. This constraint is particularly useful to consider in the bounded environment of a room or cavity, because the quality factor requirements on the matching network are even more difficult, and hence some mitigation of the room effect takes place near the bottom of the V.

To get a handle on an issue that challenges the conservatism of the model, Section 6 of the report examines the receiving properties of a short linear antenna in a bounded region (room or cavity) and how the real part of the input impedance of the antenna is affected by the wall reflections. Two canonical cavities, a sphere and a rectangular room, are examined particularly near the first fundamental modes. High frequency statistical variations and their extreme values are also considered. Reductions in the real part of the antenna input impedance are the focus since this can suppress the level of the right arm of the V-Curve. This is caused by the fact that the real part of the antenna input impedance is created by losses in the room boundary rather than radiation to infinity. Quantification of the loss associated with the room (for example, its quality factor Q) is required to set the possible variations that can be observed at the antenna terminals and more quantitatively establish the effect on the right hand part of the V-Curve; measurements of room losses are thus suggested. We also point out several mitigating factors to this effect. One is the fact that the transmitter radiated field can be suppressed at the same frequencies as the receiver impedance in high Q situations. Secondly, requirements on the quality factor of the matching network of the V-Curve will become more severe in these cases and push up the minimum matching frequency of the right arm of the V-Curve.

8 REFERENCES

[1] R. L. Parker, "Origin and Application of the 'V' Curve," Sandia National Laboratories Internal Report, unpublished, Appendix A of this report.

[2] P. F. Mohrbach, R. Thompson, R. F. Wood, and D. J. Mullen, "Monograph On Computation Of RF Hazards, Report Prepared for NASA Goddard Space Flight Center by the Applied Physics Laboratory of the Franklin Research Center, July 1968.

[3] R. E. Jorgenson, L. K. Warne, and M. E. Morris, "V-Curve Prediction of Allowable Field Strengths," Sandia National Laboratories Internal Report, to R. R. Carr, March 19, 1990, Appendix B of this report.

[4] L. K. Warne, "Matched Receiving Antenna Inside a Cavity Resonator," Sandia National Laboratories Internal Report, January 29, 1991, Appendix C of this report.

[5] L. K. Warne, "Matched Receiving Antenna Inside a Cavity Resonator: Practical Interpretation," Sandia National Laboratories Internal Report, February 1, 1991, Appendix D of this report.

[6] E. C. Jordan and K. G. Balmain, **Electromagnetic Waves and Radiating Systems**, Englewood Cliffs: Prentice-Hall, Inc., 1968.

[7] S. A. Schelkunoff and H. T. Friis, **Antennas Theory and Practice**, New York: John Wiley & Sons, 1952.

[8] S. Ramo, J. R. Whinnery, and T. Van Duzer, **Fields and Waves in Communication Electronics**, New York: John Wiley & Sons, Inc., 1965, pp. 33, 286-297, 309-311.

[9] F. W. Grover, **Inductance Calculations**, New York: Dover Pub., Inc., 1973, p. 60.

[10] K. S. H. Lee and F. C. Yang, "Trends and bounds in RF coupling to a wire inside a slotted cavity," IEEE Trans. Electromagn. Compat., vol. 34, pp. 154-160, Aug. 1992.

[11] C. A. Balanis, **Antenna Theory: Analysis and Design**, Harper & Row, New York 1982, pp. 125, 376.

[12] L. K. Warne, T. E. Koontz, and K. C. Chen, "EM Penetration Bounds," Sandia National Laboratories Internal Report, August 5, 1988.

[13] K. S. H. Lee and L. K. Warne, "Bounding Of Voltage Responses," AFWL Interaction Note 540, June 30, 1998.

[14] L. K. Warne, K. S. H. Lee, H. G. Hudson, W. A. Johnson, R. E. Jorgenson, and S. L. Stronach, "Statistical Properties of Linear Antenna Impedance in an Electrically Large Cavity," IEEE Trans. on Antennas and Prop., Vol. 51, No. 5, May 2003.

[15] R. Balian and C. Bloch, "Distribution of Eigenfrequencies for the Wave Equation in a Finite Domain. II. Electromagnetic Field. Riemannian Spaces," Annals of Physics: 64, 271-307, 1971.

[16] S. A. Schelkunoff, **Electromagnetic Waves**, New York: D. Van Nostrand Co., Inc., 1957, pp. 294-299.

[17] R. E. Collin, **Field Theory of Guided Waves**, New York: IEEE Press, pp. 387-395, 1991.

[18] W. R. Smythe, **Static and Dynamic Electricity**, New York: Hemisphere Pub. Corp., pp. 541-545, 1989.

[19] L. K. Warne, H. G. Hudson, W. A. Johnson, R. E. Jorgenson, S. L. Stronach, and K. S. H. Lee, "Input Impedance of Antennas in High Frequency Cavities, Sandia National Laboratories Report, SAND2000-3112, Dec. 2000.

[20] X. Zheng, T. M. Antonsen, Jr., and E. Ott, "Statistics of Impedance and Scattering Matrices in Chaotic Microwave Cavities: Single Channel Case," Electromagnetics, Vol. 26, No. 1, Jan. 2006, pp. 3-35.

[21] M. C. Gutzwiller, **Chaos in Classical and Quantum Mechanics**, New York: Springer-Verlag, Inc., 1990.

[22] S. Deus, P. M. Koch, and L. Sirko, "Statistical properties of the eigenfrequency distribution of three-dimensional microwave cavities," Physical Review E, Vol. 52, No. 1, July 1995.

[23] T. H. Lehman, "A Statistical Theory of Electromagnetic Fields in Complex Cavities," AFWL Interaction Note 494, May 1993.

[24] T. M. Antonsen, Jr., E. Ott, A. Chen, and R. N. Oerter, "Statistics of wave-function scars," Vol. 51, No. 1, Physical Review E, January 1995, pp. 111-121.

[25] L. K. Warne, R. E. Jorgenson, J. D. Kotulski, and K. S. H. Lee, "Two Dimensional Unstable Scar Statistics," Sandia National Laboratories Report, SAND2006-7511, December 2006.

[26] L. K. Warne, R. E. Jorgenson, J. D. Kotulski, and K. S. H. Lee, "Time Harmonic Scar Statistics in Two Dimensional Cavities," IEEE AP-S International Symposium, June 11-15, Honolulu, HI, 2007.

[27] D. A. Hill, "Linear dipole response in a reverberation chamber," IEEE Trans. Electromagn. Compat., vol. 41, pp. 365-368, Nov. 1999.

[28] L. K. Warne and K. S. H. Lee, "Some Remarks on Antenna Response in a Reverberation Chamber, IEEE Trans. on Electromagn. compat., vol. 43, no. 2, May 2001.

[29] L. K. Warne, W. A. Johnson, and R. E. Jorgenson, "An Improved Statistical Model for Linear Antenna Input Impedance in an Electrically Large Cavity," Sandia National Laboratories Report, SAND2005-1505, March 2005.

[30] L. K. Warne, H. G. Hudson, R. E. Jorgenson, W. A. Johnson, and K. S. H. Lee, "Receiving Properties of Linear Antennas in High Frequency Cavities," Sandia National Laboratories Internal Report, October 7, 2002.

[31] X. Zheng, T. M. Antonsen, Jr., and E. Ott, "Statistics of Impedance and Scattering Matrices in Chaotic Microwave Cavities with Multiple Ports," Electromagnetics, Vol. 26, No. 1, Jan. 2006, pp. 37-55.

The establishment of existing criteria for assembly/disassembly operations is based on a very simple dipole model commonly approximated by wiring used for interconnections of components associated with weapon systems. The response for electro-explosive devices (EED's) takes the form of a 'V' as shown in Figure A1. The curve depicts the required field in Volts/meter to produce the 100% no-fire current in the EED.

Right Arm of the 'V' Curve

The right arm of the 'V' assumes that the dipole is matched to the load. This assumption is reasonable since there is usually a portion of a transmission line between the dipole formed by system wiring and the load (EED bridgewire). By allowing frequency to be variable, the equivalent of a line stretcher exists between the dipole and the load. A wide variety of loads is presented to the dipole as can be observed from the Smith Chart (Reference 1) shown in Figure A2 by following the extreme outside circle of the Chart. This circle describes loads for a lossless transmission line and is normalized to the characteristic impedance of the line. The actual load for this case must exist somewhere on the outer c1rcle. Other loads would be described by circles of different radius. If the line is lossy, the loads presented to the dipole are described by a spiral from the actual load to the center of the chart as shown in Figure A2. All loads are not possible by simply varying frequency for a fixed configuration since for this to be true, all points on the Smith Chart would have to be covered rather than those representing the curve.

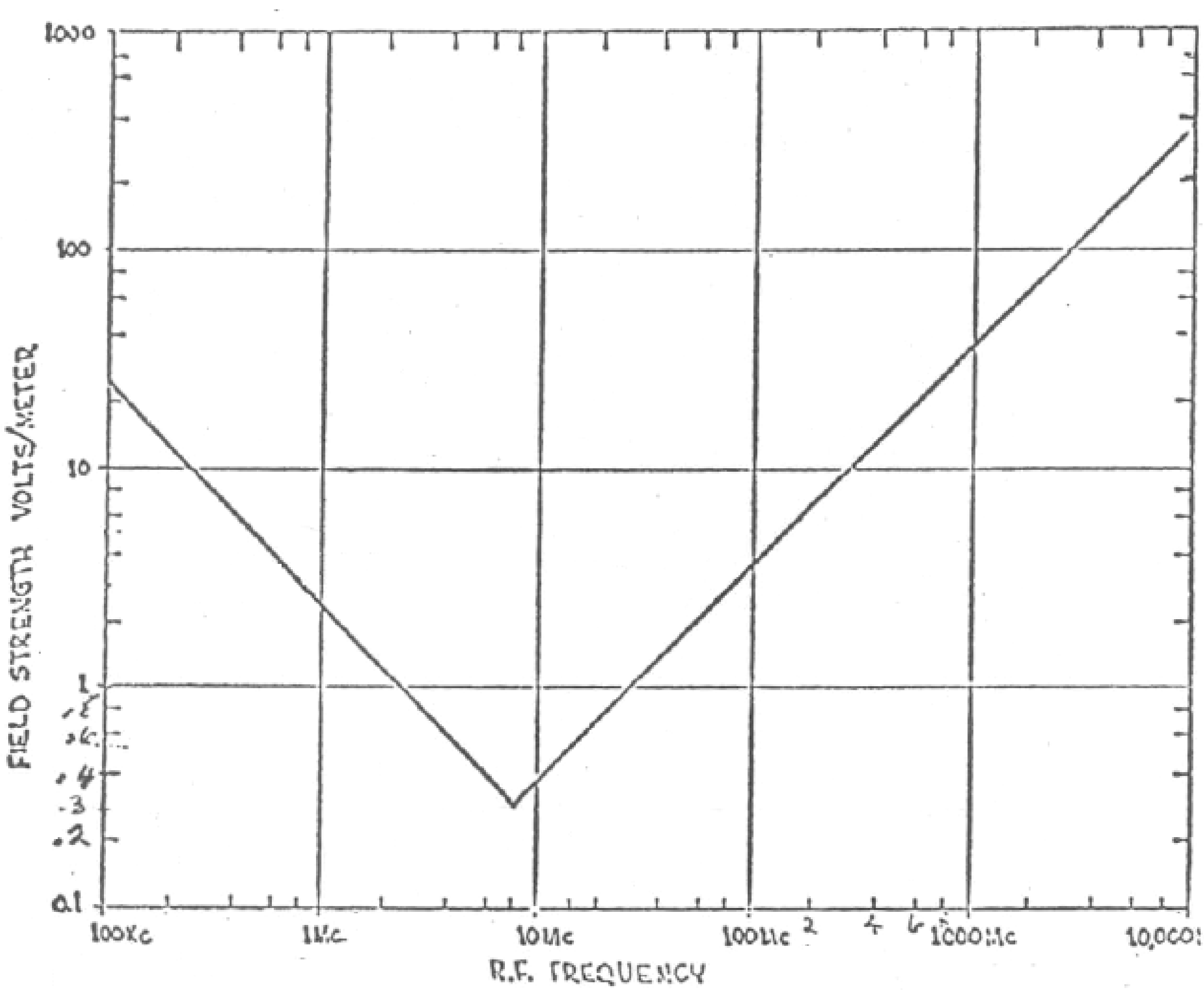

Figure A1. Field Strength Limits During Assembly-Disassembly of Weapon Systems Based on a 100mA no-fire EED.

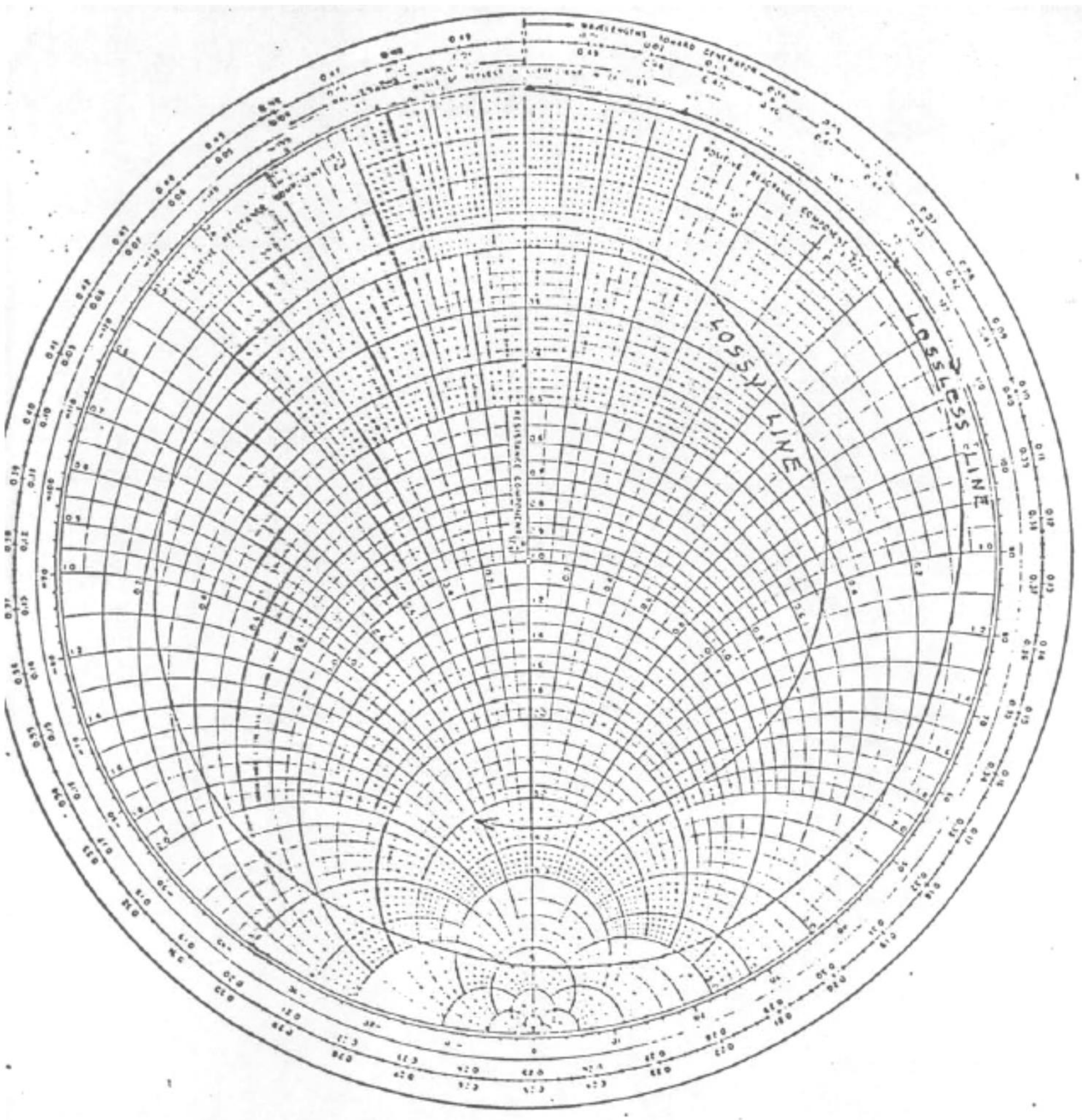

Figure A2. Smith Chart Showing Loads Reflected by a Uniform Transmission Line.

Although a greater variety of loads is available from the lossy line due to spiraling rather than retracing the same curve of the lossless line, less power is delivered to the load since much of the energy is dissipated in the line. In general, the most power will be delivered to the load by obtaining the best match on the lossless curve. The lossless line curve assumes that the transmission line is uniform (constant characteristic impedance) between the dipole and the load. In reality, such lines are usually made up of several different wire spacings representing several lines of different characteristic impedance. As observed on the Smith Chart in Figure A3, these lines introduce steps in the circular path described by varying frequency. A greater variety of loads is introduced by this factor, but as before, not all possible loads can be realized by varying frequency. Where several trips around the Smith Chart are required to obtain the match (the line is long in terms of wavelength), line loss is usually an overriding factor.

In dealing with assembly/disassembly operations, numerous different configurations may be encountered. Handling fixtures, test equipment, grounding schemes, variable exposure conditions, and changes due to removal of components are a few of the factors which affect these configurations. These factors also lead to a variety of loads. Further, the criteria should be general for many different weapons systems. This factor will significantly increase the number of loads that could be encountered. Hence, it is concluded that the only reasonable bounding condition that can be chosen is a perfectly matched load for frequencies where transmission lines might be greater than one-half wavelength long.

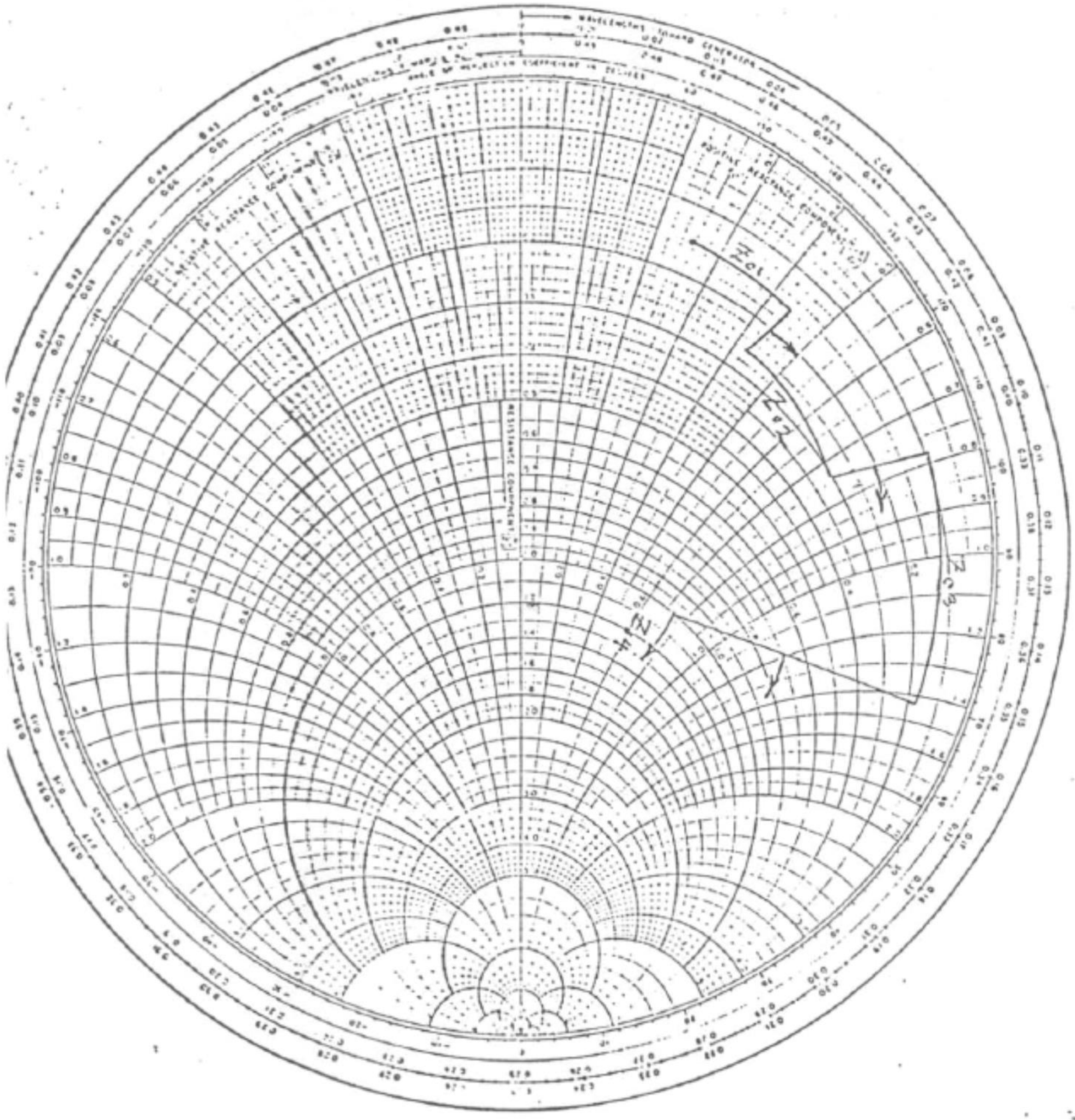

Figure A3. Smith Chart Showing Effect of Transmission Lines on Reflected Loads as Frequency is Varied.

Dipole Effective Height

The following discussion centers on the dipole and its ability to capture energy from the field. In this discussion a dipole is considered to be an antenna formed by a two element collinear array. The elements do not have to be equal in length, but their separation points are considered to be the load terminals as shown in Figure A4.

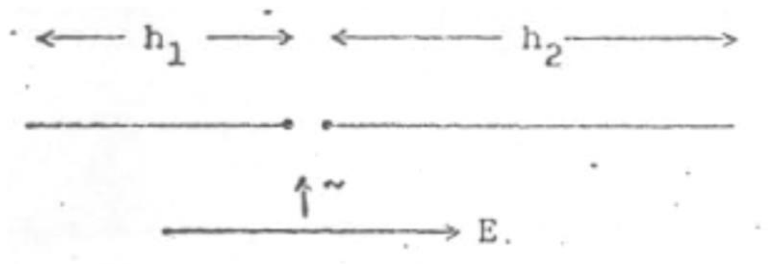

Figure A4. Pictorial Representation of a Dipole.

Since available analytical results are for $h_1 = h_2$, the discussion will center on this case, but it is believed that the results will extend to the more general case of $h_1 \neq h_2$. The effective height of a dipole is a parameter derived from analysis (Reference 2) which describes generally the capability of an antenna for extracting energy from the field. More precisely for a symmetrical dipole:

$$V_{oc} = E2h_e \tag{1}$$

V_{oc} = *open circuit voltage*

E = *incident electric field*

h_e = *effective height*

The effective height also expresses the pattern characteristics of the dipole. In the low frequency reg1on where the dipole is short in terms of wavelength the pattern characteristic is approximately a cosine function in one plane and a constant for any fixed radius in an orthogonal plane, approximately described by the shape of a doughnut as shown in Figure A5, (Reference 3). The following equation applies to a monopole short in terms of wavelength:

$$E = \frac{120\pi h I_o}{d\lambda} \cos\theta$$

I_o = *center current*

h = *height*

d = *distance*

λ = *wavelength* (Reference 4)

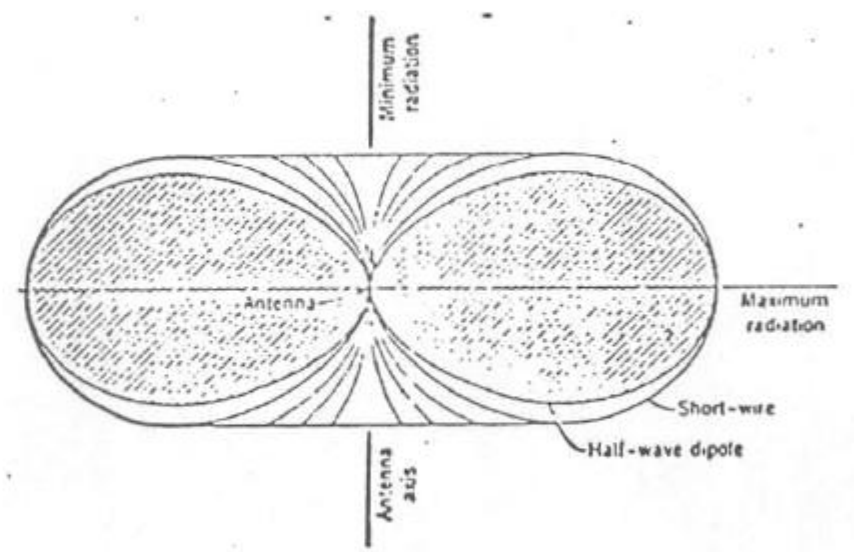

Figure A5. Power Radiation Patterns of Short-Wire Antenna and Half-Wave Dipole.

Since this pattern is essentially constant in the low frequency range, the effective height is constant as follows:

$$h_e = h/2$$

$$h = half - length\ of\ the\ dipole$$

In the high frequency range the patterns vary considerably and the number of side lobes increases as frequency increases as typified in Figure A6 (Reference 4).

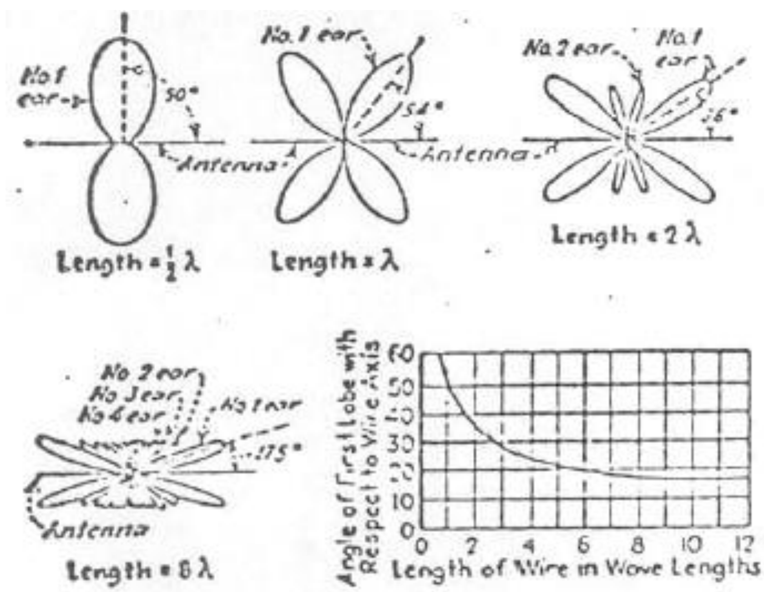

Figure A6. Polar diagram showing strength of field radiated in various directions from an antenna consisting of a wire remote from the ground. These diagrams can be considered as cross sections of a figure of revolution in which the axis is the antenna.

The effective height reflects these lobe changes in an oscillatory manner as shown in Figure A7 (Reference 5).

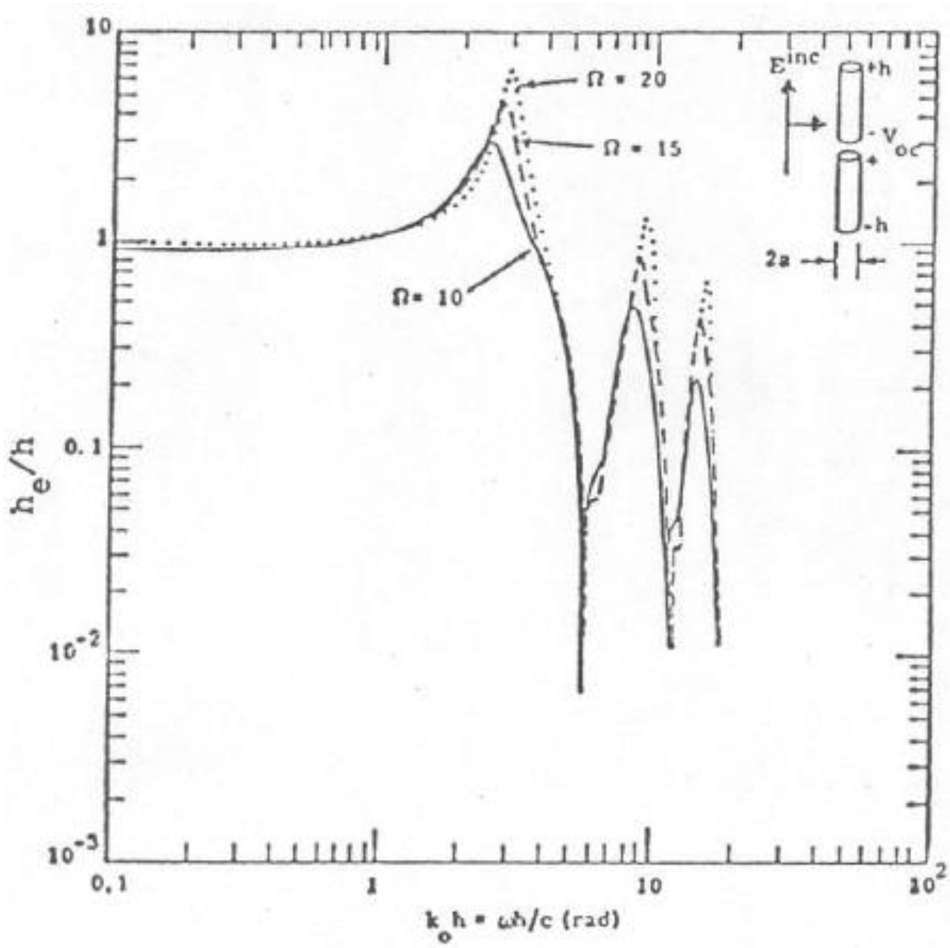

Figure A7. Normalized Open-Circuit Voltage Transfer Function for Dipole Antennas

The plot in Figure A7 is the response for broadside incidence. At any given frequency where a null occurs at broadside incidence, a ·peak of one of the lobes shown in Figure A6 can be realized by shifting the angle of incidence slightly. The peaks in effective height decrease at approximately 6 dB/octave in the high frequency range as shown in Figure A7. It is concluded that the effective height is constant in the low frequency range for broadside incidence and drops off slowly (cosine function) off broadside incidence. In the high frequency region, the peaks of the effective height roll off at 6 dB/octave with frequency and off broadside incidence the effective height varies through a series of peaks and nulls. The peaks off broadside do not generally decrease as shown in Figure A6.

Radiation Resistance and Maximum Power Transfer

The amount of power that a given source can deliver to a matched load is dependent on its open circuit voltage and its internal resistance.

For the dipole, resistance consists of wire resistance and radiation resistance. Except at very low frequencies radiation resistance will predominate. At frequencies where radiation resistance predominates, resistance will 1ncrease as follows:

$$r_r \cong \frac{2\pi\gamma}{3}\left(\frac{hf}{c}\right)^2 \qquad (2)$$

$\gamma = 120\pi = free\ space\ z$

$f = frequency$

$c = velocity\ of\ light$ (Reference 6)

Figure A8 is a plot of the radiation resistance (Reference 5). The radiation resistance is oscillatory but approaches a constant value in the high frequency limit.

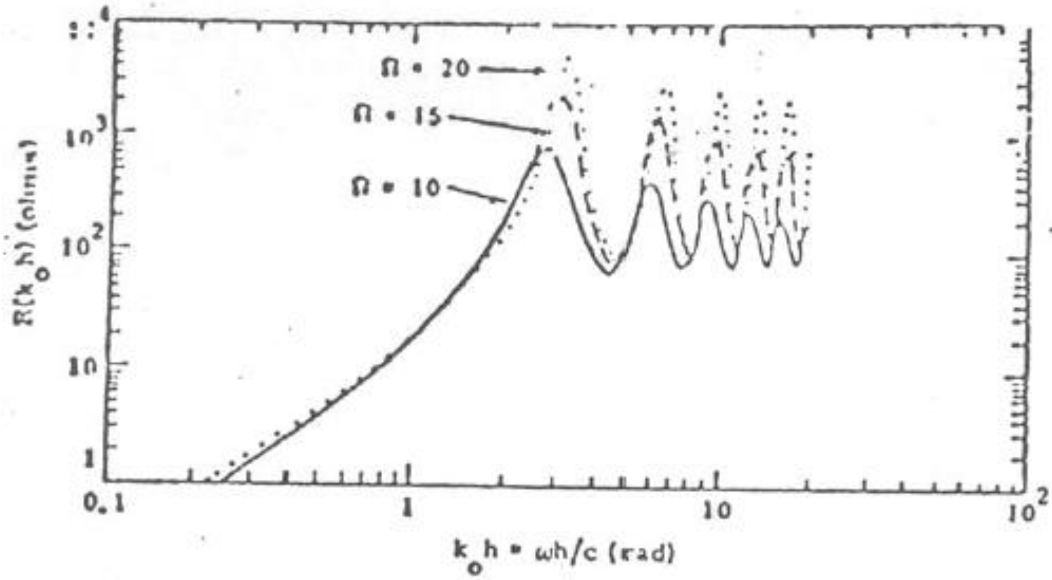

Figure A8. Radiation Resistance of a Cylindrical Dipole

Combining the frequency varying characteristics of effective height and radiation resistance as they affect power transfer, the maximum power which can be transferred is:

$$P_t = \frac{V_{oc}^2}{4r_r} = \frac{(E2h_e)^2}{4r_r} \quad (3)$$

Since it has been shown in the low frequency region that .effective height is constant as frequency is increased while radiation resistance increases as the square of frequency, the maximum power which can be transferred decreases at 6 dB/octave as frequency is increased. In the high frequency region the effective height approximately decreases at 6 dB/octave while the radiation resistance is approximately constant. These characteristics suggest that a reasonably smooth 6 dB/octave decrease in maximum power transfer is available through the mid-frequency range also. Figure A9 is a plot of computed maximum power transfer as a function of frequency for a fixed length dipole using a code developed for data in Reference 7. This is a remarkably smooth curve if one uses only the peaks in the high frequency region. It is inferred from this curve that the maximum power transferred is independent of the length of the dipole. This is clarified by the following discussion. It is well known that the power received by a resonant dipole is:

$$P_{rec} = \frac{G\lambda^2 P_f}{4\pi} = \frac{G\lambda^2 E^2}{4\pi\gamma} \tag{4}$$

$G = dipole\ gain$

$\lambda = wavelength$

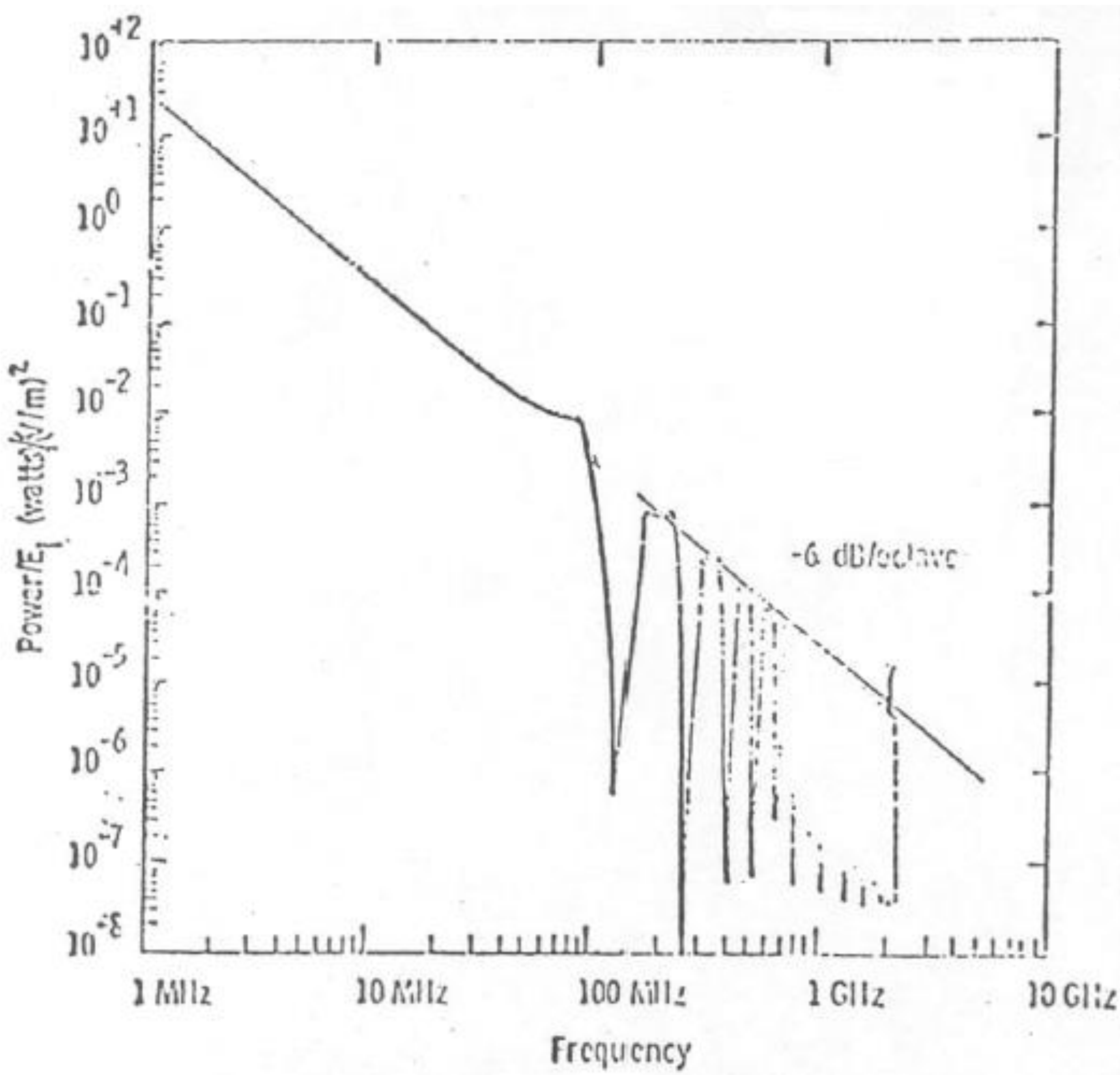

Figure A9. Response of a Matched, Fixed Length Dipole

In order to resonate the dipole it must be reduced in length directly as frequency is increased. Further, the power received decreases at 6 dB/octave as noted from equation 4 above. Hence, a resonant dipole which must be varied in length follows the same curve as a fixed length dipole. This leads one to the conclusion that the power that a dipole receives (or delivers to a matched load) is independent of the length of the dipole. It is therefore fixed absolutely by frequency alone. This, of course, excludes cases in the high frequency region where nulls occur, although a null can be shifted to a peak by turning either the dipole or the source direction slightly.

It should be emphasized that these conclusions have not been verified for an asymmetrical dipole but it is not anticipated that this increased generalization will produce different results. Although results were presented primarily for broadside incidence it was shown that levels vary slowly off broadside incidence. Further, antennas such as 'V's and arrays are conceivable with arbitrary wire arrangements, and these antennas are more efficient at collecting power from the field at certain specific frequencies. Hence, the dipole model is not in itself a worst case, but simply a reasonably good representation for arbitrary weapon configurations.

Left Arm of the 'V' Curve

The discussion has not covered the left arm of the 'V' of Figure A1. The left arm would not exist if optimum matching could be maintained. Both the dipole length and any interconnecting wiring forming a transmission line are limited in assembly areas. Somewhat arbitrarily, 8 MHz has been chosen as the frequency below which optimum matching cannot reasonably be achieved due to length constraints. Since matching cannot be achieved and the dipole is also short in terms of wavelength, a mismatch which increases as frequency decreases can be expected. This is illustrated by the equivalent circuit below:

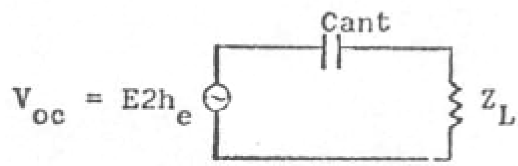

For EED's, the dipole impedance linearly increases as frequency is decreased above EED impedances which are typically five ohms or less. For semiconductors, the forward resistance is often low while back resistances are high (Mega ohms). The forward conducting region will result in more dissipation leading to the vaporization of leads than the back resistances up to a point where the forward resistance is:

$$\left(r_f = \frac{{X_c}^2}{r_r}\right)$$

as shown below:

$$I_f = \frac{V_{oc}}{-JX_c + r_f} \cong \frac{V_{oc}}{X_c} \qquad X_c \gg r_f$$

$$r_f = forward\ diode\ resistance$$

$$I_r = \frac{V_{oc}}{-JX_c + r_r}$$

$$r_r = back\ diode\ resistance$$

$$|I_r| = \frac{V_{oc}}{\sqrt{{X_c}^2 + {r_r}^2}}$$

$$|I_r|^2 = \frac{{V_{oc}}^2}{{X_c}^2 + {r_r}^2}$$

Setting $|I_r|^2 r_r = \left|I_f\right|^2 r_f$

$$\frac{r_r}{{X_c}^2 + {r_r}^2} = \frac{r_f}{{X_c}^2}$$

or

$$r_f = \frac{r_r {X_c}^2}{{X_c}^2 + {r_r}^2}$$

Since r_f is usually in the 1 - 50 ohm area and r_r in the Mega ohm area, equality of forward and reverse loss will occur when $r_r > X_c$ and

$$r_f \cong \frac{{X_c}^2}{r_r} \qquad (5)$$

At lower frequencies, the 'V' curve 1s not applicable.

Hence, it is concluded that the left half or 'V' presently used for EED's also is applicable within the above constraint for CW failures of semiconducting devices. Since the concepts developed for the matched dipole were independent of the load, the right half of the 'V' curve is also applicable to semiconductor devices.

R. L. Parker, 1553
Sandia National Laboratories

References

Reference 1. “Microwave Theory and Measurements", Hewlett Packard Co., 1962

Reference 2. RWP King, “The Theory of Linear Antennas", Harvard University Press, 1956

Reference 3. H. R. Reed, Carl M. Russell, "Ultra High Frequency Propagation", John Wiley & Sons, Inc., 1953

Reference 4. F. E. Terman, "Radio Engineers’ Handbook", McGraw-Hill Book Co., 1943

Reference 5. D. E. Merewether, A. Cooper, R. L. Parker, "Electromagnetic Pulse Handbook for Missiles and Aircraft in Flight", SC-M-710346, September 1972

Reference 6. J. D. Kraus, “Antennas", McGraw-Hill Book Co., 1950

Reference 7. G. B. Varnado, J. G. Bartlett, "Mathematical Models for the Response of Aerospace Systems to High Frequency Environments", SLA 74-0131, 1974

Appendix B 1990 Memorandum to Ralph Carr

Sandia National Laboratories

Operated for the U.S. Department of Energy by
Sandia Corporation
Albuquerque, New Mexico 87185-

date: March 20, 1990

to: Ralph R. Carr, 7212

from: R. E. Jorgenson, L. K. Warne, M. E. Morris, 7553

Roy E Jorgenson Larry Warne Marvin E. Morris

subject: V-Curve Prediction of Allowable Field Strengths

Introduction

When a weapon is assembled or disassembled or when a weapon has been severely damaged, wires connected to the interior of the weapon are exposed to electromagnetic fields that arise from sources such as hand-held communications equipment or mobile radar. These situations are of concern, because some of the exposed wires are connected to electro-explosive devices (EEDs) that will detonate if the power delivered to them, due to the current induced on the wires by the fields, becomes too high. It is necessary, therefore, to limit the strength of the electromagnetic fields in the environment or, equivalently, to fix a standoff distance within which transmitters above a given power level should not operate.

A convenient way to bound the electromagnetic field strength is by means of a curve that shows, as a function of frequency, the maximum electric field intensity that can exist in the environment without causing an EED to explode. Unfortunately, as shown in Figure B-1, the configurations of wires in the weapon system have a large degree of variation as the wire bundles are moved about the assembly area. It is impossible and undesirable, therefore, to solve an actual problem rigorously, because with every change in wire configuration a new problem would have to be solved. A better approach would be to use a simple model that demonstrates the essential physics of the problem in order to find a least upper bound for the allowed field strength for most situations and then to solve a few typical wire configurations rigorously to ensure that these bounds are indeed realistic.

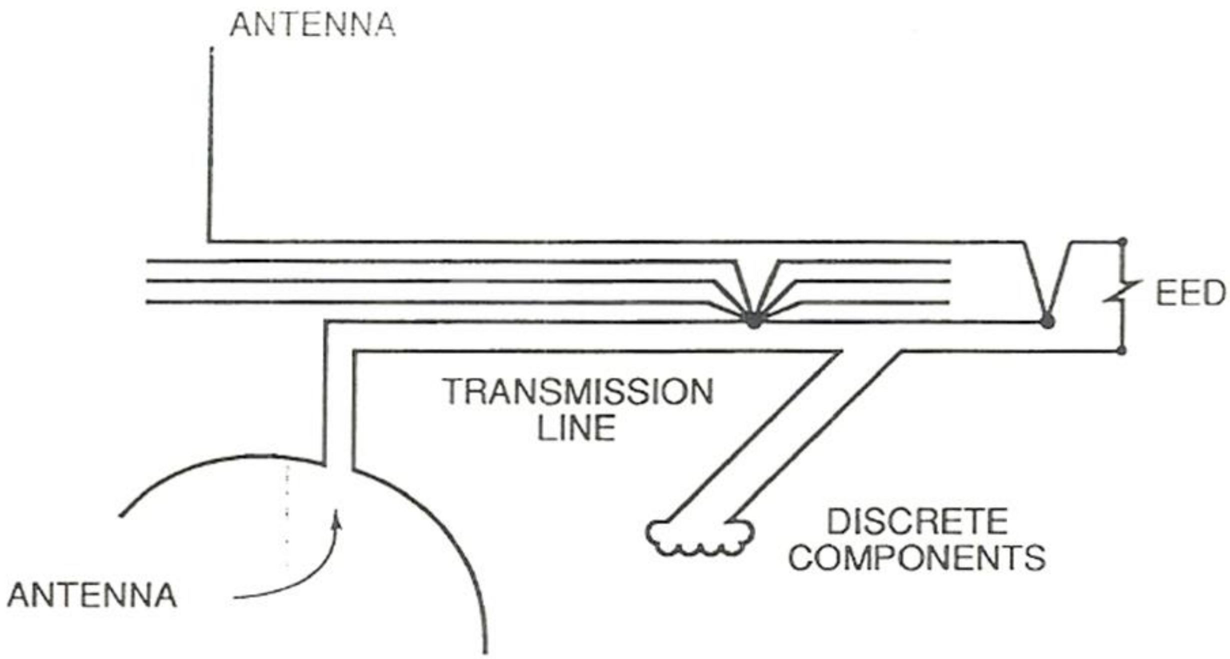

Figure B-1. Example of a wire configuration that may exist in a weapon system.

The purpose of this memorandum is to provide a simple but realistic model of a bundle of wires connected to a 100-mA, no-fire EED and to document the assumptions made in constructing and solving this model. The memorandum begins by simplifying the actual situation shown in Figure B-1 to that of a single dipole connected to an EED through a two-wire transmission line, as shown in Figure B-2. The assumptions on the model are then examined to see what parameters can be reasonably fixed. Each assumption and its consequence are documented. Next, further approximations are made to arrive at five mathematical descriptions of the model. Each of these is discussed in turn: a short dipole with no transmission line, the V-Curve, a short dipole with a transmission line, a long dipole with a transmission line, and the presently used resonant dipole with no transmission line. The field strength bounds predicted by each of these descriptions are compared with each other in the results section, and some conclusions concerning the V-Curve are drawn.

Physical Model

As discussed in the introduction, the actual physical situation shown in Figure B-1 is too variable to allow any general conclusions to be drawn from it. Figure B-1 shows a bundle of wires exposed to an electromagnetic field. Some of the wires could be separated from the main bundle, in which case they would act mainly as antennas that couple electromagnetic energy from the surrounding environment into the wire bundle. The sections of wires in the bundle would not couple energy as efficiently as the separated wires, but could act as transmission lines to transport the energy to the EED. The wires acting as transmission lines could be connected to various discrete devices along their length or could be connected to other wires. The wires could also vary in cross section as a function of length, which would cause the characteristic impedances of the transmission lines to vary also.

The first step in simplification is to break the wire bundle into three sections according to the main function of each section. The wires separated from the bundle are assumed to act solely as antennas. The wires in the bundle along with the discrete elements act as a transmission line system. This section may match the impedance of the EED to that of the antenna so that the power transferred to the EED is maximized. Energy coupled directly to the wires in the bundle from the external field is ignored. The final section of the wire bundle is the EED itself, which is characterized by a 5-ohm resistive load.

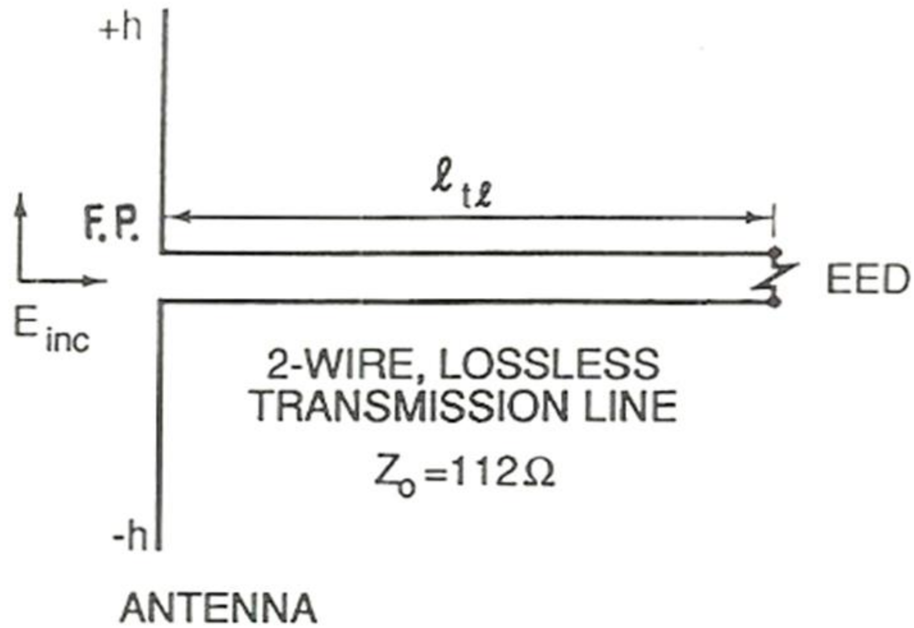

Figure B-2. Idealization of the general wire configuration to that of a dipole connected to a two-wire transmission line, which is, in turn, connected to an EED.

The antennas formed by the separated wires are approximated as dipoles in free space. Any variation of the wires from the dipole configuration is assumed to decrease the amount of energy coupled into the system. The loop antenna is the dual to the dipole, so consideration of it would add no new physics to the problem. Several wires acting as antennas could be connected to the same transmission line section forming an antenna array, which would increase the amount of energy coupled into the system, but these possibilities are ignored.

The transmission line section's main function is to impedance match the load to the antenna. This occurs at discrete frequencies for a simple transmission line of a given length. The effect of placing discrete elements at points along the transmission line, adding tuning stubs (formed by wires connected to the transmission line) and varying the characteristic impedance of the transmission line as a function of length merely shifts the location of these matching frequencies. Since the exact locations of these frequencies are not important in the calculation of a bound, the effects of the discrete elements and tuning stubs are ignored, and the transmission line section is characterized by a two-wire simple transmission line. The result of the above arguments is that the actual situation shown in Figure B-1 is simplified to that of Figure B-2—a single dipole is connected to a two-wire transmission line, which is, in turn, connected to a 5-ohm load.

Assumptions

The four components making up the simplified model are the incident field, the dipole, the transmission line, and the EED load. This section documents the assumptions made on each component and determines which parameters of the problem can be realistically fixed.

The incident field is assumed to be a plane wave, which implies that the source of the field is in the far-field of the dipole. The wave is polarized so that the H field is perpendicular to the axis of the dipole (no polarization loss). The frequency of the incident wave is between 10 MHz and 15 GHz. The plane wave is incident at an angle such that it is in the main beam of the dipole pattern, which maximizes the amount of energy received by the dipole. If the dipole is short (less than a wavelength), this direction is perpendicular to the antenna axis. As the antenna becomes longer, this main beam moves toward the antenna axis.

The dipole is made of uninsulated, perfectly conducting wire in free space. The wire, which is an extension of the wire bundle, has a gauge between #16 AWG and #20 AWG (radius between 6.454×10^{-4} meter and 4.059×10^{-4} meter). The parameter in the calculations that depends on the antenna radius is the fatness parameter, which is calculated by the formula

$$\Omega = 2 \ln\left(\frac{2h}{a}\right)$$

where h is the half-length of the dipole and a is the dipole radius. The fact that the fatness parameter varies logarithmically with the wire radius justifies fixing the radius of the antenna (and consequently that of the transmission line wires) at 5.0×10^{-4} meter, which is approximately the radius of #18 AWG wire.

The transmission line that connects the antenna to the EED is composed of two wires from the wire bundle. The wires are insulated from each other by a Teflon sheath ($\varepsilon_r = 2.1$). A bound on the transmission line characteristic impedance is needed to eliminate the possibility of a reactive match at very low frequencies. In this memorandum, the transmission line will be assumed to consist of adjacent wires. The Teflon insulation on each of the wires is assumed to be as thick as the wire radius. This means that the wires are separated from each other by approximately four wire radii, (i.e., 2.0×10^{-3} meter). The transmission line impedance Z_o depends on the logarithm of the separation distance between the lines since the wire radius has already been fixed in the fatness parameter calculation. This means that, like the fatness parameter, the transmission line impedance can be fixed at a typical value

$$Z_o = \frac{120}{\sqrt{\varepsilon_r}} \cosh^{-1}\left(\frac{b}{2a}\right) = 112 \; ohms \;,$$

where b is the separation distance between the two wires.

The EED is assumed to be a 100-mA, no-fire device. It is assumed to have an impedance of 5 ohms and a power sensitivity threshold of 50 mW.

Models

The parameters that remain to be varied are the half-length of the dipole (labeled h in Figure B-2), the length of the transmission line (labeled ℓ_{tl} in Figure B-2), and the feed position of the antenna (labeled F.P. in Figure B-2). The following sections discuss each of the five mathematical models used to generate the curves in the results section. The first two models are simple and are candidates for setting the bounds of the incident E field. The third and fourth models are more complex and will be used to verify the bounds set by the first two for typical cases. The last model is a simple model and is being used presently.

Short Dipole, No Transmission Line

In the short-dipole, no transmission line model, as shown in Figure B-4, the EED is connected directly to the dipole with no intervening transmission line. The dipole is assumed to be short in terms of a wavelength, so that the current along the dipole has a triangular distribution with respect to length. The antenna and load can be replaced by the equivalent circuit shown in Figure B-4. The antenna is replaced by an open circuit voltage (V_{oc}) in series with the radiation resistance (R_{rad}), capacitance of the antenna (C_{ant}) and inductance of the antenna (L_{ant}), all of which are defined in Appendix I of this memorandum. The equation governing the curve is then

$$E_{inc} = \frac{1}{h}\sqrt{\frac{P_t}{R_L}}\left[(R_{rad}+R_L)^2+\left(\frac{\omega^2 L_{ant}C_{ant}-1}{\omega C_{ant}}\right)^2\right]^{1/2} \quad V/m \ ,$$

where P_t is the power threshold of the EED (50 mW), R_L is the resistance of the EED, and ω is the radian frequency. This model suffers from not accounting for any matching network between the antenna and the EED. As will be seen in the results, this model will allow a larger field to exist in the environment than can be considered safe.

Figure B-3. A short dipole connected directly to the EED.

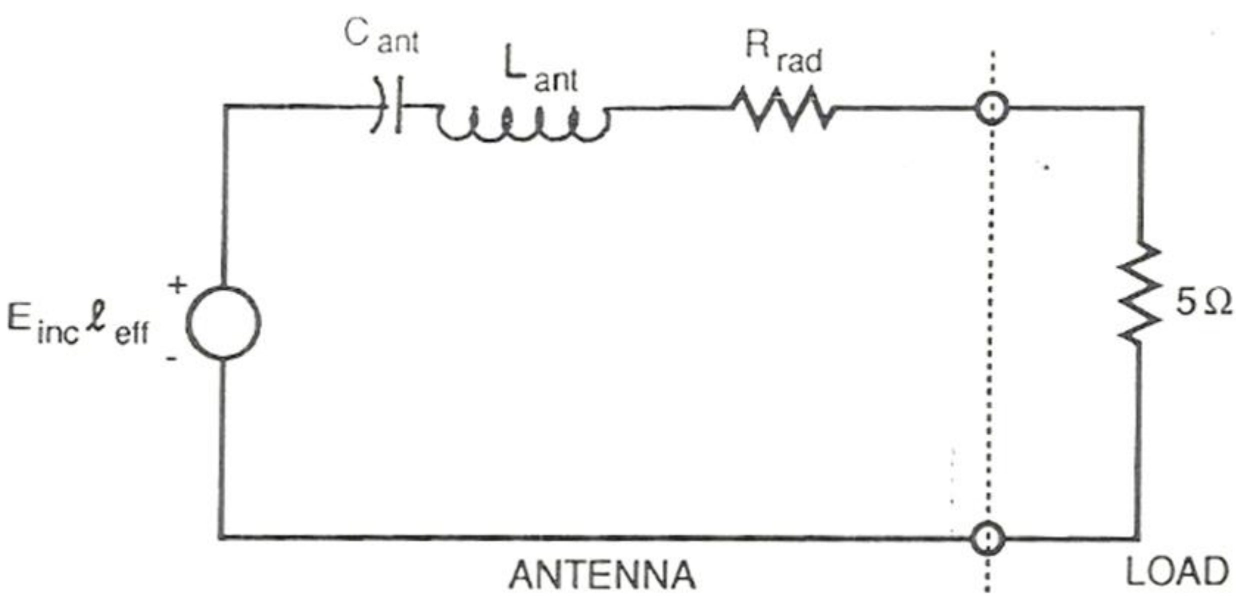

Figure B-4. The equivalent circuit for the situation shown in Figure B-3.

V-Curve Calculation

The V-Curve is the second type of simple model used to calculate the field bounds. It is well established and includes the matching effect of the transmission line between the antenna and the EED. In this model, the dipole is again considered to be short. The two arms of the V-shaped curve are generated by considering the model from two points of view. Above a certain frequency, the transmission line is electrically long enough to have a chance to match the load impedance of the EED to the impedance of the antenna. Since the transmission line configuration is so variable, the right arm of the V-Curve is generated by assuming that the transmission line perfectly matches the antenna to the load at all frequencies in this range. This situation allows the maximum power to be transferred to the EED and represents the worst-case scenario in the context of a small dipole assumption. The equivalent circuit for this case is shown in Figure B-5. The antenna is modeled by a voltage generator (V_{oc}) in series with the radiation resistance (R_{rad}). The load presented to the antenna by the transmission line is equal to the radiation resistance since it is assumed to be perfectly matched. The curve is governed by the equation

$$E_{inc} = \frac{2}{h}\sqrt{P_t R_{rad}} \;\; V/m \; .$$

Therefore, the strength of allowed field increases with frequency at a rate of 6 decibels per octave. The curve is fixed both in slope and y intercept.

The left arm of the V-Curve is generated by assuming that below a certain frequency the transmission line is electrically so short that it will never match the impedance of the EED to that of the antenna. The equivalent circuit is shown in Figure B-5b. The antenna, which is modeled by a voltage generator (V_{oc}) in series with the capacitance of the antenna (C_{ant}), is connected directly to the EED impedance. The radiation resistance and the inductance of the antenna are negligible at low frequencies. The curve is governed for small ω by the equation:

$$E_{inc} = \frac{1}{h}\sqrt{\frac{P_t}{R_L}}\left[(R_L)^2 + \left(\frac{1}{\omega C_{ant}}\right)^2\right]^{1/2} \; V/m \;,$$

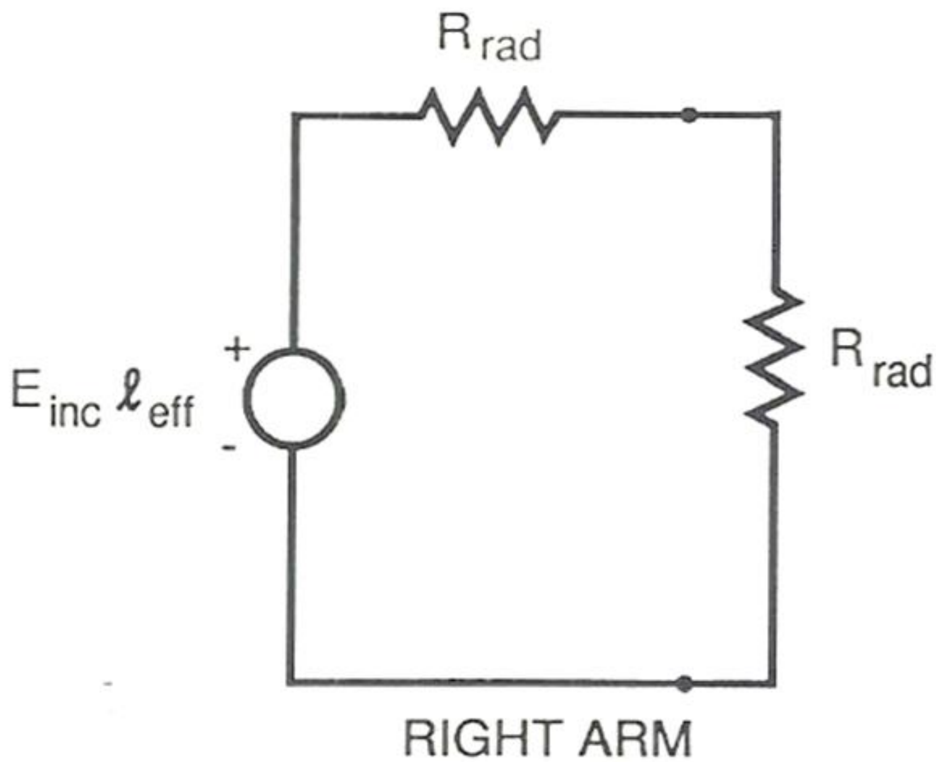

Figure B-5a. The equivalent circuit for the right arm of the V-Curve.

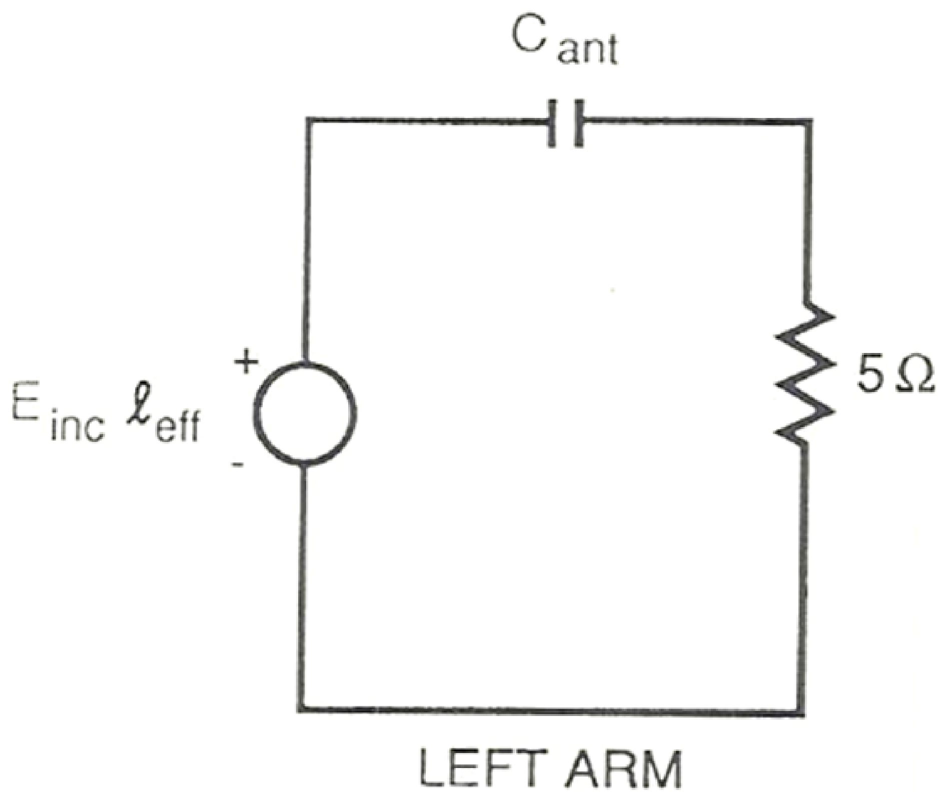

Figure B-5b. The equivalent circuit for the left arm of the V-Curve.

It can be seen, therefore, that the allowed strength of the incident field decreases with frequency at the rate of 6 decibels per octave. The left-hand portion is only fixed in slope (it is taken to vary as l/ω) because, even at low frequencies, the inductance of the transmission line begins to cancel the capacitance of the antenna, and the power delivered to the EED is greater than that indicated by the above equation. It remains to determine, therefore, the y intercept of the left arm, or equivalently, where in frequency the curve transitions from the left to right arm. Through experimentation with the more rigorous models shown below, this frequency is determined to be the smaller of the two frequencies (a) where the transmission line is one-fourth of a wavelength long, as measured in Teflon, or (b) where $f = 1/(2\pi\ L_{ant}\ C_{ant})$.

Short Dipole with Transmission Line

For the short-dipole with transmission line model, the antenna is again a short dipole. The impedance presented to the antenna is represented by the transfer of load impedance using the transmission line formula, i.e.,

$$Z_{in} \;=\; Z_o \frac{R_L \cos \beta\ell_{t\ell} \;+ jZ_o \sin \beta\ell_{t\ell}}{Z_o \cos \beta\ell_{t\ell} \;+ jR_L \sin \beta\ell_{t\ell}} \quad ohms \;\;,$$

where

$$\beta \;=\; \omega \sqrt{\mu_o \varepsilon_o \varepsilon_r} \quad .$$

The circuit is shown in Figure B-6. The curves generated are governed by the equation

$$E_{inc} \;=\; \frac{1}{h} \sqrt{\frac{P_t}{R_{in}}} \left[(R_{rad} + R_{in})^2 + \left(\frac{\omega X_{in} C_{ant} - 1 + \omega^2 L_{ant} C_{ant}}{\omega C_{ant}} \right)^2 \right]^{1/2} \quad V/m \;\;,$$

where

R_{in} is the real part of Z_{in} and X_{in} is the imaginary part of Z_{in}.

The values predicted by this model are inaccurate if the dipole becomes much longer than half a wavelength.

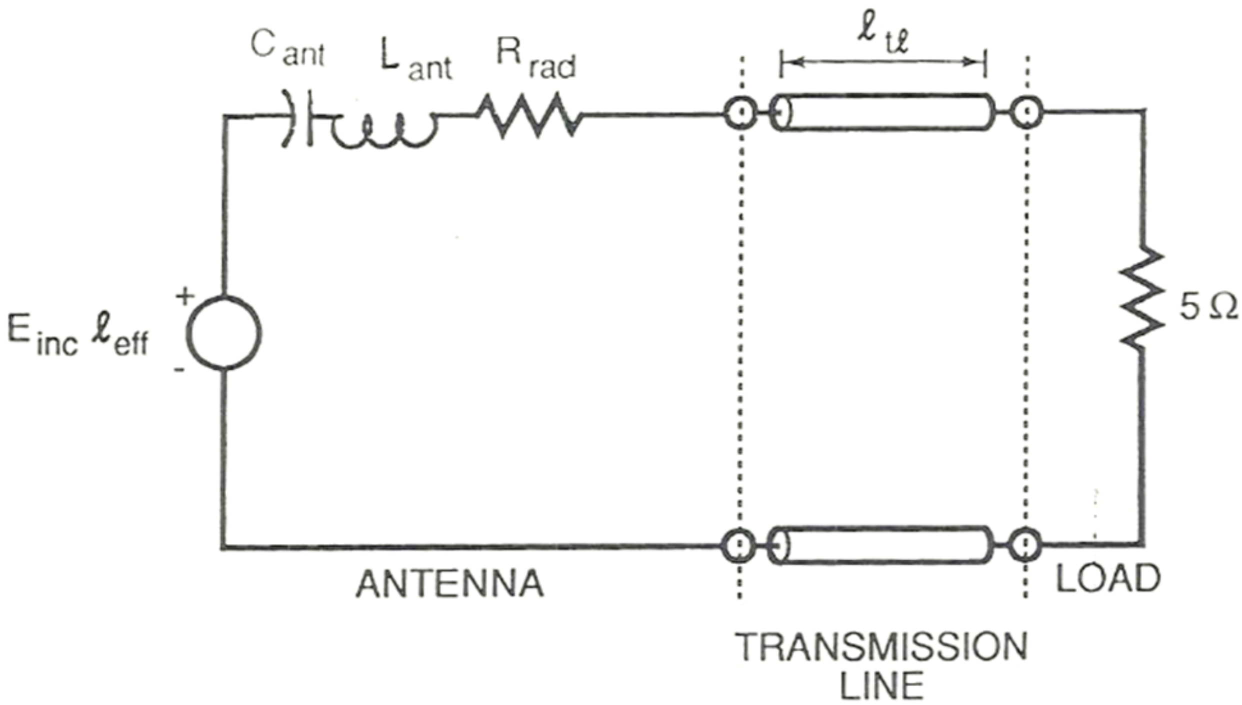

Figure B-6. The equivalent circuit for a short dipole connected to the EED through a transmission line.

Long Dipole with Transmission Line

The long-dipole with transmission line model is the most rigorous of all the models examined. The impedance presented to the antenna is calculated using the transmission line formula used in the "Short Dipole with Transmission Line" model discussed above. The dipole is modeled more rigorously than in previous calculations so that the dipole can be several wavelengths long and can be fed asymmetrically. The quantities such as the impedance of the antenna and antenna pattern are derived from a Weiner-Hopf calculation and are discussed in Appendix I of this memorandum. As the antenna increases in electrical length, the main beam of the antenna shifts from being broadside to the antenna axis to an angle closer to the axis of the antenna. The amount of voltage available at the antenna terminals must be maximized by scanning the incident field over all possible incident angles ($0 < \theta_i < \pi$). The circuit that results from these calculations is shown in Figure B-7. The formula for the curve is given as

$$E_{inc} = \sqrt{\frac{P_t}{R_{in}}} \frac{|Z_{in} + Z_{ant}|}{|J_a^R(\theta_i\ ,\ z_{FP})_{max} Z_{ant}|} \quad V/m \quad ,$$

where Z_{ant} is the impedance of the antenna. $J_a^R(\theta_i\ , z_{FP})_{max}$ is the maximum current at the feed point z_{FP} for all possible incident angles. This model for the dipole is not valid when the dipole is less than 0.12 wavelength long because the Wiener-Hopf derivation is based on calculations for semi-infinite antennas.

Resonant Dipole, No Transmission Line

The resonant- dipole, no transmission line model traditionally has been used to calculate the bounds on the incident electric field. The resulting curve is the same form as the V-Curve, but the levels predicted and the break frequency between the left and right arms are different. The right arm is calculated by using the model in Figure B-8. The physical length of the dipole is changed with frequency so that it is always a half wavelength long. The dipole is connected directly to the EED with no intervening transmission line. The resulting curve is governed by the equation

$$E_{inc} = \frac{4f}{1.273\ V_c} \sqrt{\frac{P_t}{R_L}}\ (R_{rad} + R_L) \quad V/m \quad ,$$

where R_{rad} is the radiation resistance (73 ohms) of the half- wave dipole, f is the frequency, and V_c is the speed of light. This arm increases with frequency at the rate of 6 decibels per octave.

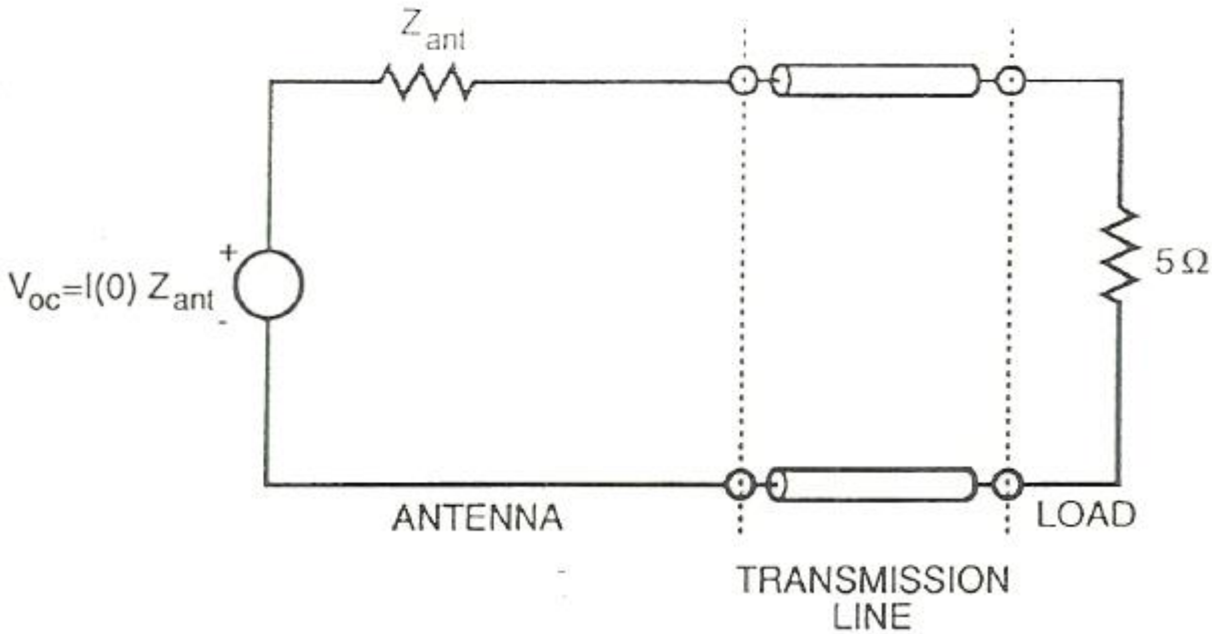

Figure B-7. The equivalent circuit for a long dipole connected to the EED through a transmission line. (The long dipole is modeled using a Wiener-Hopf approach.)

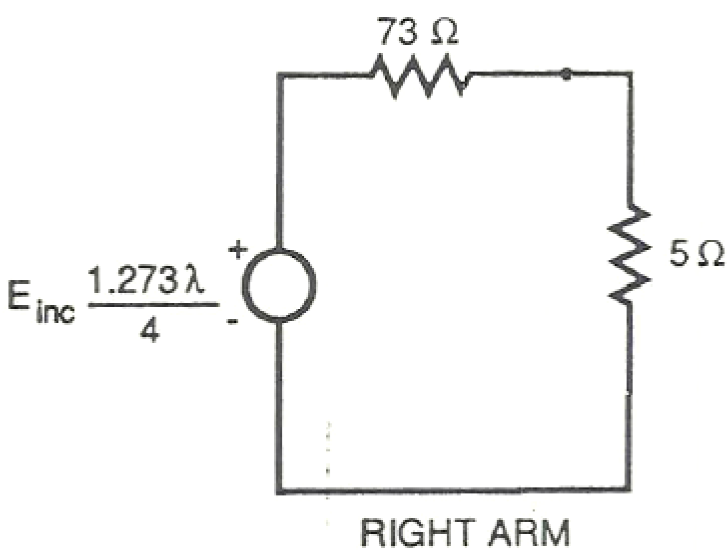

Figure B-8. The equivalent circuit for the right arm of the presently used model.

The left arm of the curve decreases with frequency at the rate of 6 decibels per octave and is generated just like the left arm of the V-Curve. The only remaining task is to pick the frequency at which the curve transitions from the left to the right arm. This point is chosen at the frequency at which the original length of the dipole is a half wavelength. So, whereas the transition frequency in the V-Curve depends on the length of the transmission line, the transition frequency in the traditional curve depends on the length of the dipole. Since there is no transmission line in this model, there is no matching between the antenna and the EED. This fact causes the bounds predicted by this model to be too liberal.

Results

Figure B-9 through Figure B-12 show plots of the bound on the electric field intensity as a function of frequency on a log-log scale as calculated by each of the first four models. The half-length of the dipole is fixed at 0.1 meter and the transmission line length is varied through the values 0.01, 0.1, 0.2, and 0.5 meter. In all cases, the V-Curve bounds the other three curves from below. The transition frequency for the V-Curve in Figure B-9 is equal to the frequency at which the dipole resonates since the dipole resonates at a lower frequency than the frequency at which the 0.01 meter transmission line is a quarter wavelength long. As the transmission line length increases (Figure B-10 through Figure B-12), the transition frequency is set at the point at which the transmission line length is a quarter wavelength. The short-dipole, no transmission line model provides a greatest upper bound on the field intensity and is therefore unsatisfactory. The bounds predicted by the models with transmission lines oscillate between the values set by the no transmission line model and the V-Curve as the transmission line matches and mismatches the load to the antenna.

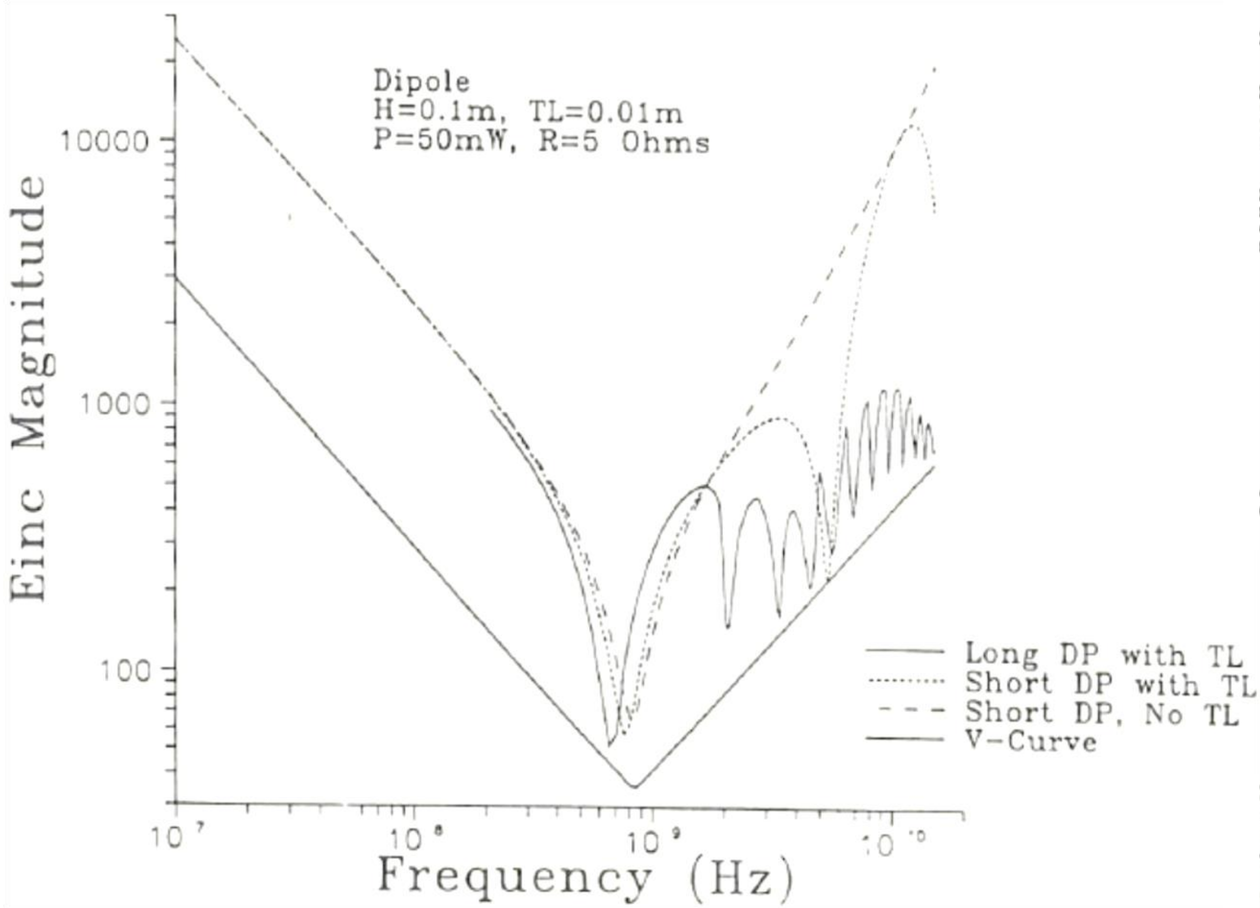

Figure B-9. Curve showing the bound on the E field as a function of frequency as predicted by four different mathematical descriptions of Figure B-2. The dipole half-length is 0.1 meter. The length of the transmission line is 0.01 meter. The load is a 50-mA, no-fire EED.

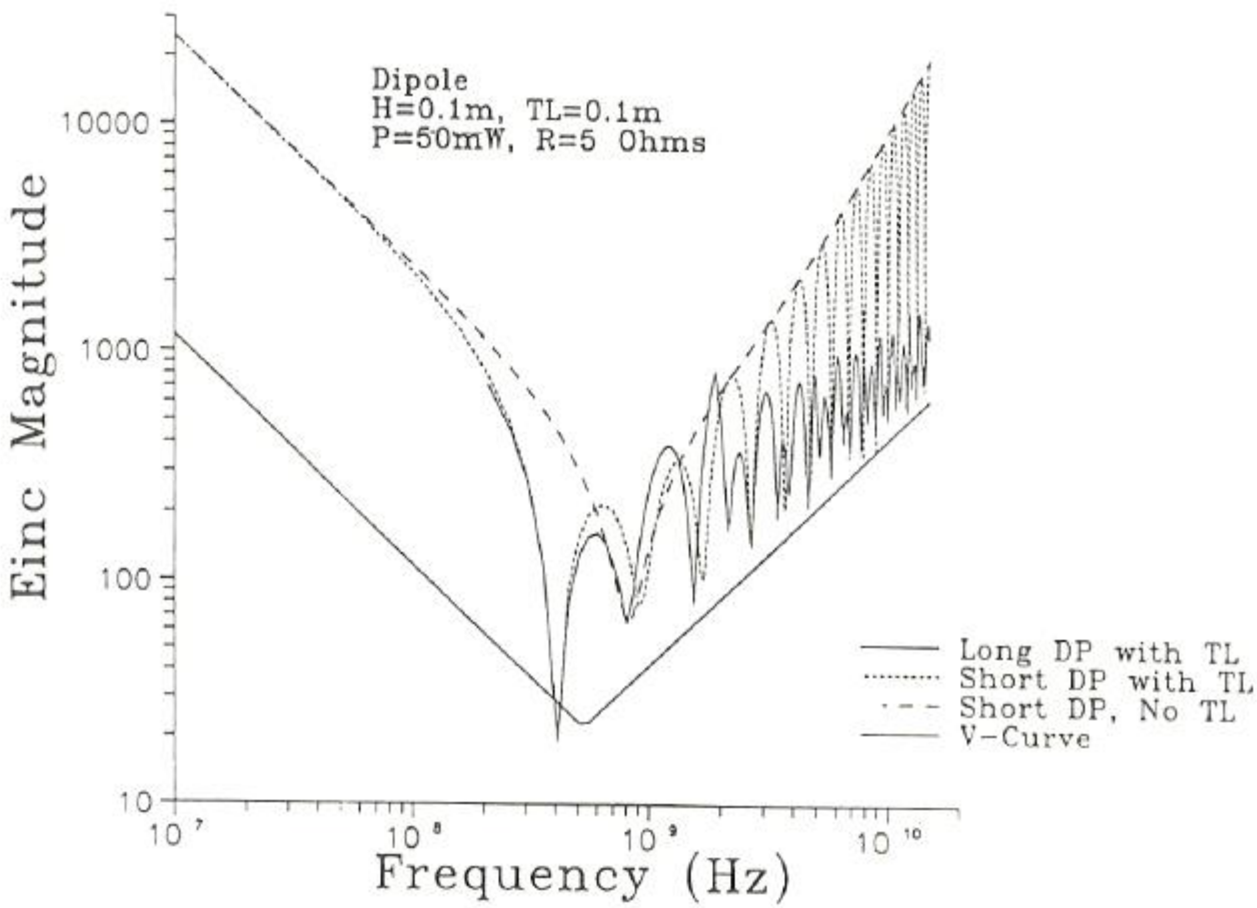

Figure B-10. Same as Figure B-9 except the transmission line length is 0.1 meter.

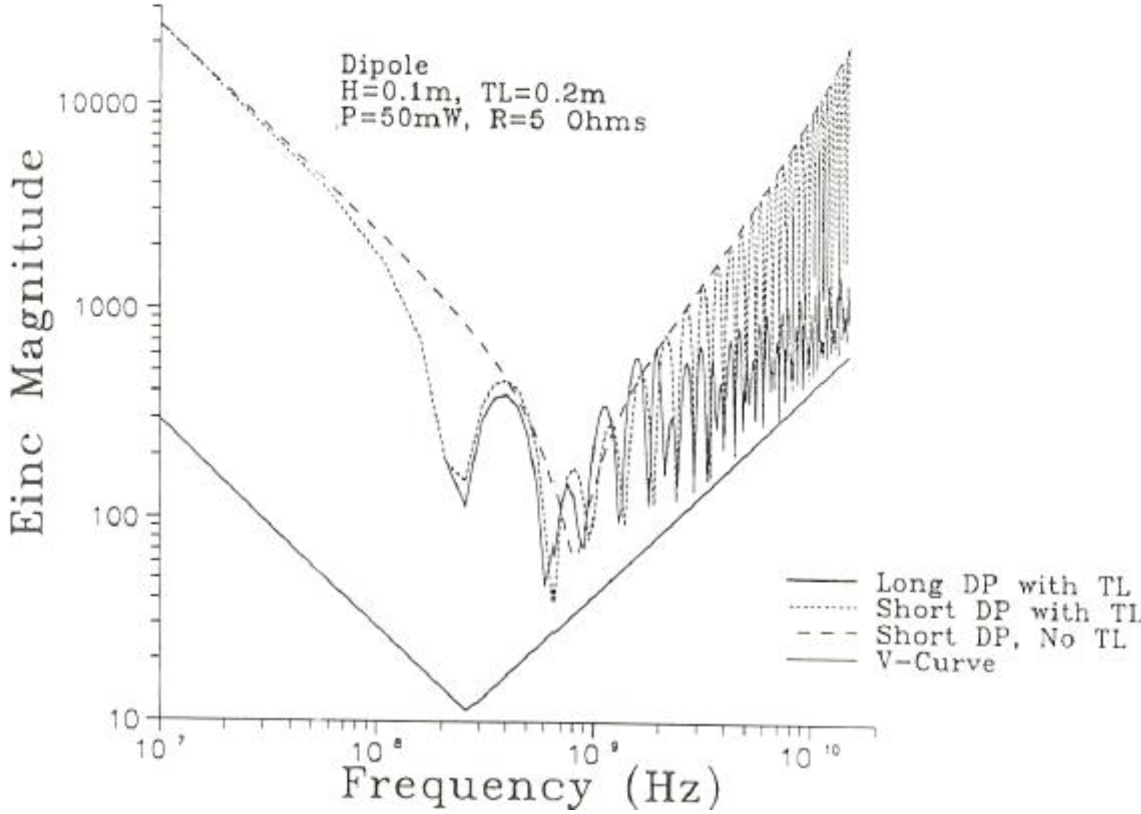

Figure B-11. Same as Figure B-9 except the transmission line length is 0.2 meter.

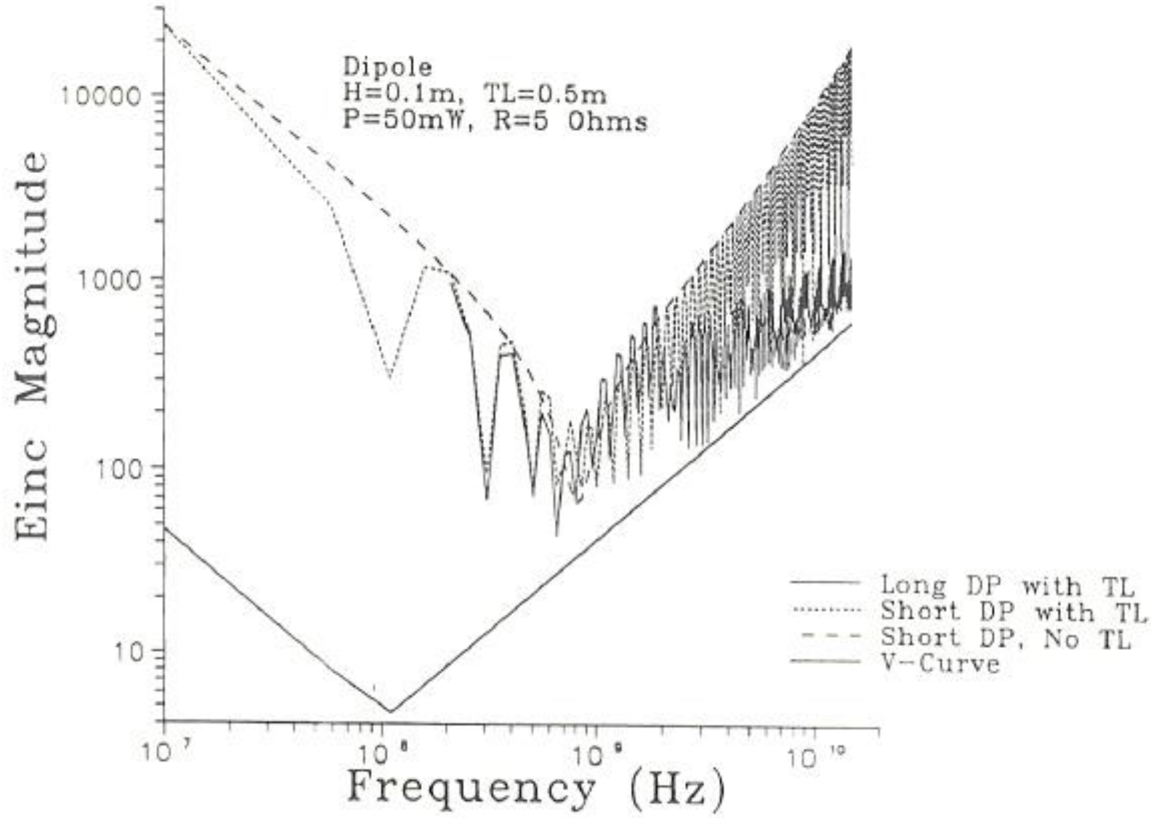

Figure B-12. Same as Figure B-9 except the transmission line length is 0.5 meter.

If the dipole becomes electrically too long, as shown in Figure B-13 and Figure B-14, the V-Curve model begins to break down. The maximum electric field predicted by the more exact long dipole model falls below that predicted by the V-Curve. This is an area for future study. It must be pointed out, however, that the failure of the V-Curve model is not drastic and that it can be used with a high degree of confidence as long as the dipole length is less than six wavelengths.

Figure B-15 shows the effect of varying the position of the antenna feed from center-fed to being fed halfway between the center and the end of the dipole. The figure shows results for a typical case when the dipole has a half-length of 0.1 meter. The position of the peaks and valleys shifts in frequency, but the overall trend remains unchanged. It can be concluded, therefore, that the V-Curve provides a suitable bound for both symmetrically and asymmetrically fed dipoles.

Figure B-16 compares the V-Curve predicted bounds to those predicted by the present model (half-wave dipole, no transmission line). Although both models are similar in shape, the levels predicted by the present model are greater than both the V-Curve and the more exact short dipole with transmission line model at the frequencies where the transmission line performs a matching function. This indicates that the effect of the transmission line must be accounted for in order to obtain a safe bound.

Figure B-17 and Figure B-18 show the safe radius as a function of frequency predicted by the V-Curve and the current model. A 1-W transmitter having an antenna with a gain of 3.5 would have to stay outside this radius to keep the field strength at the EED below the safe level. Figure B-17 is the curve for a 100-mA, 5-ohm no-fire EED and Figure B-18 is for a 1-A, 1-ohm no-fire EED. The safe distance predicted by the V-Curve is an order of magnitude greater than that predicted by the present model. All models used for this analysis are far-field models, which mean that the characteristics of the transmitting and receiving antenna are not affected by the proximity of each other. This assumption breaks down when the half-length of the dipole is 1.5 meters and the distance between antennas is less than a meter. The effect of being in the near-field of the dipole is an area of further study.

Conclusions

The present model used in setting a bound on the field intensity and, consequently, the minimum transmitter standoff distance allowed near a damaged weapon is not conservative enough. The V-Curve, on the other hand, provides conservative, yet realistic bounds for all cases unless the length of the dipole becomes greater than six wavelengths. We recommend using the V-Curve, which is as simple to construct as the presently used model and provides a safer bound than this model.

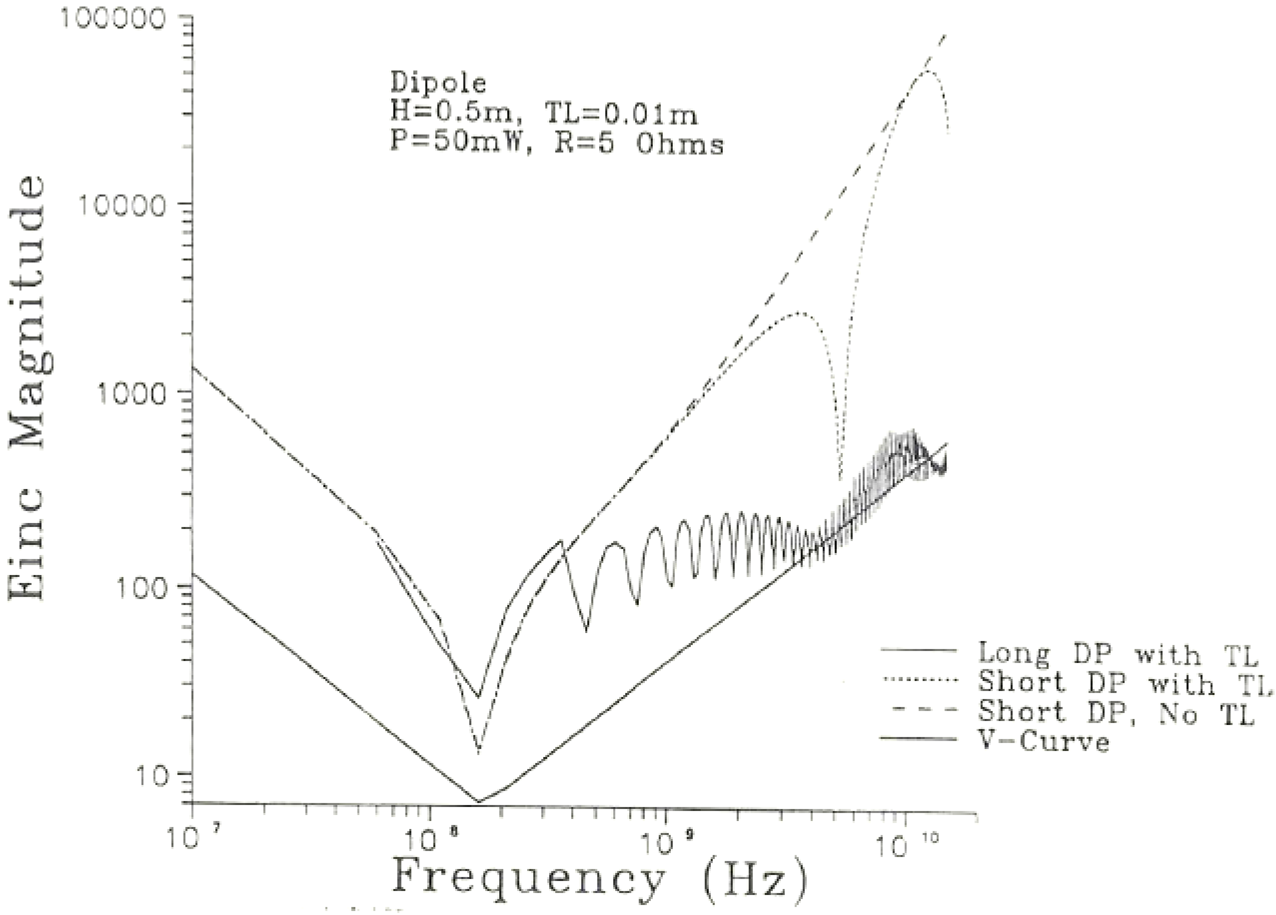

Figure B-13. Same as Figure B-9 except the dipole half-length is 0.5 meter. The E field bound predicted by the more exact long-dipole with transmission line model is less than that predicted by the V-Curve when the dipole length becomes greater than six wavelengths.

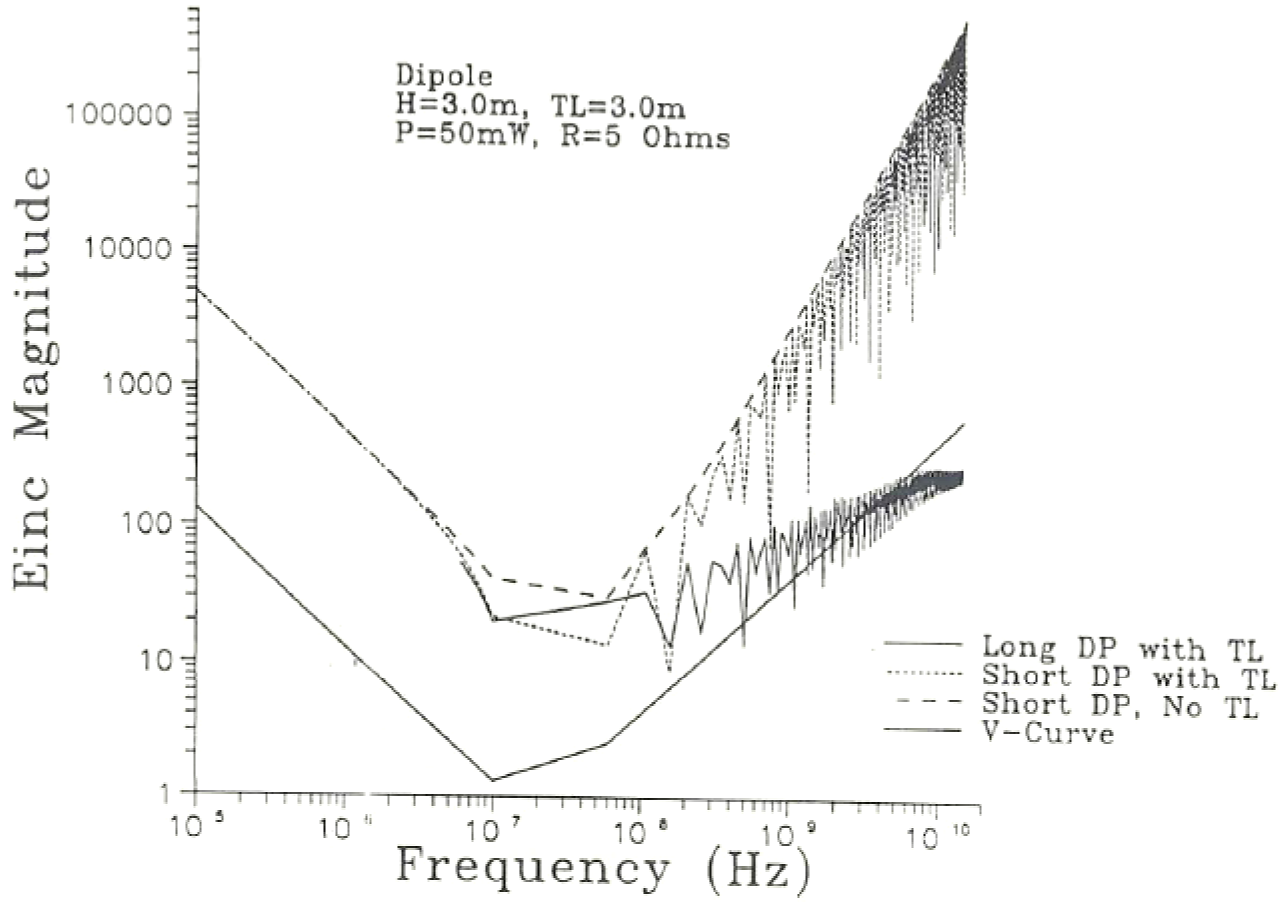

Figure B-14. Same as Figure B-13 except the transmission line is 0.1 meter long. Again, the E field bound predicted by the long-dipole model falls below that predicted by the V-Curve.

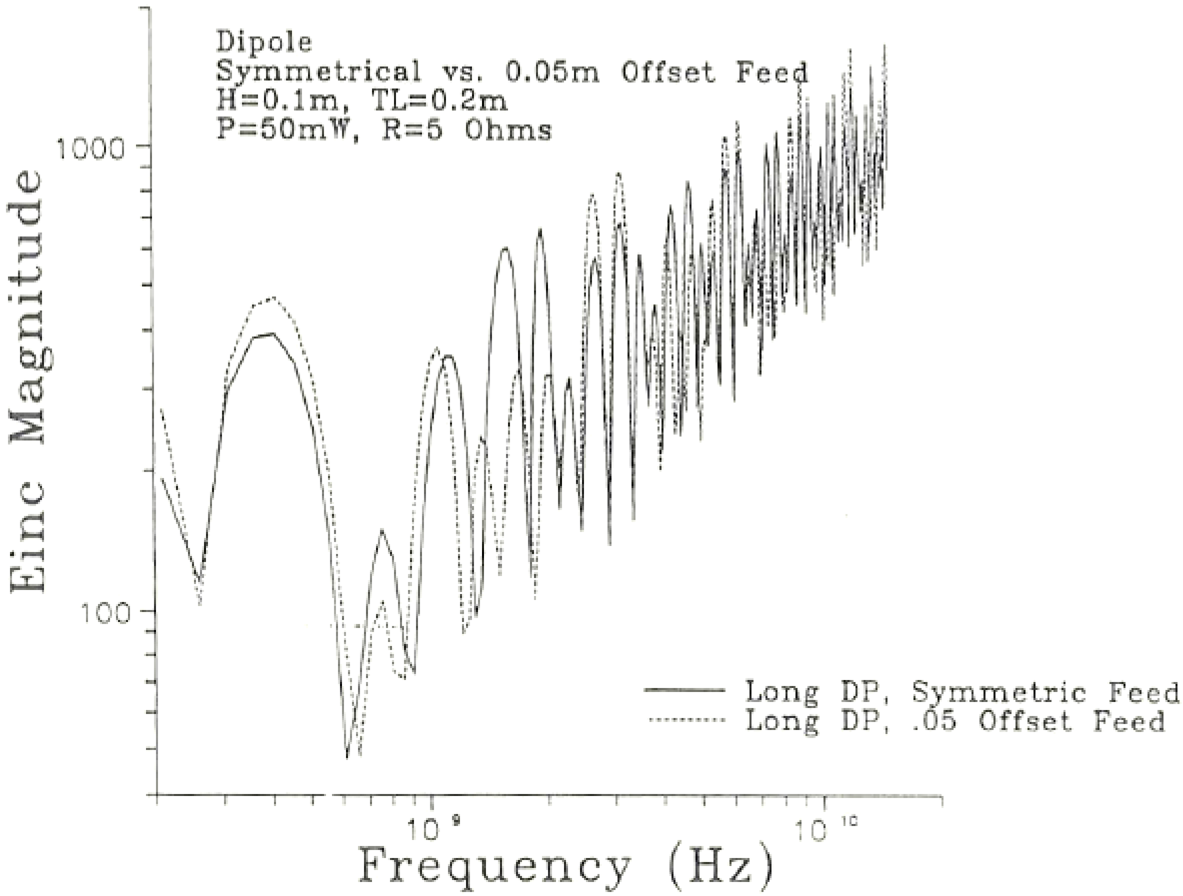

Figure B-15. Comparison of the E field predicted by the long dipole model for dipoles that are center-fed and dipoles that are asymmetrically fed. The overall bound level is the same although the positions in frequency of the peaks and valleys are shifted.

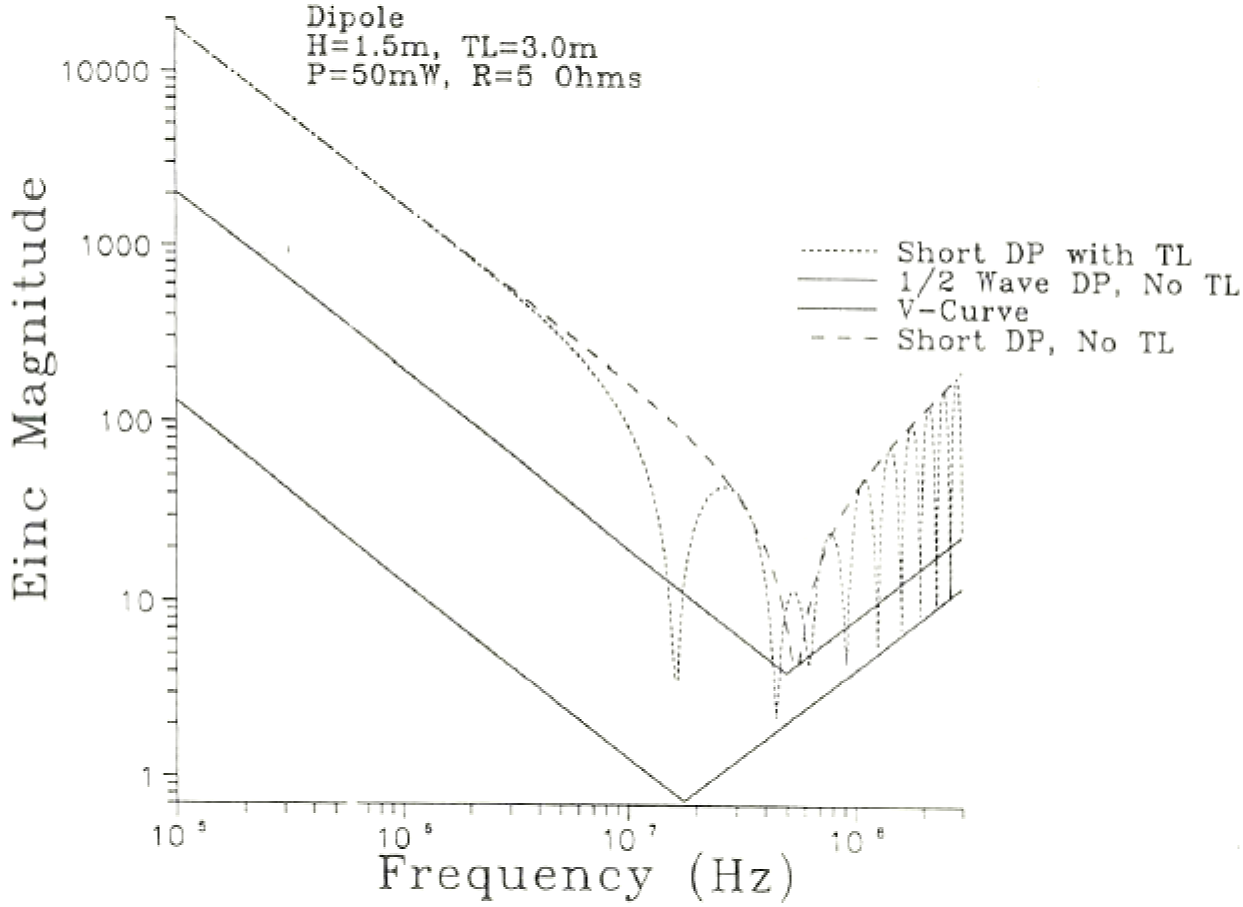

Figure B-16. Bounds predicted by the present model (resonant dipole, no transmission line) compared to those predicted by the V-Curve and the more exact short-dipole with transmission line model. The half-length of the dipole is 1.5 meters, the transmission line is 3.0 meters long, and the EED is a 100-mA, 5-ohm no-fire.

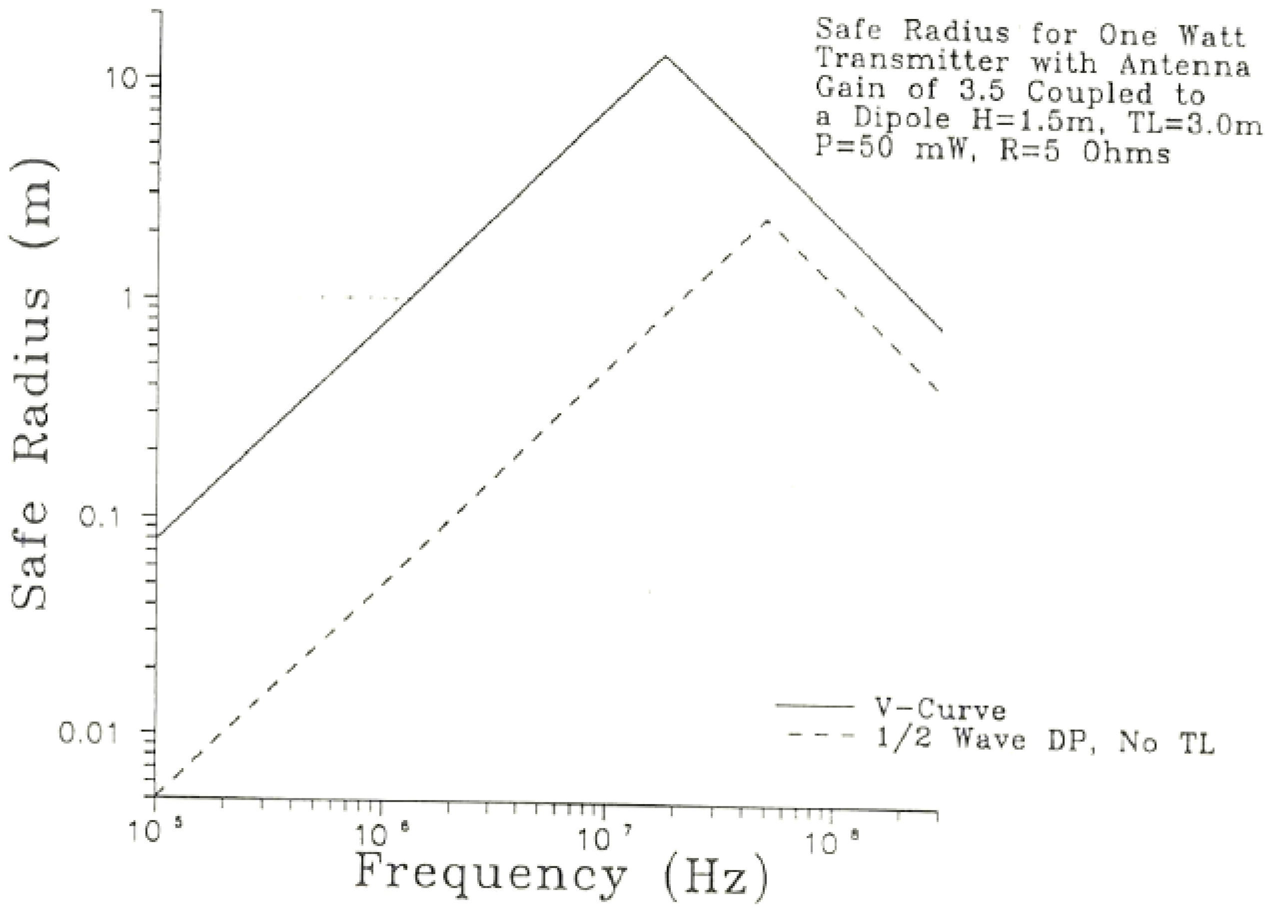

Figure B-17. The safe radius versus frequency as predicted by the present model (resonant dipole, no transmission line) compared to that predicted by the V-Curve for the same situation as Figure B-16. The transmitting antenna has an output power of 1 W into an antenna having a gain of 3.5.

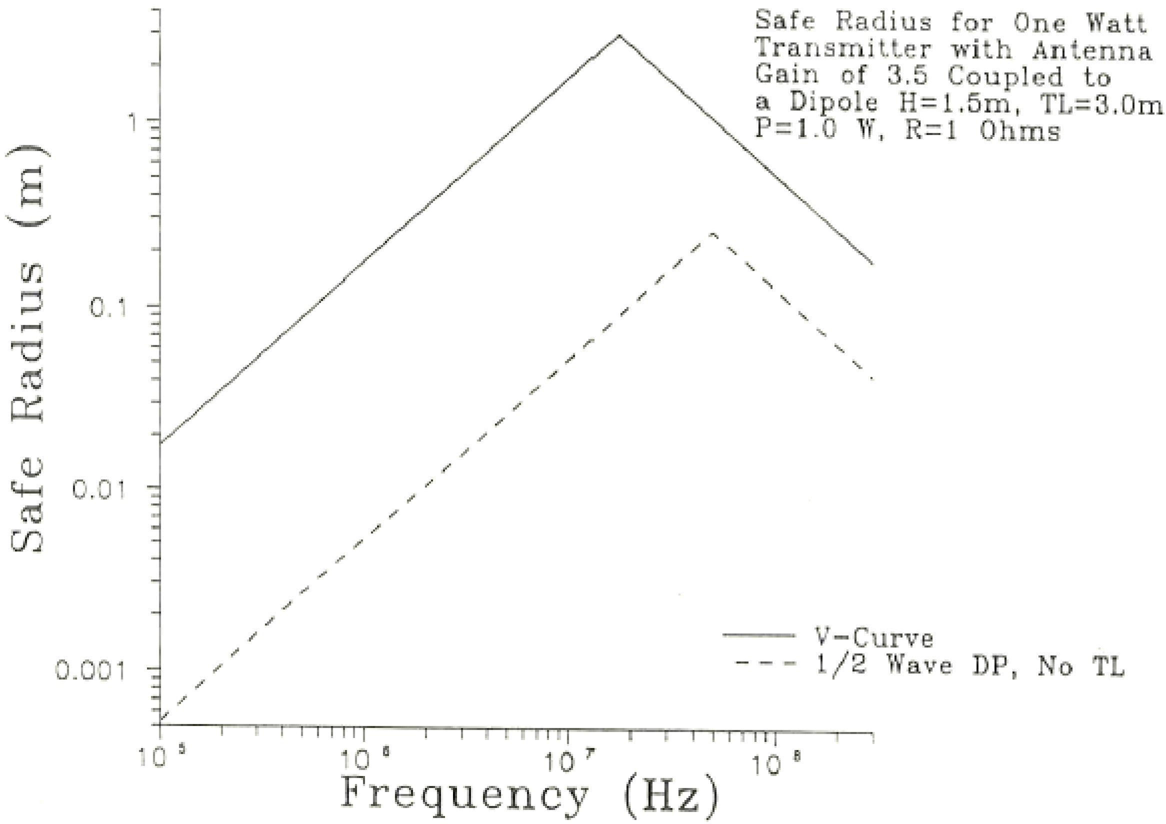

Figure B-18. Same as Figure B-17 except the EED is a 1-A, 1-ohm no-fire device.

References

[1] R. L. Parker, "Origin and Application of the 'V' Curve" , unpublished Sandia National Laboratories report.

[2] E. C. Jordan and K. G. Balmain, Electromagnetic Waves and Radiating Systems, Englewood Cliffs, NJ: Prentice Hall, 1968, Ch. 10, 11.

[3] L. W. Rispin and D. C. Chang, Antenna Handbook, Y. T. Lou and S. W. Lee, ed., New York: Van Nostrand Reinhold, 1988, Ch. 7.

[4] A. F. Regulation 127-100, Explosives Safety Standards, Washington, DC: Dept. of Air Force, 20 May 1983, Ch. 6.

[5] NAVORD OP 3565/NAVAIR 16-1- 529, Washington, DC: Dept. of Navy, 4th Revision, Ch. 3.

[6] L. K. Warne, Division 7553, Sandia National Laboratories Albuquerque, Memorandum to T. S. Edrington, 5 August 1988.

Appendix I
Short and Long Dipole Calculations

The short dipole is characterized by an open circuit voltage in series with a resistance, capacitance, and inductance. These quantities are defined as

$$V_{oc} = E_{inc}\ell_{eff} = E_{inc}h \quad \text{volts}$$

$$R_{rad} = 197.4\left(\frac{2hf}{V_c}\right)^2 \quad \text{ohms}$$

$$C_{ant} = \frac{\pi\epsilon_o 2h}{(\Omega - 2 - 2\ln 2)} \quad \text{farads}$$

$$L_{ant} = \frac{\mu_o h}{3\pi}\left(\ln\left(\frac{2h}{a}\right) - \frac{11}{6}\right) \quad \text{henries}$$

Note that the current distribution along the dipole is in the form of a triangle that is maximum at the feed point and zero at the ends of the dipole. ℓ_{eff} is the effective length of the antenna, μ_o is the magnetic permeability of free-space, and ε_o is the electric permittivity of free space.

The current on the long dipole as a function of distance is calculated by launching a primary current on the antenna that is the same as the current existing on a similarly excited infinite, thin-wire antenna, i.e.,

$$U_a^s(|z - z_o|) = \frac{-j}{\eta_o} e^{-jk_o|z-z_o|} \ln\left\{1 + \frac{j2\pi}{2C_a + \gamma - j3\pi/2 + \ln\left[k_o|z - z_o| + \left(k_o^{\,2}|z - z_0|^2 + e^{-2\gamma}\right)^{1/2}\right]}\right\}$$

where k_o *is* the free-space wave number, η_o is the impedance of free-space,

$$C_a = -\ln(k_o a) - \gamma \quad \text{, and}$$

$$\gamma = 0.577 \quad \text{is the Euler constant.}$$

When the primary currents hit the end of the dipole, they are reflected back in the opposite direction. The form of the reflected currents can be obtained by applying a

Wiener-Hopf analysis to a wave incident on a semi-infinite antenna from its end. This gives the reflected current as

$$U_a(z) = \frac{2\pi}{\eta_o} \frac{e^{-jk_o z}}{2C_a + \gamma - {j\pi}/{2} + \ln(2k_o z) + e^{j2k_o z} E_1(j2k_o z)}$$

where

$$R_a = \frac{\eta_o}{2\pi}(2C_a - j\pi)/(1+\delta_a)^2$$

$$\delta_a = Re\left\{\frac{-j}{2\pi}\ln\left(1 + \frac{j2\pi}{2C_a - j3\pi/2}\right) - \frac{1}{2C_a - j\pi + \ln 2}\right\}$$

and E_1 is the exponential integral of the first kind.

These currents continue to reflect back and forth off the ends of the antenna to give two series, which can be summed to obtain the total current at z due to an applied unit voltage at z_o, i. e.,

$$J_a^T(z;z_o) = U_a^S(|z - z_o|) - Q_a^T(h)R_a U_a(h-z) - Q_a^T(-h)R_a U_a(h+z) \quad ,$$

$$\text{for } -h < z < h \quad ,$$

where

$$Q_a^T(\pm h) = [U_a^S(h \pm z_o) - U_a^S(h \pm z_o)R_a U_a(2h)]/\Delta(h)$$

and

$$\Delta(h) = 1 - {R_a}^2 {U_a}^2(2h) \quad .$$

The input admittance of the antenna will be

$$Y_{ant} = {Z_{ant}}^{-1} = {J_a}^T(z_o, z_o) \quad .$$

Using the above current distribution, the far field pattern as a function of the angle off the antenna axis (θ_i) and the feed point z_o is

$$F(\theta_i; z_o) \; = \; \left(\frac{j2\pi}{k_o\eta_o}\right)\{e^{jk_o z_o \cos\theta_i}[W_a(h+z_o;\theta_i) + W_a(h-z_o;\pi-\theta_i)]$$

$$- R_a\big[e^{jk_o h\cos\theta_i}\, Q_a^T(h)\, W_a(2h;\theta_i)$$

$$+ e^{-jk_o h\cos\theta_i}\, Q_a^T(-h)\, W_a(2h;\pi-\theta_i)]\}$$

where

$$W_a(z;\theta_i) \; = \; \frac{1}{1+\cos\theta_i}\left[\frac{e^{-jk_o z(1+\cos\theta_i)}}{2C_a - j\pi/2 + \gamma + P(\theta_i; z)}\right.$$

$$\left. - \frac{1}{2C_a - j\pi - 2\csc^2(\theta_i/2)\ \ln(\cos(\theta_i/2))}\right]$$

and

$$P(\theta_i; z) \; = \; \ln(2k_o z) + \csc^2(\theta_i/2)\, e^{jk_o z(1+\cos\theta_i)}\, E_1(jk_o z[1+\cos\theta_i])$$

$$- \cot^2(\theta_i/2)\, e^{j2k_o z}\, E_1(j2k_o z) \quad .$$

E_1 is again the exponential integral of the first kind.

The above expression leads to a received current at the feed point z_o due to an incident plane wave having an electric field intensity of 1 V/m and having a propagation vector that makes an angle of θ_i with respect to the antenna axis, i.e.,

$$J_a^R(\theta_i, z_o) \; = \; \sin\theta_i\, F(\pi-\theta_i, z_0) \qquad 0 \; < \; \theta_i \; < \; \pi \quad .$$

The incident angle θ_i must be found that maximizes this current.

Appendix II
Safe Distance Tables

Safe distance must be maintained between mobile (including hand-portable) radio equipment and weapons involved in accidents to ensure that no weapon EEDs are initiated. Guidance provided below is based on the V-Curve calculations for a transmission line length of 3 meters (10 feet), which has been selected as an upper-bound length for exposed weapon wiring. The transmission line is connected to a monopole. The transmitter is assumed to have all its power transmitted through a short monopole antenna. Older EEDs have 4.5-ohm bridgewires and 100% no-fire current ratings of 100 mA. More modern EEDs have l-ohm bridgewires and no-fire current ratings of 1 A.

To use Tables 1 and 2, transmitter power and operating frequency of mobile communication equipment must be known. If the type of EED in the weapon is not known, the distance scale for 4.5-ohm, 100-mA devices should be used (Table 1). If neither the type of EED nor the power and frequency of the mobile equipment are known, a minimum distance of 378 meters (1260 feet) would be prudent. Observe safe distance until exposed wiring has been effectively shielded.

Table 1. 4.5-Ohm, 100-mA No-Fire Device (Distance in Meters)

Transmitter Power	Frequency (MHz)							
(Watts)	1	2	5	10	20	50	100	300
1				10.8	16.9	6.8	3.4	1.2
2				15.3	23.9	9.5	4.8	1.6
5				24.2	37.7	15.1	7.5	2.5
10				34.2	53.3	21.3	10.7	3.6
20			24.2	48.3	75.4	30.2	15.1	5.0
50			38.2	76.4	119.3	47.7	23.9	8.0
100		21.6	54.0	108.1	168.7	67.5	33.7	11.2
200		30.6	76.4	152.9	238.6	95.4	47.7	15.9
500	24.2	48.3	120.9	241.7	377.8	150.9	75.4	25.1

Table 2. 1-Ohm, 1-A No-Fire Device (Distance in Meters)

Transmitter Power	Frequency (MHz)							
(Watts)	1	2	5	10	20	50	100	300
1				2.3	3.6	1.4	0.8	0.3
2				3.2	5.1	2.0	1.0	0.4
5				5.1	8.0	3.2	1.6	0.5
10				7.3	11.3	4.5	2.3	0.8
20			5.1	10.3	16.0	6.4	3.2	1.1
50			8.1	16.2	25.3	10.1	5.1	1.7
100		4.6	11.5	22.9	35.8	14.3	7.2	2.4
200		6.4	16.2	32.4	50.6	20.2	10.1	3.4
500	5.1	10.3	25.6	51.3	80.0	32.0	16.0	5.3

Copy to:

5111	D. N. Bray
5113	R. W. Jorgensen
5114	W. D. Ulrich
5122	J. N. Baker
5126	W. D. Chadwick
5127	M. J. Eaton
5128	B. E. Bader
5131	G. N. Beeler, Act'g.
5132	S. D. Meyer
5133	G. H. Whiting
5141	C. A. Harris
5143	R. D. Robinett
5144	D. E. Ryerson
5145	D. H. Schroeder
5147	G. L. Maxam
5151	W. C. Nickell
5153	S. L. Jeffers
5154	R. L. Alvis
7212	J. W. Mead
7231	H. D. Bickelman
7550	R. A. David
7554	L. D. Scott
7555	B. Boverie
8131	W. R. Bolton
8132	A. S. Rivenes
8133	A. C. Skinrood
8134	M. H. Rogers
8154	D. J. Havlik
8155	R. G. Miller
8156	M. E. John
8161	M. H. Reynolds
8162	C. T. Yokomizo
8163	W. G. Wilson
7553	M. E. Morris
7553	R. E. Jorgenson
7553	L. K. Warne

Appendix C 1991 Memorandum to Marvin Morris

Date: January 29, 1991

To: M. E. Morris, 7553

Larry Warne

From: L. K. Warne, 7553

Subject: Matched Receiving Antenna Inside a Cavity Resonator

Introduction

This memo considers the question of whether the usual "V curve" requirement, based on a matched dipole antenna in an infinite free space, is applicable to the interior of a cavity formed, for example, by the walls of a building or the exterior case of a weapon system (The "V curve" is primarily used to set the allowable electromagnetic field levels in assembly areas where cabling is attached to hotwire electroexplosive devices.). A simple canonical spherical problem is used to yield closed form solutions for this simple special case. It is found that there can be significant reductions in the real part of the dipole input impedance resulting in significant increases in received power.

Short Dipole in an Infinite Free Space:

The typical "V curve" requirement is based on a resonant matched dipole model. However, an electrically short dipole leads to very similar results and is much simpler to treat in the current problem. Figure C-1 shows a circuit model for a center-driven electrically-short dipole of length 2 dh and radius a. The circuit elements are

$$R_{ant} = R_{rad} \approx \frac{\eta_o}{6\pi}(k\,dh)^2 \quad , \tag{1}$$

$$C_{ant} \approx \frac{2\pi\epsilon_o\,dh}{\Omega - 2 - 2\ln 2} \quad , \tag{2}$$

$$V_{oc} \approx E_o\,dh \quad , \tag{3}$$

where $\Omega = 2\ln(2\,dh/a)$ is the antenna fatness parameter, E_o is the incident field at the location of the antenna (in rms units), $\eta_o = \sqrt{\mu_o/\epsilon_o} \approx 120\pi$ ohms is the free space impedance, $k = \omega\sqrt{\mu_o\epsilon_o}$ *is* the wavenumber, ϵ_o is the permittivity of free space, and μ_o is the permeability of free space. The load, in the matched case for maximum power transfer, is taken to have $\omega L_{ld} = 1/(\omega\, C_{ant})$ and $R_{ld} = R_{ant}$. The power received by the load in the matched case is thus

$$P_{rec} = |V_{oc}|^2/(4R_{ant}) \quad . \tag{4}$$

Obviously the minimum value that R_{ant} attains is important in determining a bound for P_{rec}. Using (1) and (2) in (4) and noting $k = 2\pi/\lambda$, where λ is the free space wavelength, we obtain the familiar result from antenna theory

$$P_{rec} = \frac{\lambda^2}{4\pi} G\,|E_o|^2/\eta_o \quad , \tag{5}$$

where the directivity gain of a short dipole antenna is $G = 3/2$.

Short Dipole in a Spherical Resonant Cavity:

We now consider the short dipole when placed at the center of a spherical enclosure of radius b as shown in Figure C-2. The walls of the enclosure are lossy and are described by the impedance boundary condition

$$\underline{n} \; x \; \underline{E} = Z_s \; \underline{n} \; x \; \underline{n} \; x \; \underline{H} \quad , \tag{6}$$

where $\underline{n}$ is the unit inward normal to the sphere, $\underline{E}$ is the electric field vector, $\underline{H}$ is the magnetic field vector, and Z_s is the surface impedance. The dipole current density $\underline{J}$ is approximately

$$\underline{J} = I \, \delta(x) \, \delta(y) \, f(dh - |z|)/dh \; \underline{e}_z \quad , \tag{7}$$

where I is the current amplitude at the center, δ(x) is the delta function, $\underline{e}_z$ is a unit vector in the z direction, f(u) = u for u > 0 and f(u) = 0 for u < 0. In the limit as k dh, dh/b → 0 we can take

$$\underline{J} = I \, dh \, \delta(\underline{r}) \; \underline{e}_z \; , \tag{8}$$

where $\underline{r}$ is the three dimensional position vector.

The source vector potential (time dependence $e^{-i\omega t}$ is used throughout) in free space is

$$\underline{A}^s(\underline{r}) \; = \; \mu_o \int_V \; \underline{J}\,(\underline{r'}) \; \frac{e^{ik|\underline{r} - \underline{r'}|}}{4\pi \; |\underline{r} - \underline{r'}|} \; dV' \quad . \tag{9}$$

The potential in this case only has a z component and is given for r > > dh by

$$A_z^s \; = \; \mu_o \; I \; dh \; \frac{e^{ikr}}{4\pi r} \quad . \tag{10}$$

Using $\nabla \; x \; \underline{A} \; = \; \mu_o \underline{H}$ we obtain

$$H_\varphi^s = I\, dh\, \frac{e^{ikr}}{4\pi r} \left(-ik + \frac{1}{r}\right) \sin\theta \quad , \tag{11}$$

where r, θ, φ are the usual spherical coordinates. Using $\nabla\, x\, \underline{H} = -i\omega\epsilon_o \underline{E}$ we obtain

$$-i\omega\epsilon_o E_\theta^s = I\, dh\, \frac{e^{ikr}}{4\pi r} \left(-k^2 - \frac{k}{r} + \frac{1}{r^2}\right) \sin\theta \quad . \tag{12}$$

The impedance boundary condition requires the addition of a solution of the source free Helmholtz equation

$$A_z^r = \mu_o\, I\, dh\, \frac{\sin(kr)}{4\pi r}\, R \quad , \tag{13}$$

where R is a constant to be determined. The associated fields are

$$H_\varphi^r = I\, dh\, \frac{\sin\theta}{4\pi r} \left[-k\, \cos(kr) + \frac{1}{r} \sin(kr)\right] R \quad , \tag{14}$$

$$-i\omega\epsilon_o\, E_\theta^r = I\, dh\, \frac{\sin\theta}{4\pi r} \left[\left(-k^2 + \frac{1}{r^2}\right) sin(kr) - \frac{k}{r} \cos(kr)\right] R \quad . \tag{15}$$

The boundary condition (6) becomes

$$E_\theta^s + E_\theta^r = Z_s \left(H_\varphi^s + H_\varphi^r\right) \,,\ r = b \quad , \tag{16}$$

which gives

$$-e^{-ikb} R = \frac{1 - \frac{1}{k^2 b^2} + \frac{i}{kb} - \frac{Z_S}{\eta_O}\left(1 + \frac{i}{kb}\right)}{\left(1 - \frac{1}{k^2 b^2}\right) \sin(kb) + \frac{1}{kb} \cos(kb) + i\frac{Z_S}{\eta_O}\left[\cos(kb) - \frac{1}{kb} \sin(kb)\right]} \,. \tag{17}$$

The real part of the antenna input impedance can be evaluated by means of the Poynting vector method. The time average power input to the antenna terminals is

$$P_{ant} = Re(VI^*) = Re(Z_{ant})\,|I|^2 \quad , \tag{18}$$

where Z_{ant} is the antenna input impedance and again rms units are used for I. But the time average power supplied to the antenna is radiated away and absorbed by the sphere at r = b; thus

$$P_{ant} = Re\left[\int_0^{\pi} 2\pi r^2 S_r \, \sin\theta \; d\theta\right] \quad , \tag{19}$$

where the radial component of the Poynting vector is

$$S_r = (E_\theta^s + E_\theta^r)\left(H_\varphi^s + H_\varphi^r\right)^* \quad . \tag{20}$$

Carrying out (19) at r = b, so that (16) can be used in (20), we obtain

$$P_{ant} = Re(Z_s)\,|I|^2 \frac{(k\,dh)^2}{6\pi} \left| -i + \frac{1}{kb} - Re^{-ikb}\left[\cos(kb) - \frac{1}{kb}\sin(kb)\right]\right|^2 . \tag{21}$$

Inserting (17) and referring to (18) gives

$$\frac{Re(Z_{ant})}{R_{rad}} = \frac{R_{ant}}{R_{rad}} =$$

$$Re(Z_s/\eta_o)\Big/\left|\left(1 - \frac{1}{k^2b^2}\right)\sin(kb) + \frac{1}{kb}\cos(kb) + i\frac{Z_s}{\eta_o}\left[\cos(kb) - \frac{1}{kb}\sin(kb)\right]\right|^2 \tag{22}$$

where R_{rad} in (22) is given by (1). Thus the right-hand side of (22) represents a multiplicative correction to R_{rad} which defines the real part of the input impedance R_{ant}.

To obtain a feel for the size of (22) let us simplify it by allowing the spherical cavity to be several wavelengths in radius (kb is large)

$$\frac{R_{ant}}{R_{rad}} = Re(Z_s/\eta_o)/|\sin(kb) + i\,(Z_s/\eta_o)\cos(kb)|^2 \ . \tag{23}$$

Now for small surface impedances $Z_s << \eta_o$, typical of metallic conductors, the minimum of (23) occurs when sin(kb) equals unity

$$R_{ant}/R_{rad} = Re(Z_s/\eta_o) \ . \tag{24}$$

Obviously the quantity in (24) can be quite small compared to unity and thus we would expect the received power (4) to be increased considerably. However, it must be noted that other losses in specific cavities of interest (losses resulting from radiation through apertures or lossy dielectrics) must actually be included to obtain realistic estimates of the decrease in R_{ant}. Nevertheless, this simple canonical model does point out the need for further consideration of this important problem.

For illustration purposes if we take $\sigma = 2.61 \times 10^7$ *S/m* for commercial aluminum and f = 800 MHz (note $Re(Z_s) = R_s = \sqrt{\omega\mu_o/(2\sigma)}$) $Re(Z_s/\eta_o) \approx 1/185^2$. This means that the standard "V curve" electric field value at 800 MHz, 0.2 V/m (800 MHz/8 MHz) ≈ 20 V/m is reduced by a factor of 185 to 0.1 V/m. Figure C-3 gives a rough sketch of the resulting curve. Of course we emphasize again in practical cases other losses must be included which will raise the level of the dashed curve.

Conclusions:

It has been demonstrated by means of a simple canonical problem, consisting of a short dipole at the center of a spherical cavity, that the real part of the input impedance can be decreased significantly from the value when the dipole is situated in empty space. This implies that the received power into a matched load is considerably increased relative to that predicted by the "V curve. " Several questions remain to be answered before use can be made of such a result: 1) how do other losses including aperture radiation and dielectric loss influence the result; 2) how does the special geometry assumed here generalize; 3) how do limitations on the matching network of the load (typically a transmission line), including losses, influence the result.

Distribution:

2512 J. G. Harlan
2513 D. E. Mitchell
2514 L. L Bonzon
2515 P. D. Wilcox
5113 R. W. Jorgensen
5114 W. D. Ulrich
5131 J. O. Harrison
5132 H. J . Abeyta
5140 W. C. Nickell
5141 C. A. Harris
5143 R. D. Robinett
5144 D. E. Ryerson
5145 D. H. Schroeder
5147 G. L. Maxam

5147 L. E. Stevenson
5210 C. C. Hartwigsen
7210 D. L. McCoy
7212 J. W. Mead
7213 H. D. Bickelman
7290 E. G. Franzak
7533 F. H. Mathews
7550 R. A. David
7553 M. E. Morris
7553 K. C. Chen
7553 R. D. Jones
7553 R. E. Jorgenson
7553 L. K. Warne
7554 R. J. Fisher
7555 B. Boverie
7555 R. H. Bonn
7555 H. G. Hudson
7555 J. G. Kostas
7555 G. A. Seely
7555 J. E. Solberg
7555 J. S. Yu
8133 A. C. Skinrood
8133 K. A. Mitchell
8162 C. T. Yokomizo
8162 D. S. Post
9333 O. L. Burchett

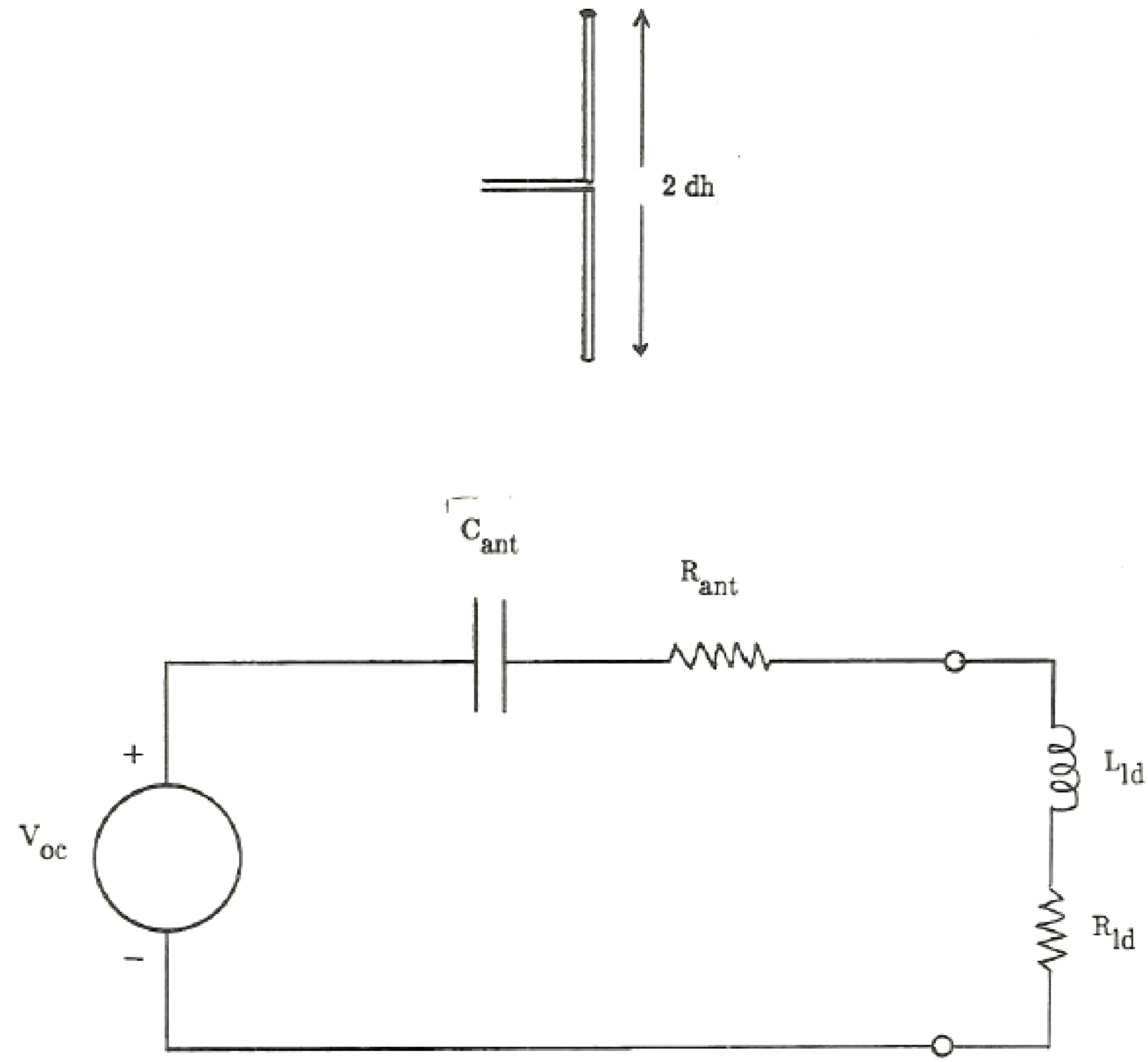

Figure C-1. Circuit model for an electrically short dipole of length 2 dh and radius a with attached load.

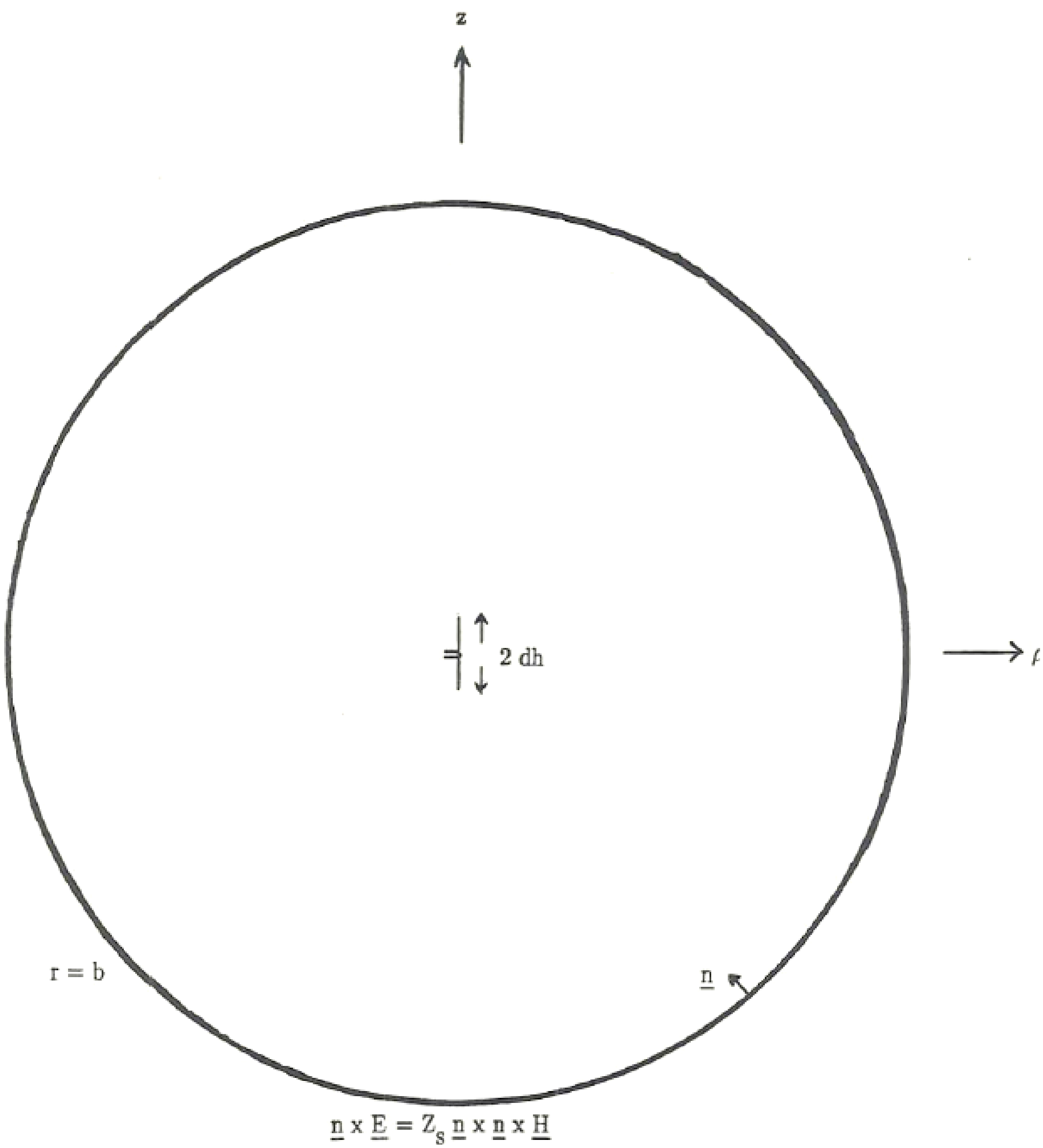

Figure C-2. Electrically-short dipole of length 2 dh at the center of a spherical enclosure of radius b with impedance boundary condition at the spherical enclosure.

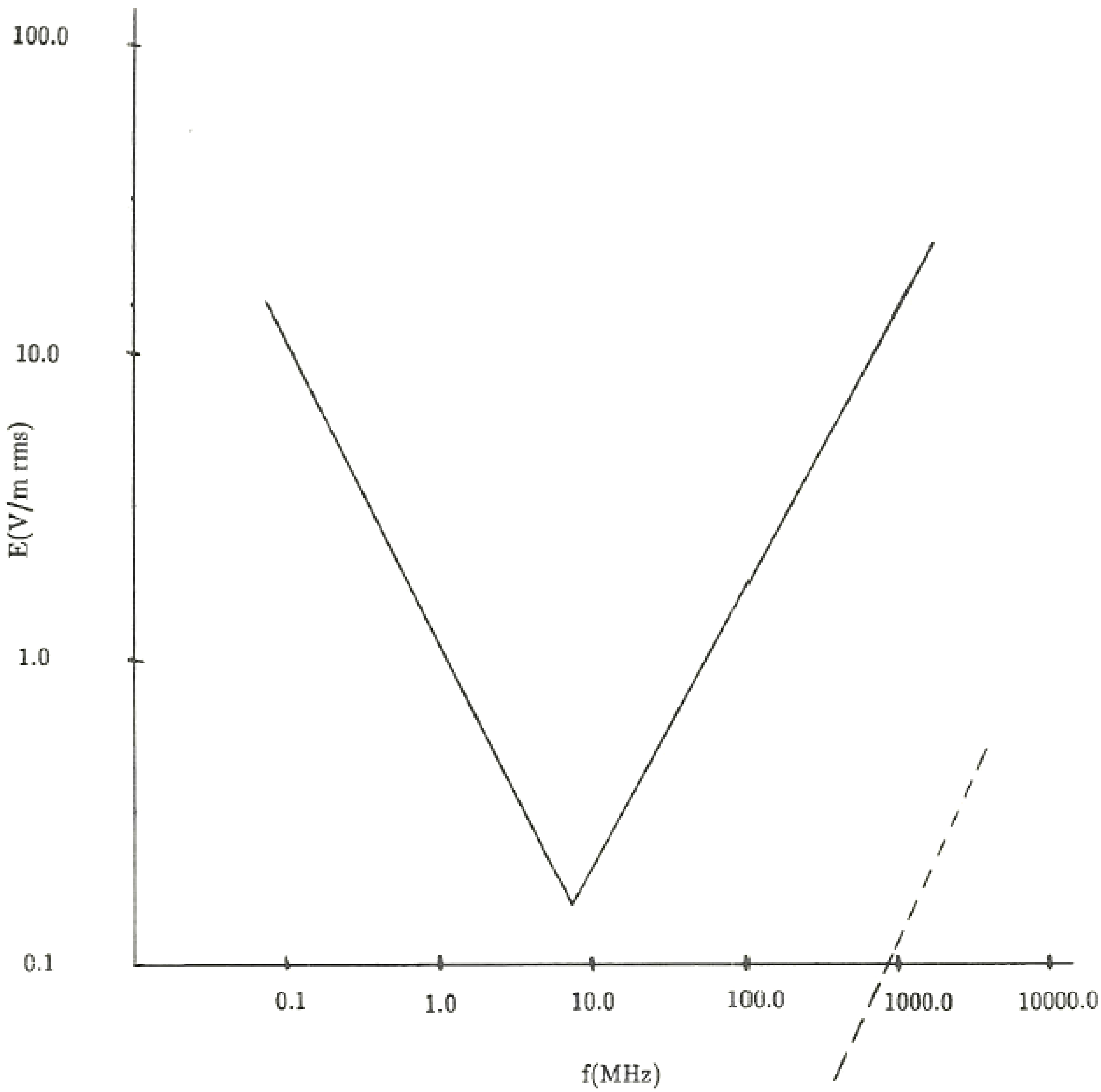

Figure C-3. Typical "V curve" (solid) with modification introduced for commercial aluminum wall material (dashed).

Appendix D 1991 Memorandum to Marvin Morris

Date: February 1, 1991

To: M. E. Morris, 7553

Larry Warne

From: L. K. Warne, 7553

Subject: Matched Receiving Antenna Inside a Cavity Resonator: Practical Interpretation

Introduction

This memo attempts to interpret the results of [1] from a practical point of view for real geometries. The discussion here is of a somewhat qualitative nature because the quantitative details in a more realistic geometry have yet to be worked out. Nevertheless the considerations given are believed to put the previous memo [1] in the proper perspective.

The real part of the input impedance $R_{ant} = Re(Z_{ant})$ to an infinitesimal dipole of length 2 dh placed at the center of a spherical cavity of radius b with surface impedance Z_s was calculated in [1] to be

$$\frac{Re(Z_{ant})}{R_{rad}} = \frac{R_{ant}}{R_{rad}} =$$

$$Re(Z_s/\eta_o) \Big/ \left| \left(1 - \frac{1}{k^2 b^2}\right)\sin(kb) + \frac{1}{kb}\cos(kb) + i\frac{Z_s}{\eta_o}\left[\cos(kb) - \frac{1}{kb}\sin(kb)\right] \right|^2 , \tag{1}$$

where R_{rad} is the radiation resistance of the infinitesimal dipole in free space

$$R_{rad} \approx \frac{\eta_o}{6\pi}(k\,dh)^2 \ , \tag{2}$$

the wavenumber is $k = \omega\sqrt{\eta_o \epsilon_o}$, the impedance of free space is $\eta_o = \sqrt{\mu_o/\epsilon_o}$, μ_o is the free space permeability, and ϵ_o is the free space permittivity.

Reference [1] discussed the simplification when kb was large. However, in general if

$$\tan(kb) = kb \ , \tag{3}$$

then (1) becomes

$$\frac{R_{ant}}{R_{rad}} = Re(Z_s/\eta_o) \ , \tag{4}$$

the same result given in [1] for kb large. But an empty perfectly conducting spherical resonator has TM_{n01} modal solutions for [2]

$$\tan(kb) = \frac{kb}{1-(kb)^2} \ . \tag{5}$$

Equation (1) at the frequencies (5) becomes

$$\frac{R_{ant}}{R_{rad}} = Re(Z_s/\eta_o)\left|\frac{\eta_o}{Z_s}\right|^2\left(1 - \frac{1}{k^2b^2} + \frac{1}{k^4b^4}\right) \ . \tag{6}$$

Now for small Z_s/η_o the result (4) indicates that there is a decrease in the real part of the input impedance whereas the result (6), at a different set of frequencies, yields an increase in the real part of the input impedance. To explain these results, note the field components generated by the boundary are [1]

$$H_\varphi^r \ = I\ dh\frac{\sin\theta}{4\pi r}\left[\cos(kr) - \frac{1}{kr}\sin(kr)\right](-k)R \ \ , \tag{7}$$

$$-i\omega\epsilon_o E_\theta^r \ = I\ dh\frac{\sin\theta}{4\pi r}\left[\left(1-\frac{1}{k^2r^2}\right)\sin(kr) + \frac{1}{kr}\cos(kr)\right](-k^2)R \ \ . \tag{8}$$

Notice that if kb satisfies (5) then E_θ^r = 0 at r = b. However for small Z_s the total field E_θ^S + $E_\theta^r \approx 0$ (where E_θ^S is the field resulting from a dipole in empty space [1]) at r = b. This means that the constant R becomes very large and the magnetic field (7) is very large at r = b. This results in large power dissipation at the wall and thus the large value of the observed real part of the input impedance (6).

Alternatively if kb satisfies (3) then $E_\theta^r \neq 0$ at r = b (This is also true as long as we are well away from the resonant frequencies (5).). The constant R can be taken as an order unity quantity and the total magnetic field at the wall is relatively small. Thus the power dissipation at the wall is small and the real part of the input impedance is the relatively small quantity (4).

This idealized geometry allows these limits to exist even if kb is large. However in a real cavity, which has a finite size antenna and possibly complex structure, many modes other than TM_{n01} (represented by (7) and (8)) will be excited when kb is large. As the number of resonant modes grows with kb, the resonant frequencies tend to overlap as a result of the broadening due to the finite losses at the walls (It is no longer possible to be well away from the modal resonant frequencies.). Many of these modes will thus have large values of the tangential magnetic field at the cavity walls. Thus it appears it is not possible in real situations with large kb to achieve the small values of the real part of the input impedance (6). The solution considered in [1], because of the high degree of symmetry, is basically a one dimensional radial solution; whereas, the three dimensional character of practical geometries results in a very much larger number of resonant modes at high frequencies.

This multimode problem is not present when kb is order unity. However the question of whether limitations on the matching network to the antenna (usually a transmission line) severely limits the power received in this case still remains to be answered.

Conclusions:

It has been pointed out that in large realistic cavities the multimode nature of the field is likely to prevent achieving situations where the real part of the input impedance becomes small. This may not be the case, however, when the frequency is low enough that the cavity is operating in the range of its lowest order modes (the wavenumber times the cavity dimension is order unity).

References:

[1] L. K. Warne, memo “Matched Receiving Antenna Inside a Cavity Resonator,” January 29, 1991.

[2] S. Ramo, J. R. Whinnery, and T. Van Duzer, Fields and Waves in Communication Electronics. New York: John Wiley & Sons, Inc., 1965, pp. 556-558.

Distribution:

2512 J. G. Harlan
2513 D. E. Mitchell
2514 L. L Bonzon
2515 P . D. Wilcox
5113 R. W. Jorgensen
5114 W. D. Ulrich
5131 J. O. Harrison
5132 H. J. Abeyta
5140 W. C. Nickell
5141 C. A. Harris
5143 R. D. Robinett
5144 D. E. Ryerson
5145 D. H. Schroeder
5147 G. L. Maxam
5147 L. E. Stevenson
5210 C. C. Hartwigsen
7210 D. L. McCoy
7212 J. W. Mead
7213 H. D. Bickelman
7290 E. G. Franzak
7533 F. H. Mathews
7550 R. A. David
7553 M. E. Morris
7553 K. C. Chen
7553 R. D. Jones
7553 R. E. Jorgenson
7553 L. K. Warne

7554 R. J. Fisher

7555 B. Boverie

7555 R. H. Bonn

7555 H. G. Hudson

7555 J. G. Kostas

7555 G. A. Seely

7555 J . E. Solberg

7555 J. S. Yu

8133 A. C. Skinrood

8133 K. A. Mitchell

8162 C. T. Yokomizo

8162 D. S. Post

9333 O. L. Burchett

DISTRIBUTION

Number	Mail Stop	Name	Dept.
1 (electronic)	MS0405	K. O. Merewether	0434
1 (electronic)	MS0447	E. G. Garavaglia	2221
1 (electronic)	MS0481	N. J. Dereu	2222
1	MS0492	K. C. Chen	0411
1	MS1152	L. I. Basilio	1352
10	MS1152	R. E. Jorgenson	1352
1	MS1152	W. L. Langston	1352
10	MS1152	L. K. Warne	1352
1	MS1152	R. K. Howard	1353
1	MS1152	H. G. Hudson	1353
1 (electronic)	MS1152	M. Jursich	1353
1 (electronic)	MS1152	R. A. Salazar	1353
1 (electronic)	MS1168	B. V. Oliver	1352
1 (electronic)	MS1394	P. R. Huffman	0427
1 (electronic)	MS9154	G. A. Lopez-Diaz	8237
1 (electronic)	MS0899	RIM - Reports Management	9532

Sandia National Laboratories